# BIOGAS UPGRADE THROUGH EXHAUST GAS REFORMING PROCESS FOR USE IN CI ENGINES

**by**

**CHIA SHENG LAU**

**A thesis submitted to the**
**University of Birmingham**
**for the degree of**
**DOCTOR OF PHILOSOPHY**

School of Mechanical Engineering
University of Birmingham
March 2012

# Abstract

Biogas is not ideal for combustion in diesel engines mainly due to its low energy content. The upgrading of biogas into high quality syngas through catalytic reforming reactions was investigated.

Studies on the effect of temperature, space velocity and $O_2/CH_4$ molar ratio on various basic biogas reforming processes were done. The dry reforming of biogas was found to be active at high reactor temperatures with syngas production and reduction of carbon dioxide. The promotion of simultaneous dry and oxidative reforming by adding oxygen improves syngas production at conditions of low temperature and high space velocity.

Subsequently, the biogas exhaust fuel reforming process was done by feeding real engine exhaust together with biogas into the reforming reactor. Reforming process efficiency of 95% (ratio of energy content of reformate to biogas) was achieved at high space velocity and high content of steam in exhaust at medium engine load (300°C exhaust temperature). Further improvement was observed when reformed exhaust gas recirculation (REGR) was applied due to increased exhaust steam content in the engine – reactor system which promoted the endothermic steam reforming reaction. Moreover, improved engine thermal efficiency and lower emissions were found during reformate gas-diesel operation compared to biogas-diesel operation.

*"Dedicated to my family members and*

*to my long time girlfriend Julin Lee"*

# Acknowledgements

These three years as a research student in the University of Birmingham has been a life changing experience for me. Not only have I gained invaluable technical knowledge in the field of research, I have also met with a group of wonderful friends who came from all around the world. As such, I would like to take this opportunity to show my deepest gratitude to the people who have given me a helping hand along the way.

Firstly, I would like to sincerely thank my supervisor, Dr. A. Tsolakis for his relentless help and guidance in both research work and in daily life. I wished to thank Professor Miroslaw L. Wyszynski for his supervision and experience contributed throughout this research project. Many thanks also to the lab technicians for their technical knowledge for the duration of the project.

School Scholarship provided by the School of Mechanical Engineering and the industrial support from Johnson Matthey plc is gratefully acknowledged.

Special thanks to all my colleagues, Dr Jose Martin Herreros, Dr Dale Turner, Dr Kampanart Theinnoi, and the good lads in room G47A: Simaranjit Gill, Joshua Shenker, Hendry Sakke Tira, Wentao Wang, Danny Fennel, Thomas Hoskins and Ekarong Sukjit.

I would like to say thank you to both my parents, Eng Lim Lau and Sock Eng Ng for their unyielding love and moral support since day one and lastly to my long time girlfriend Julin Lee for her patience and care throughout all these years.

Chia Sheng Lau

March 2012

# Table of Contents

# List of Illustrations

# List of Tables

# Nomenclature

| Symbol | Units | |
|---|---|---|
| GHSV | $h^{-1}$ | Gas hourly space velocity |
| $LCV_{fuel\ in}$ | MJ $kg^{-1}$ | Lower calorific value of fuel input |
| $LCV_{fuel\ prod}$ | MJ $kg^{-1}$ | Lower calorific value of fuel produced |
| $\dot{m}_{fuel\ in}$ | kg $s^{-1}$ | Mass flow rate input |
| $\dot{m}_{fuel\ prod}$ | kg $s^{-1}$ | Mass flow rate produced |
| n | | Number of carbon atoms in Diesel |
| p | bar | Pressure (Absolute) |
| $\eta_{th}$ | % | Engine indicated thermal efficiency |
| $\lambda$ | | Excess air/fuel ratio in the engine |
| $\Phi$ | | Total equivalence ratio ($1/\lambda$) |

# List of Abbrevations

| | |
|---|---|
| AD | Anaerobic digestion |
| AFR | Excess air/fuel ratio |
| APU | Auxiliary power units |
| AR | Aspect ratio |
| ATR | Autothermal reforming |
| BDC | Bottom dead centre |
| BSFC | Brake specific fuel consumption |
| CAD | Crank angle degree |
| CHP | Combined heat and power |
| CI | Compression ignition |
| CNG | Compressed natural gas |
| $CO_2/CH_4$ | Carbon dioxide-to-methane |
| COV | Coefficient of variation |
| DRR | Dry reforming reaction |
| EGR | Exhaust gas recirculation |
| EOC | End of combustion |
| EOI | End of injection |
| FSL | Flame spread limit |
| FT-IR | Fourier transform infrared |
| GC | Gas chromatograph |
| GHG | Green house gases |
| $H_2/CO$ | Hydrogen-to-carbon monoxide |
| $H_2O/CH_4$ | steam-to-methane |
| HC-SCR | Hydrocarbon selective catalytic reduction |
| IC | Internal combustion |
| IDI | Indirect injection |
| IMEP | Indicated mean effective pressure |
| ISG | Idle stop and go |
| LPG | Liquified petroleum gas |
| ND-IR | Non-dispersive infrared |

| | |
|---|---|
| Ni | Nickel |
| O.D. | Outer diameter |
| $O_2/CH_4$ | Oxygen-to-methane |
| POX | Partial oxidation |
| PPM | Parts per million |
| PSA | Pressure swing adsorption |
| Pt | Platinum |
| REGR | Reformed exhaust gas recirculation |
| Rh | Rhodium |
| ROHR | Rate of heat release |
| SI | Spark ignition |
| SMPS | Scanning mobility particle sizer |
| SOC | Start of combustion |
| SOI | Start of injection |
| SRR | Steam Reforming Reaction |
| Syngas | Synthesis gas |
| TDC | Top dead centre |
| ULSD | Ultra low sulphur diesel |
| WGSR | Water gas shift reaction |

# CHAPTER 1

# INTRODUCTION

## 1.1 World Energy Outlook

The increase in human population across the globe and the emergence of energy-intensive nations has driven up the global energy demand. In 2010 alone, there is a growth of 5% in the energy consumption among the G20 countries (Enerdata, 2011) and globally, total energy consumption grew from 4,675 to 8,286 million tons of oil equivalent between 1973 and 2007 (IEA, 2009). With the prediction by the United Nations showing that by 2050 the earth's population will be around 9 billion people, an approximate 30% increase, there will only be an upward trend on the global demand for energy (Kibert, 2008).

Fossil fuels still remain the most common form of energy source being converted into utilizable forms such as liquid (oil), gas and solid (coal), mainly due to its high energy density and the presence of readily available infrastructure networks. However, the heavy reliance of the world on fossil fuels comes with a heavy price tag. Firstly, fossil fuels are recognized as non-renewable sources of energy, signifying that the depletion of these resources occurs faster than the rate at which they can be regenerated. Apart from that, the price per barrel of oil has skyrocketed these past years due to the increased difficulty and cost of deep-water oil drilling.

Secondly, the use of fossil fuels and the generation of greenhouse gas (GHG) come in tandem. It is a known fact that the earth is warming, with the average surface temperature 0.8°C warmer during the 1st decade of the 21st century than that of the 20th century and most of it is attributed to the releasing of carbon dioxide and GHG through burning of fossil fuels

(NRC, 2010). And finally, the strong dependence on fossil fuels for energy consumption increases the risk in energy security for a nation as fossil fuels supply is unevenly distributed across the globe. A good example would be the recent upheaval among the oil supplying nations which affects the global crude oil market, hence driving up the commodity prices especially for energy intensive consumer nations. Events such as these have greatly exposed the vulnerability in energy security for a nation.

## 1.2 Renewable Energy

### 1.2.1 Biogas as a Renewable Energy Source

In view of all these factors, countries have turned to renewable energy sources in order to meet their energy consumption demand and also to meet international commitments in reducing the GHG emissions set by the United Nations Framework Convention on Climate Change (UNFCCC) under the Kyoto Protocol to fight global warming (United Nations, 2008). Among the different sources of renewable energy (e.g. hydropower, solar, geothermal and etc), the implementation of biomass technology was deemed to be attractive as it not only helps to reduce carbon emissions but also improves the energy security of a nation if fuels were sourced and produced locally. Biofuels have been widely use, especially in European Union (EU) countries whereby there is a target use of 5.75% for biofuels in the transport sector (REN21, 2009). However, there are growing concerns over the use of biofuels as it reduces the land usage for growing food crop and might also promotes monoculture, which in turn affects the global food supply (UNEP, 2009).

Biogas, on the other hand has the potential as the future biomass energy source due to its ability to recycle waste and its versatility for energy conversion and for various applications. Essentially, biogas is a gaseous fuel derived from any biomass types, such as

crops, woods, bio-waste, etc. as long as they contain carbohydrates, proteins, fats cellulose and hemicelluloses as their main components (Deublein and Steinhauser, 2008). Compared to other renewable energy sources, biogas is arguably the most versatile energy source mainly because its production is independent of factors such as geographical location and season (Pöschl et al., 2010). Many European countries have now established favourable domestic conditions for production of electricity from biogas, with Germany leading the group having almost 4000 biogas plants (AEBIOM, 2009).

In general, biogas is a mixture of methane (45-70%), carbon dioxide (30-45%) and nitrogen (1-15%), with small quantities of hydrogen sulphide and sulphur dioxide present (Rasi et al., 2007). The quality of biogas produced is a measurement of the amount of methane present in the gaseous fuel (i.e. the combustible portion of biogas) and this is largely dependable on the feedstock type used and the production environment of the biogas. Based on current available technology, biogas comes from the four main sources (Jönsson, 2004):

- Sewage treatment plants
- Landfills
- Cleaning of organic industrial waste streams
- Mesophilic and thermophilic anaerobic digestion of organic waste

### 1.2.2 Biogas Production and Usage

Currently, landfills account for the largest proportion of biogas produced, with almost 40% of biogas in Europe is produced from landfill. However, due to the heavy land usage and the risk of produced methane escaping into the atmosphere (methane has a global warming potential of 23 times greater than carbon dioxide (Themelis and Ulloa, 2007)), the use of anaerobic digestion (AD) plant to produce biogas has been seen as an attractive option. Figure

1.1 shows the simplified layout of a typical biogas AD plant. The production of biogas and its usage as an energy source is considered to be a low carbon technology or even carbon neutral as the carbon dioxide produced through the combustion of biogas is subsequently retrieved through the photosynthesis of the feedstock (Mezzullo, 2010).

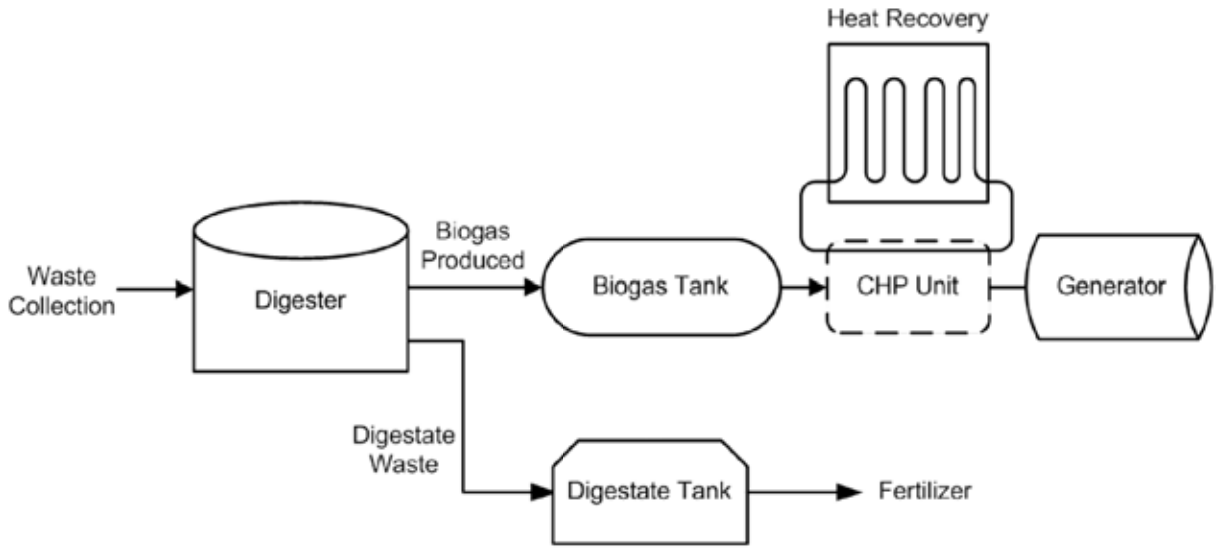


Figure 1.1: Simplified process layout of a biogas AD plant.

Biogas is mainly used for generating heat and electricity, especially in rural areas and countries where providing electrical infrastructure is expensive. In Austria, 294 biogas plants were producing green electricity for the country with an average size of 263 kWe of installed power (AEBIOM, 2009). The electricity generation is done by simply combusting the biogas produced from the digester (Figure 1.1) in a power generator, be it a gas engine or a gas turbine. In addition, the heat generated from the combustion process could be recovered for heating purposes in the AD plant or to warm up the digester. The excess electricity and heat produced could even be transmitted outside the plant for economic purposes, making it energetically sustainable. This process is called combined heat and power (CHP) and this

form of energy usage increases the conversion efficiency up to 85-90% (Deublein and Steinhauser, 2008).

In terms of domestic usage, biogas is commonly used for cooking purposes in the rural areas of developing nations. For the farming industry, the digested waste (digestate) from an AD plant makes a good source of natural fertilizer provided it meets the quality and legislation standards, hence recycling the nutrient from waste back into the agricultural sector. It has been reported that the use of digestate as fertilizers in farming has increased the crop yield up to 20% compared to using organic substrates such as cow manures (El-Shinnawi et al., 1988). In addition, digestate could also be used as a solid fuel for combustion processes (Kratzeisen et al., 2010). From the socioeconomics point of view, the use of biogas is beneficial as it not only supplies electricity and heat for daily usage, a biogas plant also acts as sanitisation facility for municipal and industrial wastes disposals. Hence, the use of biogas has the potential to simultaneously satisfy the three main renewable energy policies concerning a nation, which are: (i) agricultural policy, (ii) waste policy and (iii) energy policy.

However, the one major drawback of biogas is its lower energy content compared to other fuels such as natural gas, mainly due to the large portion of carbon dioxide present. As such, various biogas upgrading options have been made available to increase the usability of biogas. The most common biogas upgrading technologies are the water scrubber technology and the pressure swing adsorption (PSA) technology. Both technologies work by separating the carbon dioxide and sulphur contaminants from the biogas, hence making it into a higher quality methane-enriched gaseous fuel called biomethane. Biomethane can then be injected into the natural gas grid for domestic usage, reducing the dependency on fossil derived natural gas. In addition, biomethane has been widely used as vehicle fuels in Sweden whereby in 2006, there were over 6000 biogas fuelled vehicles registered (Jönsson et al., 2007).

## 1.3 The Transportation Sector

### 1.3.1 The Comeback of CI Engines

Today, a large proportion of the total world energy consumption can be attributed to the transportation sector, in particularly the burning of gasoline, diesel and other fuels derived from petroleum through the use of internal combustion (IC) engines. According to the European Environment Agency (EEA), transport accounts for approximately a third of the total final energy consumption among the EEA member countries and for more than a fifth of the GHG emissions (EEA, 2011). As such, governments and environmental agencies are putting immerse pressure on automotive manufacturers to come out with new innovations for cleaner and more efficient compression ignition (CI) and spark ignition (SI) engines by implementing legislative automotive emission standards such as the EURO emission standards.

For the past few years, CI engines have become increasingly popular, especially among European nations due to its higher thermal efficiency and increased torque characteristics compared to SI engines. In addition, CI engines are built to resist high compression ratios, making them more reliable and durable. However, the downside of CI engines is the comparatively higher emissions of particulate matters (PM) and nitrogen oxides (NOx). Nonetheless, current breakthroughs in catalytic exhaust after-treatment systems have managed to tackle this problem substantially. Another benefit of using CI engines is their flexibility in fuel source usage (a proportion of biodiesel has been commonly used in CI engines throughout Europe without any engine modification) and this has currently driven the interest in researchers to explore the benefits and challenges of using alternative renewable

gaseous fuels in CI engines, which could potentially be more environmentally beneficial than liquid biofuels (Patterson et al., 2011).

### 1.3.2 Engine Waste Energy Recovery for Biogas Upgrade

With the engine thermal efficiency typically ranging from 30 – 40% (Stone, 1992), technologies to improve engine thermal efficiency for CI engines have been a much researched field. Apart from advancements in the combustion technologies, automotive manufacturers are now looking into ways of how to improve fuel economy by reducing the generation of engine waste energy and also how to recover this waste energy if its generation is inevitable. Technologies such as the idle stop and go (ISG) technology and the turbocharger system are examples of the more common technologies currently available in the market. In terms of thermal energy loss, the rule of thumb is that about one third of the total chemical energy input is being converted into waste heat energy dissipated through the engine exhaust. Therefore, the engine exhaust gas can be considered as the main heat source for thermal energy recovery (Lee et al., 2011).

Biogas, on the other hand has been widely used in certain countries for generating heat and electricity (Deublein and Steinhauser, 2008). Nonetheless, due to its low calorific value resulting from the high proportion of carbon dioxide present, CI engines fuelled with biogas suffer from low engine thermal efficiency and high unburned hydrocarbons in exhaust emissions, especially at part load operations (Bari, 1996, Karim and Wierzba, 1992, Kobayashi et al., 2007). Fuel upgrading measures have been recommended for biogas to be used as a fuel source for CI engines (Jönsson, 2004) but these upgrading techniques require external energy input (i.e. approximately 3-6% of biogas energy output), hence decreasing the overall energy efficiency of biogas.

This thesis aims to explore the concept of potentially recovering the engine exhaust waste heat for the purpose of upgrading the biogas and to achieve on-demand supply of high quality gaseous fuels for transport vehicles. This technique is called the exhaust gas fuel reforming process and it involves the catalytic reaction of engine exhaust gas with biogas to produce synthesis gas (i.e. syngas, a gas mixture of hydrogen and carbon monoxide) for use in the combustion process of CI engines.

## 1.4 Research Objectives

The main objective of this research work is to investigate the upgrading of low energy content difficult to use biogas into high quality syngas fuel for CI engines through catalytic fuel reforming processes. To achieve this, the research work is divided into two main parts.

(i) To understand and optimise the biogas exhaust gas fuel reforming process by:

- Identifying the effect of different temperatures and gas hourly space velocity conditions on the dry reforming process (DRR, $CH_4 + CO_2 \rightarrow 2CO + 2H_2$) of biogas in producing syngas.
- Investigating the feasibility of adding oxygen into the reforming reactor to achieve low temperature simultaneous dry and partial oxidation reforming of biogas (POX, $CH_4 + 0.5O_2 \rightarrow CO + 2H_2$).
- Determining the effect of different engine exhaust compositions and biogas input into the reforming reactor on the exhaust gas fuel reforming process.

(ii) To study the implementation of the engine – reactor system by:

- Investigating the effect of the closed coupled engine – reactor system formed through feeding reformate gaseous fuel into the engine intake (REGR) on the biogas exhaust gas fuel reforming process.
- Analyzing the engine thermal efficiency and exhaust gas emission trends for the reformate gas-diesel dual fuel operation.

## 1.5 Thesis Outline

In Chapter 1, an overview on the world energy outlook together with the emerging trend of using biogas as a source of renewable energy has been presented. The increasing popularity of CI engines and the engine waste heat recovery techniques have also been discussed to provide the fundamental knowledge required in the coming chapters. The remainder of this thesis is organised as follow:

**Chapter 2: Literature Review**

This chapter is essentially divided into two main parts, the first being an overview discussion on the engine performance and exhaust emission trends on the usage of different gaseous fuels in gas-diesel dual fuel engines. The first part ends with discussions on the application and technical difficulties associated with biogas for use in dual fuel operations. The second part of this chapter reviews the theory of the main fuel reforming reactions for hydrogen production and the operating principles of the exhaust gas fuel reforming process and the engine – reactor system.

**Chapter 3: Experimental Setup**

This section presents the experimental facilities used in this research work, which includes the engine test rig, engine instrumentations, the design of the reforming mini reactor, reforming catalyst preparation procedure, reformer product gas and engine exhaust gas emissions analysis system and selected properties of the fuels (i.e. biogas and diesel fuel) used in the test.

**Chapter 4: Biogas Upgrade to Syngas via Dry and Oxidative Reforming**

This part of the thesis presents a study on the fuel reforming process using biogas. Equilibrium prediction method followed by experimental studies were done to understand the effect of temperature and gas hourly space velocity conditions on the dry reforming process of biogas to produce syngas and to simultaneously reduce the carbon dioxide content of biogas, hence achieving fuel upgrade. Subsequently, oxygen is being fed into the reforming reactor to study the feasibility of promoting syngas production at low temperatures (i.e. to simulate low exhaust temperature conditions) via simultaneous dry and oxidative reforming reactions.

**Chapter 5: Biogas Upgrade through Exhaust Gas Fuel Reforming Process with Engine Exhaust Waste Heat Recovery**

This section describes the exhaust gas fuel reforming process in which the biogas is catalytically reacted with real engine exhaust obtained from a single cylinder diesel engine to produce syngas. The main aim of this chapter is to study the reforming reaction profiles for the main reforming reactions (i.e. dry reforming, steam reforming and etc. which will be explained in Chapter 2) involved in the exhaust gas reforming process. In addition, the effects of different reactor biogas feed rate and gas hourly space velocity conditions on the reforming reactor product gas distributions and the overall reforming process efficiency were also being

investigated. Lastly, the optimum engine and reforming reactor operating conditions were indentified and these conditions were to be used in the engine – reactor system.

**Chapter 6: Performance of the Biogas Exhaust Gas Fuel Reforming Process and the Gas – Diesel Dual Fuel Operation with REGR**

In this chapter, with reference to Chapter 5 the reformed exhaust gas recirculation (REGR) was implemented in the engine – reactor system by coupling the catalytic exhaust gas fuel reforming reactor to the single cylinder diesel engine. The real reformer product gaseous fuel was fed directly into the engine and the reformate gas-diesel dual fuel operation was investigated. For the reforming section, the effect of REGR on the reactor gas product distribution and the overall process efficiency were analyzed and compared to that in Chapter 5. Subsequently, the effects of introducing the reformer gaseous fuel into the diesel engine were studied by analyzing the engine thermal efficiency, exhaust gas emissions and percentage fossil diesel fuel replacement at various engine operating conditions. Lastly, comparison studies between pure diesel, biogas-diesel and reformate gas-diesel operations were done and the beneficial effects of implementing the engine – reactor system were concluded.

**Chapter 7: Conclusions and Future Work**

An overall summary on the key findings obtained from this current research work and the motives and general linking behind each chapter are presented. In addition, the recommendations for potential future work in this research subject are given.

# CHAPTER 2

# LITERATURE REVIEW

## 2.1 CI Engine

### 2.1.1 Basic Operating Principles

The basic working idea of an IC engine is to convert the chemical energy of the supplied fuel (i.e. either in liquid form or in gaseous form) into thermal energy through the combustion process, to provide for the desired power output. CI engines work by utilizing the heat generated through the compression of air to initiate the ignition of the fuel inside a combustion chamber. Compared to SI engines, the higher compression ratios (typically from 12:1 to 24:1) and the ability to operate in lean fuel mixture together with the absence of throttling have led to higher efficiencies in CI engines.

A typical CI engine operates on four-stroke cycle, meaning two revolutions of crankshaft are required to provide one power stroke. To understand the combustion characteristics of CI engines, the rate of heat release (ROHR) diagram (derived from the in-cylinder pressure data) is used for explaining each phase that occurs during the combustion process. For a typical four stroke CI engine, the combustion of fuel takes place in a short period of time around the top dead centre (TDC) which is, at the end of the compression stroke and at the early stage of the expansion stroke. The combustion process is divided into four main phases, as illustrated in Figure 2.1.

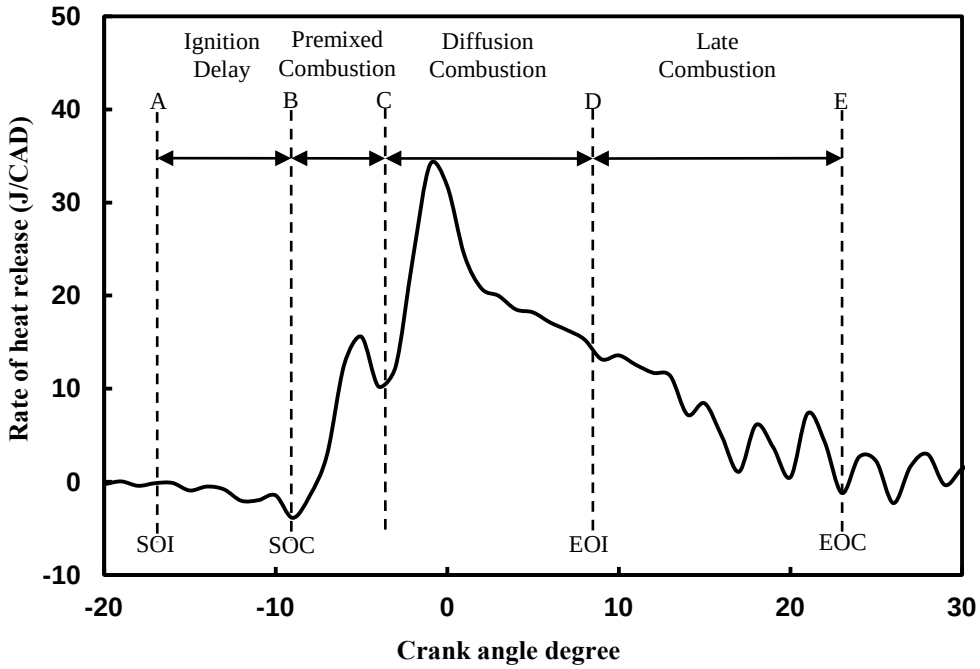


Figure 2.1: Typical ROHR diagram for a direct-injected diesel fuelled CI engine.

**A-B: Ignition delay** is defined as the period between the start of injection (SOI) to the start of combustion (SOC) in which the injected fuel undergoes the vaporisation process and mixes with the intake air, resulting in the negative value of ROHR.

**B-C: Premixed combustion**, whereby the premixed air-fuel mixture has reached the flammability limit and combusts within a very short period of time. This gives rise to the sudden sharp peak in the ROHR diagram.

**C-D: Diffusion combustion** commences once the premixed combustion stopped and it ends at the end of injection (EOI). In this phase, the main combustion process of the injected fuel occurs and the heat release rate are mainly controlled by the availability of the air-fuel mixture for the combustion reaction.

**D-E: Late combustion** is the final combustion phase which extends into the expansion stroke. The heat release during this phase is due to the combustion of small fractions of

unburned fuel with very low heat release rate (primarily due to the decreasing cylinder temperatures during the expansion stroke) and this phase completes at the end of combustion (EOC).

The whole cyclic process is then repeated again, starting with the induction of air in the intake stroke for the new engine cycle.

## 2.2 Dual Fuel Concept

### 2.2.1 Gas – Diesel Dual Fuel Operating Principles

Traditionally, CI engines are operated on liquid diesel fuels. However, due to the recent rise in oil prices and the availability of cheaper gaseous fuels such as natural gas, CI engines operating on gaseous fuels have gained much interest. With relatively simple modification and conversion processes, diesel CI engines can be made to operate on gaseous fuels efficiently in what is known as “dual fuel CI engine”. Unlike normal diesel operation whereby only fresh air is inducted (as explained in earlier section), in dual fuel engine a homogenous mixture of gaseous fuel and air is compressed and then ignited through the injection of a smaller amount of diesel fuel. With the overall combustion process being similar to that of diesel cycle, dual fuel CI engine tends to retain most of the positive trades of diesel operation (i.e. high thermal efficiency and power output) (Badr et al., 1999). Papagiannakis et al. (2008) suggested two operating modes, (i) conventional dual fuel operation and (ii) pilot ignited dual fuel operation.

Under conventional dual fuel operation, at a given engine speed, enough amount of liquid diesel is provided to achieve the certain percentage of the required engine power output. The rest percentage of engine power output required is then achieved by supplying gaseous

fuel into the system. As such, only small amounts of gaseous fuel is used and this operating mode is suitable for low engine load operations (Abd Alla et al., 2000). For pilot ignited dual fuel operation, a constant quantity of diesel fuel (pilot injection) is used mainly as the ignition source for the gaseous fuel. In this case, the small quantity pilot diesel injected (i.e. between 10% and 20% of the operation on diesel alone) covers approximately the mechanical losses of the engine and the remaining required engine power output is achieved using the gaseous fuel supplied. This operating mode allows for high substitution level of liquid diesel but suffers from low thermal efficiency and high unburned hydrocarbon (UHC) emissions at low engine load (Bedoya et al., 2009).

### 2.2.2 Dual Fuel Combustion

In dual fuel engines, the combustion process is dependent on the spray and ignition characteristic of the pilot fuel used and also on the type and concentration of gaseous fuel present in the combustion chamber. Nonetheless, a typical ROHR diagram for a dual fuel engine can be considered as a process being made up of three over-lapping components (Figure 2.2) as suggested by Karim (2003). The first component (I) is mainly due to the combustion of the pilot fuel, hence resulting in the almost similar level of ROHR in Figure 2.2 (a) and (b) at both heavy and light load respectively. For the second component (II), the proportion of gaseous fuel that is in the immediate vicinity of the ignition and combustion centres of the pilot is being burnt rapidly. And lastly, the third component (III) is due to the subsequent turbulent flame propagation advancing through the remainder of the premixed gaseous fuel-air charge present in the combustion chamber.

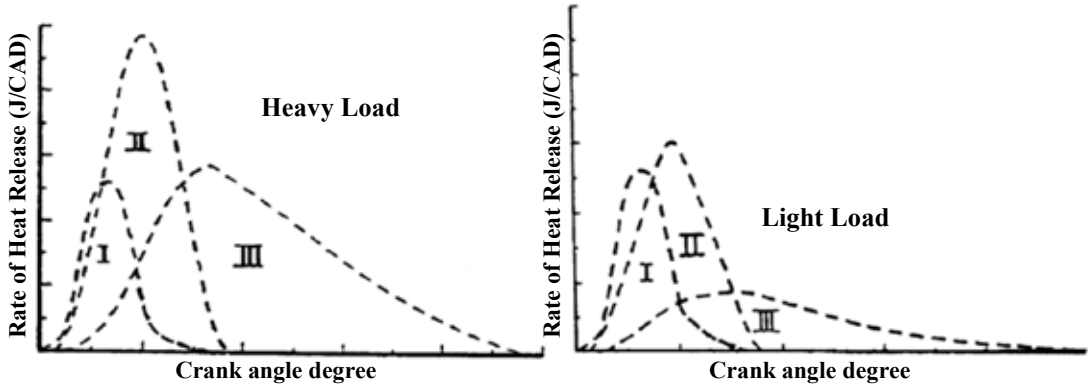


(a) (b)

Figure 2.2: Schematic representation of the different components of the combustion ROHR diagram in a dual fuel engine at: (a) heavy load (b) light load (Karim, 2003).

From Figure 2.2 (b), it can be seen that with very lean gaseous fuel-air mixture or at light engine load, the bulk of the energy release only comes from the ignition and subsequent rapid combustion of the small pilot zone together with part of the gaseous fuel-air mixture entrained into the pilot zone. The energy release also comes from the combustion of the immediate surrounding zones where the local temperatures are higher. This is mainly due to the absence of consistent flame propagation from ignition centre to the gaseous fuel, resulting in the low ROHR for component (III) as shown in Figure 2.2 and the high amount of UHC emission in the engine exhaust as mentioned earlier. It was suggested that by increasing the quantity of the pilot fuel, the effectively larger amount of mixtures entrained within the larger pilot combustion zone promotes partial flame propagation and consequently producing a higher amount of total energy release at engine part load operations (Wierzba et al., 1995).

Equally important in the combustion process is the variation in ignition delay of a dual fuel engine compared to that of a diesel engine, which has a profound effect on the subsequent combustion process, engine performance and engine emissions. Karim (2003) studied the effect of introducing different types of gaseous fuel into a dual fuel engine at constant pilot quantity and found out that the ignition delay trend is significantly different from those seen

in similar diesel operating conditions, as shown in Figure 2.3. It can be seen that the trend is very much dependable on types of gaseous fuel used and the ignition delay tends to increase with increasing amount of gaseous fuel up to a certain point followed by a dip before reaching the total stoichiometric ratio (based on combined gaseous and liquid fuel with the air available). Liu and Karim (1998) explained that the introduction of gaseous fuel into a diesel engine together with the air intake charge resulted in both the physical ignition delay (i.e. change in charge temperature, pressure, pre-ignition energy release and heat transfer) and the chemical ignition delay (i.e. chemical interactions between the gaseous and diesel fuel, such as the formation of radicals), depending strongly on the type of gaseous fuel used and its concentration in the combustion chamber.

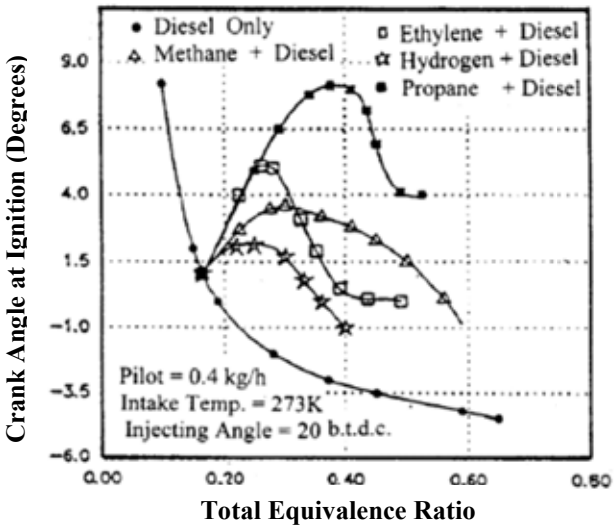


Figure 2.3: Variations of the ignition point with total equivalence ratio for gaseous fuels at a constant pilot quantity together with the corresponding diesel operation (Karim, 2003).

The main factor contributing to the physical ignition delay of a dual fuel engine is the decrease in charge temperature when gaseous fuel is introduced together with the intake air. Prakash et al. (1999) showed that the induction of gaseous fuel replaced part of the intake air, hence decreasing the oxygen partial pressure activity inside the charge during the compression stroke and subsequently reduces the charge temperature. Secondly, the use of gaseous fuel increases the overall specific heat capacity, leading to a significant drop in charge temperature at the TDC (Papagiannakis and Hountalas, 2004). Nielsen et al. (1987) too came to the same conclusion by concluding that the use of gaseous fuel with higher specific heat capacity increases ignition delay further in a dual fuel engine compared to that of a gaseous fuel with lower specific heat capacity.

In terms of chemical delay, it was shown that the homogenous gas fuel-air mixture in the vicinity of the pilot zone can undergo some chemical reactions during the compression stroke (i.e. rise in cylinder temperature), forming intermediates which competes with the pre-ignition process of diesel fuel. This is supported by Nielsen et al. (1987) whereby it was discovered that the induction of diatomic gaseous fuels (i.e. hydrogen, carbon monoxide and nitrogen) with comparable specific heats produces different ignition delay periods, suggesting that the difference in ignition delay is predominantly caused by chemical effects.

### 2.2.3 Dual Fuel Emissions

The emissions of a diesel fuelled engine remains a concern for causing environmental pollutions, in particularly the generation of PM and NOx through the combustion process. Research work investigating the emissions of dual fuel engines have shown that the application of gas-diesel dual fuel operation is capable of reducing both PM and NOx, simultaneously, hence capable of potentially breaking the PM-NOx trade off resulted from

diesel combustion. Nonetheless, the downside for dual fuel operation is the increased emissions of both carbon monoxide (CO) and unburned hydrocarbons (UHC), which are almost negligible in the case of diesel fuel operation.

**Nitrogen Oxides (NOx)** emissions consist of nitric oxide (NO) and nitrogen dioxide ($NO_2$) formed through the combination of dissociated oxygen with nitrogen, with NO being the dominating species (Heywood, 1988). As shown in Figure 2.4, NOx formation is affected considerably by the introduction of gaseous fuel, generally showing lower levels of formation compared to that of diesel at similar operating conditions (engine speed and load). It is commonly known that the formation of NOx is mainly determined by the cylinder charge temperature and the local oxygen access ratio (Papagiannakis et al., 2007). At low engine loads, the lower rate of premixed controlled combustion of the gaseous fuel resulted in lower charge temperature inside the combustion chamber compared to normal diesel operation, hence resulting in the lower NOx emissions (Figure 2.4). At higher engine loads, apart from the lower charge temperature effect, the low oxygen concentration in the charge due to the higher level of gaseous fuel inducted reduced NOx formation even further. Nonetheless, it was shown that too high gaseous fuel concentration at high engine loads led to an increase in the rate of energy released and consequently increased the NOx formation due to higher in-cylinder maximum temperature (Abd-Alla et al., 2000 ).

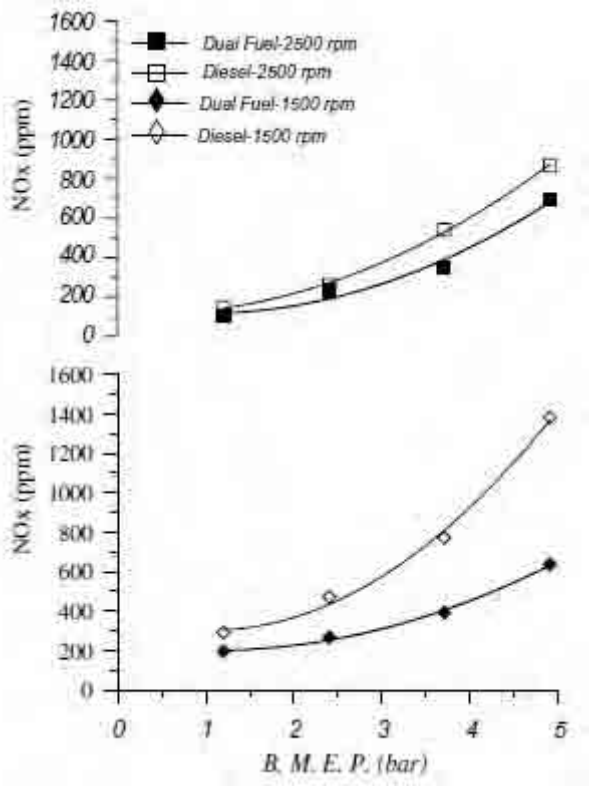


Figure 2.4: Variation of NOx emissions under diesel and pilot ignited dual fuel operation versus load at 1500 and 2500 rpm engine speed (Papagiannakis and Hountalas, 2004).

**Particulate Matters (PM)** emissions are formed from unburned hydrocarbon fuel which nucleates from the vapour phase to a solid phase in fuel-rich regions and at elevated temperatures. After which, hydrocarbons or other available molecules may condense on, or be absorbed by the particulate, depending on the surrounding conditions (Tree and Svensson, 2007). For normal diesel operation, high PM emissions are observed at high engine loads and it decreases with decreasing engine load. At high engine loads, the increasing amount of liquid diesel injected into the combustion chamber for the diffusion combustion process and the corresponding increase in total equivalence ratio promotes soot formation. Nonetheless, significant amount of reduction in PM emissions are found in dual fuel operations, with up to 70% reduction being reported (Mustafi and Raine, 2008). As the majority of PM is formed from liquid diesel fuel, the reduction in liquid diesel fuel due to the gaseous fuel substitution

simply reduces PM emissions at the same time. In addition, most of the gaseous fuel type used (e.g. methane, propane and etc.) are lower members of the paraffin with no aromatic compounds and the high hydrogen/carbon ratio decreases the PM formation tendency (Tree and Svensson, 2007). At dual fuel high engine loads, the increased charge temperature contributes to the oxidation of PM, hence further reducing its emission.

**Unburned Hydrocarbons (UHC)** emissions are in essence partially burned hydrocarbon fuels found in the engine exhaust. For normal diesel operation, UHC exists only in small quantities and does not have significant effect on overall diesel emissions. Despite that, UHC emissions are considerably higher in dual fuel operation, especially at low engine loads as shown in Figure 2.5. The formation of UHC emissions are influenced by the quality of engine combustion process. At low engine load, the lower charge temperature and excess air/fuel ratio (AFR, $\lambda$) caused the suppression of turbulent flame propagation from ignition regions of pilot, allowing small quantities of gaseous fuel to escape the combustion process (Liu and Karim, 1997). In addition, the higher ignition delay for dual fuel operation also caused an increase in UHC emissions (Karim, 2003).

It was shown that an effective approach to decrease UHC emissions at low engine load would be to increase the quantity of pilot diesel injected and to decrease the gaseous fuel inducted. By doing so, the pilot ignition centre could be increased, hence more gaseous fuel that is entrained by or in the immediate vicinity of the larger ignition centre will burn (Abd Alla et al., 2000). Apart from the combustion process, there are contributions from crevice volumes whereby some gaseous fuel-air mixture is forced into during the compression process and remained unburned. In addition, valve overlapping between intake and exhaust stroke for scavenging purposes could also increase UHC emissions as unburned gaseous fuel-air mixture is blown out of the cylinder (Weaver and Turner, 1994).

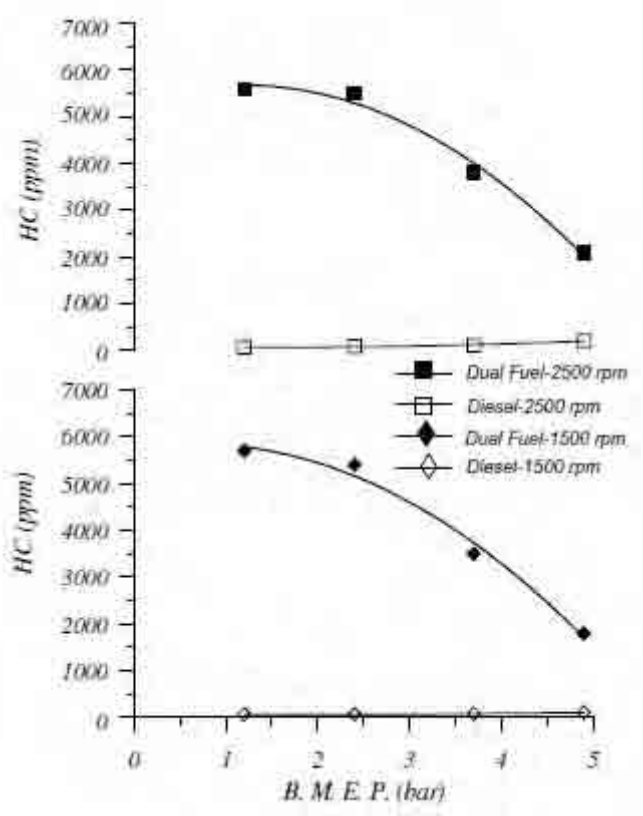


Figure 2.5: UHC emissions under normal diesel operation and duel fuel operation versus load at 1500 and 2500 rpm engine speed (Papagiannakis and Hountalas, 2004).

**Carbon Monoxide (CO)** emissions are a result of incomplete combustion of fuel due to insufficient oxygen concentration. Therefore, its formation is controlled primarily by the total equivalence ratio (Heywood, 1988). Much of the CO produced is formed at the early stage of combustion process and most of it is oxidised further to $CO_2$, thus the low CO emissions level for normal diesel operation. In dual fuel operation, CO emissions are significantly higher (Papagiannakis and Hountalas, 2004) and its formation is thought to be resulted from the partial oxidation of gaseous fuel in regions within and adjacent to the burning pilot zone (Bittner and Aboujaoude, 1992). It was shown that at similar equivalence ratio test condition, increasing pilot quantity increases the size of the burning zone, hence resulting in higher CO emission for dual fuel operation (Karim, 2003).

The **UHC – CO Emissions Trend** was suggested by Badr et al. (1999) to summarize the relation between the two main emission constituents for dual fuel operation. At constant pilot quantity, the UHC-CO trend is affected by the total equivalence ratio and it can be represented as four different operating regions (Figure 2.6). For Region I, at extremely low equivalence ratio (i.e. low gaseous fuel admission), there was low level of CO formation produced mainly from the incomplete combustion of pilot diesel. However, due to the limiting combustion of surrounding gaseous fuel, UHC emissions are high in this region. In Region II, the consumption of gaseous fuel (i.e. decreasing UHC) and formation of CO continues with increasing amount of inducted gaseous fuel. The start of Region III signifies the beginning of flame initiation through the gaseous fuel surrounding the pilot zone. It can be seen from Figure 2.6 that further increasing the equivalence ratio into Region III allows some limited flame propagation through the gaseous fuel, hence decreasing both UHC and CO emissions simultaneously. In Region IV, the flame spread limit (FSL) is reached and flame propagation now extends to all parts of gaseous fuel in the combustion chamber, producing high rates of heat release with the smallest value of UHC and CO emissions. In general, it can be said that limiting values of equivalence ratio at $\Phi_1$, $\Phi_2$ and $\Phi_3$ (Figure 2.6) may signify the start of local partial oxidation, flame initiation and the successful spread of flame propagation through the gaseous fuel-air mixture respectively.

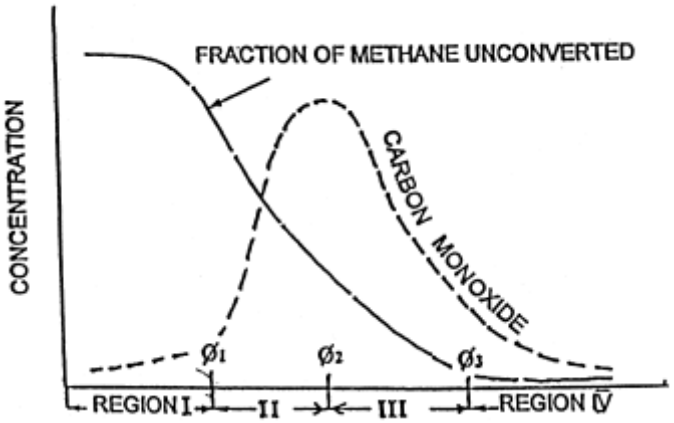


Figure 2.6: Schematic variations of UHC and CO emissions with total equivalence ratio, showing various operating regions (Badr et al., 1999).

### 2.2.4 Biogas – Diesel Dual Fuel Operation

The engine performance and emission characteristics for gas-diesel dual fuel operations are largely dependent on the types of gaseous fuel used, as shown earlier in Figure 2.3. In the past, compressed natural gas (CNG, which comprised mainly of methane) and liquified propane gas (LPG) have shown greatest potential to be applied as gaseous fuels for dual fuel operation. Due to their high octane rating; those fuels are not susceptible to the knocking phenomenon which is common in CI engines with high compression ratio. Table 2.1 shows the comparison of fuel properties between various alternative gaseous fuels suitable for dual fuel operation and liquid diesel fuel. Nevertheless, both CNG and LPG are categorized as non-renewable sources of energy; hence their usage contributes to the emission of GHG into the atmosphere.

Biogas, as mentioned earlier in Chapter 1 is a type of clean and renewable gaseous fuel derived from the anaerobic digestion of organic mass. Table 2.2 shows the various properties of biogas. In biogas, the main constituent contributing to the fuel heating value is methane and therefore the performance of biogas usage in dual fuel operation is largely

determined by the amount of diluents (mainly carbon dioxide) present in it (Bedoya et al., 2009). Tests were carried out by Bari (1996) to investigate the effect of carbon dioxide on the biogas-diesel dual fuel engine performance by introducing pure carbon dioxide at various substitution levels together with methane gas at a constant engine speed and load. It was shown that when the percentage induction of carbon dioxide increases, the biogas supply needed to provide the same engine power output also increases, hence resulting in a higher brake specific fuel consumption (BSFC).

Table 2.1: Various properties for alternative gaseous fuels and diesel (Owen and Coley, 1995).

| **Fuels** | **Hydrogen** | **CNG** | **LPG** | **Diesel** |
|---|---|---|---|---|
| Chemical Formula | $H_2$ | $CH_4$ | $C_3H_8$ | $\sim C_{15}H_{29.13}$ |
| Molecular Weight | 2.016 | ~17.06 | 44 | ~170 |
| Density @ 15°C (kg/m$^3$) | 0.082 | 0.46 | 0.5 | ~835 |
| LHV (MJ/kg) | 120.0 | 50.01 | 92 | 42.9 |
| Stoich Air/Fuel | 34.3 | 17.19 | 15.6 | 14.5 |
| (RON+MON)/2 | - | 124.5 | 102.5 | ~0 |
| CN | - | - | - | 52-60 |
| Flammability (Upper) | 75.0 | 15 | 9.5 | 7.5 |
| Limits (%vol.) (Lower) | 4.0 | 5 | 2.1 | 0.6 |

Henham and Makkar (1998) also reported that the overall efficiency of the dual fuel operation decreases with the addition of carbon dioxide and this effect is even more pronounced at high engine speed. Duc and Wattanavichien (2007) studied the effect of using biogas produced from a pig farm in an indirect injection (IDI) diesel engine at different engine load conditions and showed that at high engine load, the engine thermal efficiency for the biogas-diesel dual fuel system is comparable to that of normal diesel operation. Nonetheless, the engine thermal efficiency deteriorates greatly at low and medium engine load when biogas is used.

Table 2.2: Properties of biogas (Yoon and Lee, 2011).

| Properties | Data |
|---|---|
| Methane (%, by vol.) | 30-73 |
| Carbon dioxide (%, by vol.) | 20-40 |
| Nitrogen (%, by vol.) | 5-40 |
| Hydrogen (%, by vol.) | 1-3 |
| Oxygen (%, by vol.) | 0-5 |
| Boiling point (°C) | (-) 126-162 |
| Density (kg/m$^3$) | 0.65-0.91 |
| Octane number | 130 |
| Auto-ignition temperature (°C) | 632-813 |
| A/F ratio (by vol.) | 17.2 |
| Lower heating value (MJ/kg) | 26.17 |

To understand the emissions characteristics resulted from biogas-diesel operation, Mustafi and Raine (2008) investigated the effect of using three biogas composition, (i) BG1: 80% methane, 20% carbon dioxide (ii) BG2: 70% methane, 30% carbon dioxide and (iii) BG3: 60% methane, 40% carbon dioxide on the emissions of dual fuel operation compared to that of using pure methane at high engine load conditions. It was concluded that while increasing carbon dioxide present in biogas does not affect the formation of CO emissions, there was a minor increase in the emission of UHC when biogas is used and the emission is increased with increasing amount of carbon dioxide present. On the contrary, as shown in Figure 2.7, both NOx and PM emissions were reduced tremendously when biogas is used. The experiment conducted by Yoon and Lee (2011) also showed that at low engine load, both NOx and soot emissions decreased with the use of biogas compared to normal diesel operation. Nonetheless, they also concluded that there is a significant increase in CO and UHC emissions at low engine loads for biogas-diesel dual fuel operation.

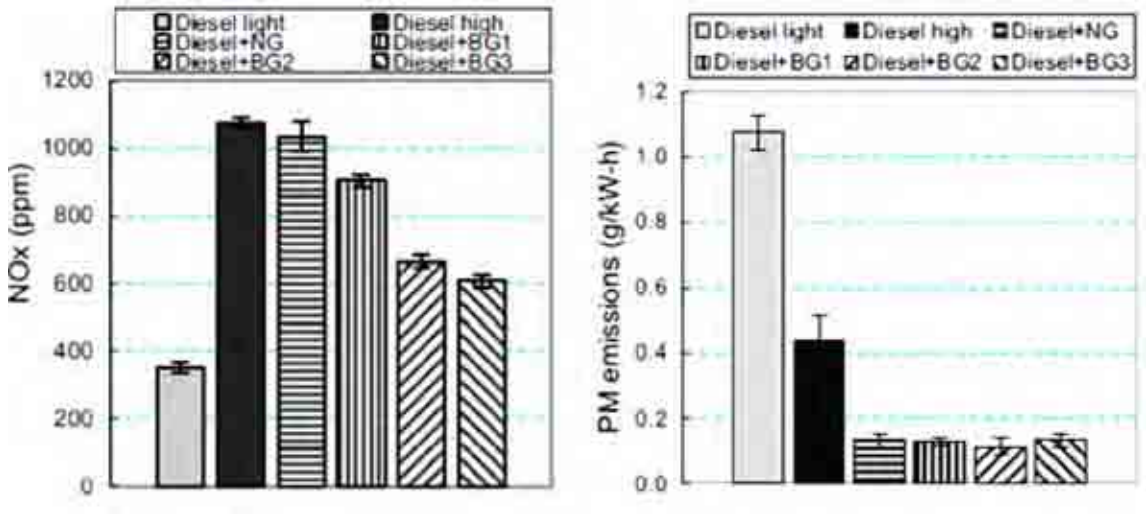


Figure 2.7: NOx concentration and PM mass emission for diesel and dual fuelling (engine speed: 1750 rpm; torque: 3 Nm (light load) and 28 Nm for others), (Mustafi and Raine, 2008).

It was explained that the reduced engine power output in biogas-diesel dual fuel operation is mainly due to the higher biogas induction (due to the low energy content) compared to other gaseous fuels such as CNG, which resulted in a higher fresh air substitution level (Henham and Makkar, 1998). Hence, there is a drop in the engine volumetric efficiency and less power is being generated. In addition, it was also shown that the presence of diluents (carbon dioxide) in biogas further increases the heat capacity of the cylinder charge per unit mass of fuel, reducing the flame temperature and inhibiting flame propagation at the same time (Abd-Alla, 2002). The reduction in charge temperature contributes to the prolonged ignition delay for biogas-diesel dual fuel operation, which in turn is beneficial in reducing the NOx and PM emissions simultaneously. A thorough investigation was done by Kobayashi et al (2007) to understand the characteristics of methane-air mixture turbulent premixed flames diluted with carbon dioxide. The study concluded that with the presence of carbon dioxide, the local turbulent burning velocity was reduced and the combustion oscillation of the premixed gaseous fuel-air mixture was restrained, hence resulting in less gaseous fuel being burnt.

### 2.2.5 Hydrogen for Enhancing Biogas – Diesel Dual Fuel Operation

It was clear that even though the use of biogas for the gas-diesel dual fuel operation provides better NOx and PM emissions, it resulted in lower engine thermal efficiency together with higher CO and UHC emissions at low and medium engine load operating conditions. Bedoya et al. (2009) suggested that gaseous fuels with high burning rates could be used to improve the combustion process of the biogas-diesel dual fuel engine, especially at part load operations. Hydrogen, as shown in Table 2.1 has very high mass lower heating values and its wide flammability limits allow a wide range of engine power output at various mixture equivalence ratios, rendering it superior to other gaseous fuels. It was shown that the minimum ignition energy of hydrogen-air mixture is an order magnitude lower than that of methane-air mixture at atmospheric condition (Ono et al., 2007).

An experimental study was done by Roy et al. (2011) to investigate the effect of adding hydrogen at various substitution levels into low quality producer gas for combustion at constant pilot injection pressure and quantity. The result shows that the average values of maximum engine thermal efficiency increases with increasing hydrogen substitution level and concluded that it was contributed by the higher ratio of specific heats and flame speed of hydrogen. In addition, lower UHC and CO emissions were reported with increased hydrogen substitution level. Nonetheless, it was shown that there was an increase in NOx emissions when more hydrogen was being introduced into the dual fuel system. Gomes Antunes et al. (2009), on the other hand reported an approximately 20% drop in NOx levels with the use of direct injected hydrogen into a diesel engine, stating that the presence of hydrogen reduces high-temperature zones inside the combustion chamber, which acts as the main factor for NOx formation. A detailed experimental study on the combustion of natural gas and hydrogen mixture by Tinaut et al (2011) also reported that the addition of hydrogen increases burning

velocity of the gaseous fuel-air mixture, which in effect reduces the overall combustion duration.

## 2.3 Fuel Reforming

### 2.3.1 Hydrogen Production, Storage and Applications

Despite the superior properties of hydrogen compared to other conventional gaseous fuels, serious technical and economical challenges are to be overcome in utilizing hydrogen as an energy carrier. This is due to the fact despite being the lightest and most abundant element on earth, hydrogen can only be found in compound forms such as water ($H_2O$) and hydrocarbon (HCs) fuels. Therefore, in order to make use of hydrogen as an energy carrier for transportation applications, it must first be generated and subsequently stored on-board a vehicle, making it energetically inefficient. In current technology, hydrogen fuels are produced either from the reforming and gasification processes with hydrocarbons as feedstock or through the electrolysis process using water.

There are in general three main ways for storing hydrogen on-board, either through physical or material-based storage methods. The simplest method would be to store hydrogen as a compressed gas. With this approach, hydrogen is being compressed to approximately 350-700 bar pressure and stored in either metal-lined or polymer-lined pressurized vessels. Nonetheless, due to the inherent disadvantage of being a low density gas, this option requires storage tanks with a large volume capable of storing enough hydrogen to allow for a driving range of more than 500 km (DOE, 2009), making it impractical for automotive applications. The second approach is to store hydrogen in the form of cryogenic liquid. Despite the fact that hydrogen stored in this manner has a much higher volumetric capacity than compressed form, the high energy inefficiency incurred for hydrogen liquefaction and the unavoidable loss of

hydrogen during extended parking and refilling substantially reduces the overall energy efficiency of a vehicle. It was suggested that these problems could potentially be overcome by using insulated pressure vessels in the cryo-compressed hydrogen storage system (Ahluwalia et al., 2011). The third method is the use of metal hydrides systems. Metal hydrides such as aluminium hydride ($AlH_3$) have the potential for reversible hydrogen storage and release at the optimum pressure-temperature operating window. Nonetheless, the low gravimetric capacity, the slow uptake and release kinetics and the high cost associated with the metal hydride system makes it unsuitable for vehicular applications (DOE, 2008).

Apart from applications in IC engines as mentioned earlier, hydrogen fuel also acts as the main fuel source for fuel cell applications in power generations and transport applications (Andújar and Segura, 2009). Today, over 2500 fuel cell plants have been installed for stationary power generation purposes and portable fuel cells are also available for providing electricity in rural areas or for military purposes. In terms of transportation purposes, apart from providing the usual mechanical power output required by a vehicle, it was also proposed that fuel cell could be used secondarily as auxiliary power units (APU) to supply electricity in long haul trucks. Nonetheless, present applications related to fuel cells in the transportation sector are still considered to be in the research, development and testing stage.

### 2.3.2 Main Fuel Reforming Reactions

Fuel reforming processes using hydrocarbon fuels for hydrogen production can be done either catalytically or non-catalytically. A catalytic reformer normally consists of precious metals such as platinum (Pt), rhodium (Rh) and nickel (Ni) and the key variables in choosing a suitable catalyst includes the nature of precious metals, precious metal loading, and composition of the catalyst support (Peucheret et al., 2006). The presence of transition

metals is usually being utilized as an active catalyst to perform reforming processes (Frusteri et al., 2004). For instance, Rh has been known for high reactivity and stability during the dry reforming process (Richardson et al., 2003) while Pt is active in both the water gas shift reactions and oxidative reforming processes (Horn et al., 2007). In addition, different precious metals are also reactive towards different types of fuels, e.g., for the steam reforming process of different hydrocarbon fuels, the activity of Rh is $C_2H_6$>$C_2H_4$>$CH_4$ while that of Pt is $CH_4$>$C_2H_6$/$C_2H_4$ (Graf et al., 2007). A combination of different metals in a bimetallic catalyst could be used to provide higher catalytic stability and to reduce cost.

A catalyst works by decreasing the activation energy of the various reactions taking place during the reforming processes, hence providing a catalytic reformer with the advantage of having lower operating temperatures compared to a non-catalytic reformer. On top of that, lower temperatures also simplified materials selection for construction of the reforming reactor to a certain degree. Nonetheless, there are potential problems associated with catalytic reforming, such as the occurrence of sulphur poisoning, carbon masking of catalytic sites and thermal damage to the catalyst. In this section, methane (the main constituent of biogas) is used as the main hydrocarbon fuel for the explanation of each fuel reforming reactions.

**Steam Reforming Reaction (SRR)** is the most common method for large scale hydrogen production commercially. This process is extremely reactive with high hydrogen yield (Eq. 2.1). But since it is endothermic in nature, high heat energy input is required to drive this process which also resulted in substantial energy loss. The production of hydrogen through SRR using methane is typically carried out at temperatures ranging from 700 to 900 °C and at pressures ranging from 20 to 40 bar (Ryi et al., 2009). In industrial applications, these energy demand is supplied by inter stage heaters or external burners.

$$CH_4 + H_2O \rightarrow CO + 3H_2 \qquad (\Delta Hr = +226.81\ kJ/mol) \qquad (2.1)$$

**Water-Gas Shift Reactions (WGSR)** can also take place following the SRR reforming reaction in a two stage reforming reactor model as shown in Figure 2.8. Downstream the SRR reforming reaction, the CO present reacted with the excess steam to form the secondary WGSR reaction, producing additional hydrogen together with carbon dioxide (Eq. 2.2) at reactor temperatures ranging between 550 to 700 °C (Tsolakis and Golunski, 2006).

$$CO + H_2O \rightarrow CO_2 + H_2 \qquad (\Delta Hr = -33.86\ kJ/mol) \qquad (2.2)$$

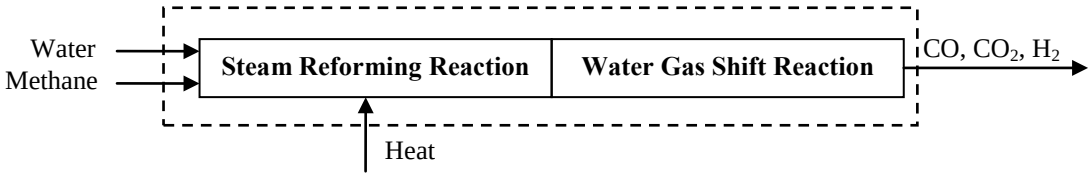


Figure 2.8: Thermodynamics model for steam reforming and water gas shift reactions.

**Partial Oxidation (POX)** is an exothermic reforming process whereby methane is partially oxidised in a limited supply of oxygen to produce hydrogen and carbon monoxide (Eq. 2.3). POX is a self-sustaining reaction with intrinsically faster transient response than other endothermic processes; hence making it favourable to be used in transient operations (Tomishige et al., 2001). Nonetheless, due to the exothermic nature of POX process, the produced hydrogen enriched gaseous fuel has a lower calorific value than that of methane feed gas (Lee, 2001). Moreover, regulation on the air to fuel mass ratio is crucial to avoid the occurrence of complete oxidation which is undesirable in terms of hydrogen production, as shown in Eq. 2.4.

$$CH_4 + 0.5O_2 \rightarrow CO + 2H_2 \quad (\Delta Hr = -22.63 \text{ kJ/mol}) \tag{2.3}$$

$$CH_4 + 2O_2 \rightarrow CO_2 + 2H_2O \quad (\Delta Hr = -891.64 \text{ kJ/mol}) \tag{2.4}$$

**Dry Reforming Reaction (DRR)** is another highly endothermic reaction that occurs at high temperature range (>800 °C). This process is of particular interest for this thesis since both the main components of biogas (i.e. methane and carbon dioxide) are consumed to produce hydrogen, as shown in Eq. 2.5. However, the DRR is a slow reacting process and it is affected by the contact time between the reactor gas feed and the catalyst active sites (Jing and Zheng, 2006).

$$CH_4 + CO_2 \rightarrow 2CO + 2H_2 \quad (\Delta Hr = +260.62 \text{ kJ/mol}) \tag{2.5}$$

**Autothermal Reforming (ATR)** combines both the POX and SRR processes in a single reforming reactor. As shown in Figure 2.9, methane, water and oxygen are introduced simultaneously into the reactor to produce hydrogen enriched product gas. In this configuration, the fast reacting POX process is initiated at the front of the reactor through complete combustion of part of the methane fuel, extending to the middle section. The SRR process then utilizes part of the heat generated by the exothermic oxidative processes, leading to lowered catalyst temperature (Ding and Chan, 2008). The general form of the reaction for ATR can be described as in Eq. 2.6. In addition, WGSR could occur downstream the reactor if there is excess steam present and the temperature requirement is reached, further improving hydrogen production. Depending on the extend of each individual reforming reactions required (i.e. either exothermic or endothermic), appropriate selection of metals and supports for catalyst design are crucial in achieving the desired product selectivity and to improve reforming efficiency (Ahmed and Krumpelt, 2001).

$$CH_4 + xO_2 + (1-2x)H_2O \rightarrow CO + (3-2x)H_2 \tag{2.6}$$

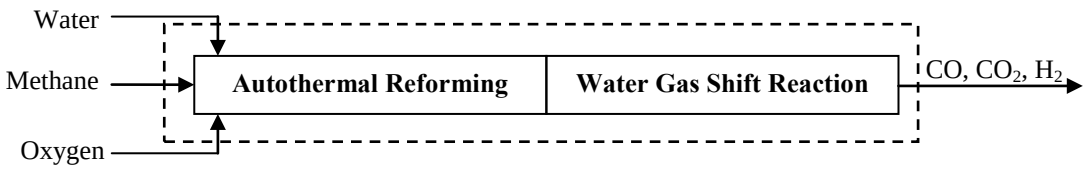


Figure 2.9: Thermodynamics model for autothermal reforming reaction.

### 2.3.3 Exhaust Gas Fuel Reforming

For on-demand hydrogen production in automotive applications, the reformer reactor hardware must satisfy the criteria of being both compact and lightweight to avoid imposing weight penalty on a vehicle. In addition, the hydrogen production system should be self-sustaining, without the requirement for external energy input and capable of utilizing various hydrocarbon fuels for the reforming process.

A promising technique would be the use of exhaust gas fuel reforming process. The reforming reaction profiles in exhaust gas fuel reforming are practically similar to that of ATR, involving both SRR and POX as the main reforming reactions. Since the diesel operation is always lean, there exists a considerable amount of oxygen and steam in the engine exhaust. While a separate source of water and oxygen is needed for the ATR process, exhaust gas fuel reforming utilizes both the steam and oxygen which is readily available in the engine exhaust for the reforming reactions. Therefore, the extent of each reforming reactions (i.e. either exothermic or endothermic) is dependable on the engine operating conditions which in turn affects the diesel engine exhaust compositions. The reactions for both the combustion of a typical diesel fuel and the exhaust gas fuel reforming of biogas can be described as follow (Tsolakis and Megaritis, 2004):

$$C_nH_{1.88n} + 1.47n\lambda(O_2 + 79/21N_2) \rightarrow nCO_2 + 0.94nH_2O + 1.47n(\lambda\text{-}1)O_2 + 1.47n\lambda(79/21)N_2 \quad (2.7)$$

$$[aCH_4 + bCO_2] + x[nCO_2 + 0.94nH_2O + 1.47n(\lambda\text{-}1)O_2 + 1.47n\lambda(79/21)N_2] \rightarrow yCO + zH_2 + 1.47nx\lambda(79/21)N_2 \quad (2.8)$$

where n is the number of carbons in the diesel fuel molecule, both a and b are the amount of methane and carbon dioxide compositions of biogas and x represents the volume of exhaust gas required to achieve stoichiometric reaction with one unit volume of biogas. y and x are the number of kmols of carbon dioxide and hydrogen produced respectively.

Experimental investigations on the exhaust gas fuel reforming process of diesel fuel were done by Tsolakis et al. (2004). It was shown that even at low catalyst bed temperature of 290 °C; up to 16% hydrogen content of the reactor gas product was achieved through the exhaust reforming process with diesel engine exhaust as reactor feed gas. Moreover, water addition into the reforming reactor up to a certain level reduced power losses in the reforming process and enhanced the hydrogen production by SRR process, with up to 15% more hydrogen produced compared to that without water addition. Despite the beneficial effects, further increasing the water addition only resulted in increased WGSR process and no significant addition in hydrogen production by the SRR process was observed (Tsolakis and Megaritis, 2004).

### 2.3.4 Engine – Reactor System

The schematic diagram of the engine – reactor system is shown in Figure 2.10. In the catalytic fuel reformer, the hydrocarbon fuel (i.e. biogas feed in this thesis) gets in direct contact with hot engine exhaust gas to generate hydrogen and carbon monoxide (syngas) as described in Eq. 2.8. Nonetheless, the unused engine exhaust gas and unreacted biogas in the catalytic fuel reformer would mix with the produced syngas, generating the reforming reactor

product gaseous fuel termed 'reformate'. The potential heat energy required in the catalytic fuel reformer is met by combusting part of the biogas feed and also through heat exchanging process with the surrounding surplus exhaust gas, hence achieving engine waste heat energy recovery. Reformate produced is then fed back into the engine by mixing it with fresh intake charge, supplying reformate gaseous fuel into the engine through reformed exhaust gas recirculation system (REGR). This operating concept is called the engine – reactor system, with the formation of an REGR loop as shown in Figure 2.10. Unlike conventional exhaust gas recirculation (EGR) systems whereby the only adjustable configurations are the flow rate and the temperature of the recycled gas (i.e. either hot or cooled EGR), the composition of REGR could be altered by controlling the exhaust gas intake and fuel feed into the catalytic reformer (Tsolakis and Golunski, 2006).

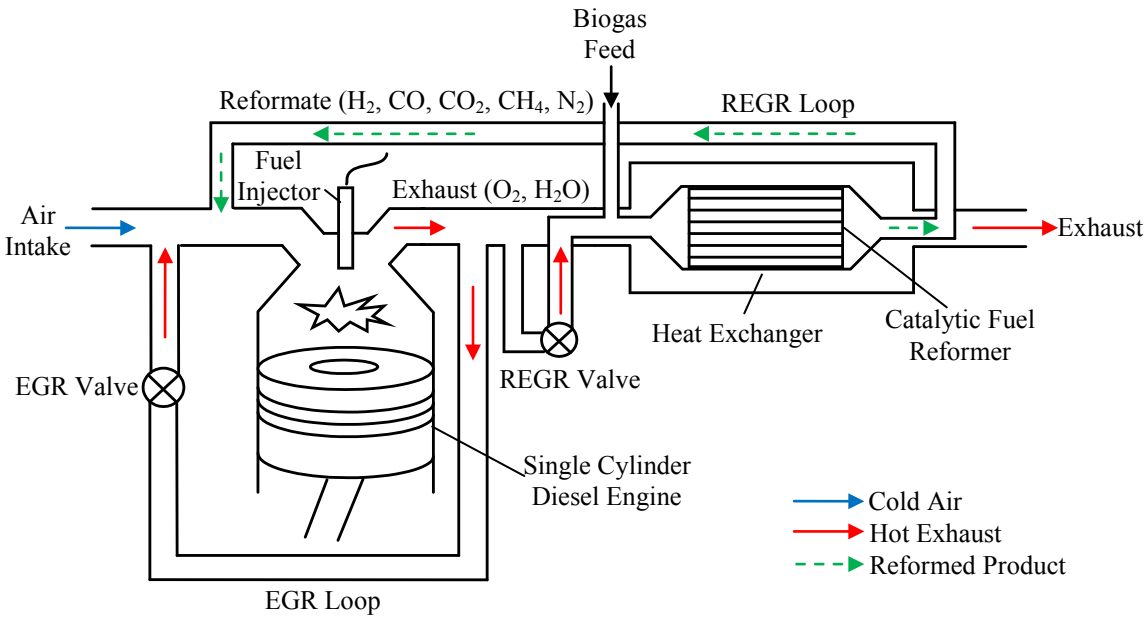


Figure 2.10: Schematic for exhaust gas fuel reforming system using biogas (Tsolakis, 2004).

Based on Figure 2.10, it can be seen that instead of feeding the hydrogen enriched reformate gas back into the engine intake, alternatively it could also be routed to provide reformate for various engine after-treatment devices. Despite having a positive impact on the

combustion process of a gas-diesel dual fuel engine as discussed earlier, the use of hydrogen has also shown beneficial effects in after-treatment systems. For instance, adding hydrogen into the engine exhaust stream improves the hydrocarbon selective catalytic reduction (HC-SCR) catalyst performance in reducing NOx under lean diesel condition, especially at lower temperature region (Abu-Jrai and Tsolakis, 2007). Nonetheless, a penalty is imposed on the overall engine fuel economy as more hydrocarbon fuels would be needed to produce the required hydrogen enriched gas in the engine – reactor system for after-treatment purposes.

## 2.4 Summary

Based on the literature review presented in this chapter, it is clear there are a lot of research work investigating the potential of using gas-diesel dual fuel operation for better CI engine emissions and energy security purposes. Even though both NOx and PM are substantially reduced in dual fuel operations, the inevitable releases of both UHC and CO in the engine exhaust emissions and poor engine performance, especially at low engine load operating conditions is a concern.

Biogas, being clean and renewable has shown tremendous benefits to be used as an energy carrier. In addition, the digestate waste produced from the anaerobic digestion process could be recycled back into the carbon chain as fertilizers for farming purposes, potentially making production and usage of biogas carbon neutral. Nonetheless, due to the high amount of diluents gas (i.e. carbon dioxide) present, the biogas-diesel dual fuel operation suffers from low engine thermal efficiency and high UHC emissions at low and medium load engine operating conditions.

Hydrogen is a highly efficient and low polluting gaseous fuel suitable for power generation, heating and transportation purposes. The introduction of hydrogen into the biogas-diesel dual fuel operation is able to improve the engine thermal efficiency and exhaust emissions concurrently. Nonetheless, utilizing pure hydrogen for vehicular applications still proves to be impractical with the aforementioned problems related to the production and storage of hydrogen. In the following chapters of this thesis, the catalytic reforming of biogas to produce hydrogen enriched syngas and the effect of introducing the engine – reactor system on a CI engine operation will be presented.

# CHAPTER 3

# EXPERIMENTAL FACILITIES

## 3.1 Test Engine and Engine Instrumentation

This chapter mainly describes the experimental facilities used for this research. The test setup and data or sample acquisitions performed in this thesis for both the engine experimental tests and fuel reforming tests are described. Typical testing data sheets used for monitoring results during the tests are presented in the Appendix B.

### 3.1.1 Test Bench Engine

The test engine used in this research work is the Lister Petter TR1 engine, which is a naturally aspirated and air-cooled single-cylinder direct injected diesel engine as shown in Figure 3.1. An externally cooled EGR system was also implemented in this engine. For fuel injection parameters, the fuel injector has an opening pressure of 180 bar and the injection timing is set by the manufacturer at 22 crank angle degree (CAD) before TDC. The detailed engine specifications for TR1 are given in Table 3.1.

Table 3.1: Test engine specifications.

| Engine Specification | Data |
|---|---|
| Number of cylinders | 1 |
| Bore/stroke | 98.4 mm/101.6 mm |
| Displacement volume | 773 $cm^3$ |
| Connecting rod length | 165 mm |
| Compression ratio | 15.5:1 |
| Related power (kW) | 8.6@ 2500 rpm |
| Peak torque (Nm) | 39.2@ 1800 rpm |
| Injection system | Three holes pump-line-nozzle |

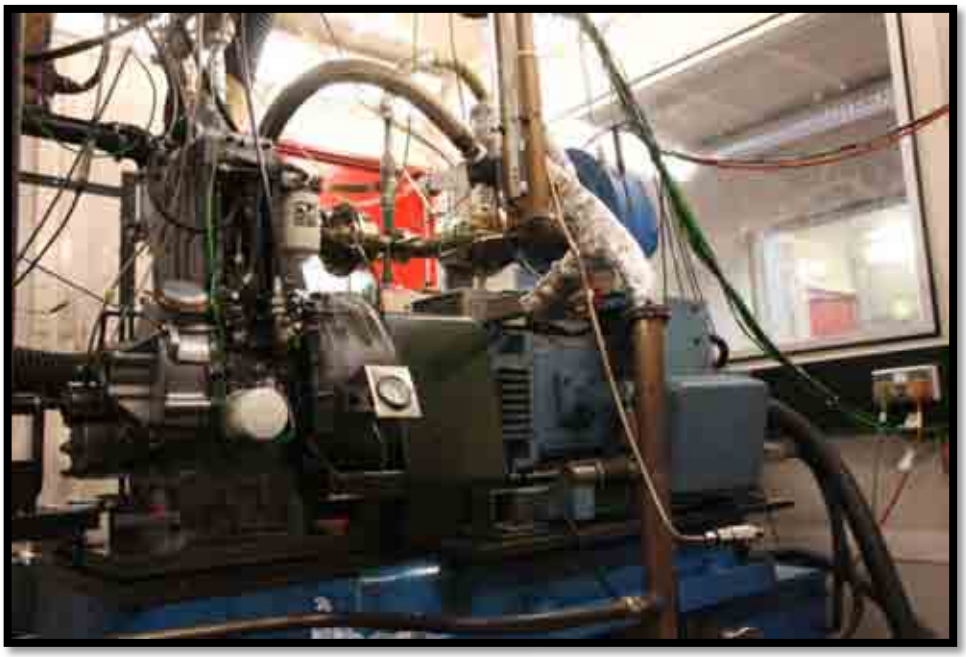

Figure 3.1: Lister Petter TRI Test Engine.

### 3.1.2 Engine Instrumentation

The main part of the single cylinder test engine instrumentation is the thyristor-type air-cooled Thrige Titan DC electric dynamometer which was used to load and motor the engine. The external cooled EGR system was controlled using a valve and the EGR level was determined volumetrically as a percentage reduction in the volumetric flow rate of air at a certain engine speed and load. The in-cylinder pressure traces were recorded using a Kistler 6125B pressure transducer mounted at the cylinder head and connected to a National Instruments data acquisition board via a Kistler 5011 charge amplifier. The corresponding crankshaft positions were measured using a digital shaft encoder. In-house developed LabVIEW based software is then used to obtain the pressure data and the combustion analysis which includes peak engine cylinder pressure, values of indicated mean effective pressure (IMEP), percentage coefficient of variation (COV) of IMEP, indicated power and heat release. Multiple k-type thermocouples were used at various points on the test engine to measure the

oil, inlet manifold and exhaust temperatures and the data is recorded for use in combustion analysis.

## 3.2 Reforming Tests

### 3.2.1 Reforming Catalyst

The reforming catalyst used in this research is a monolith catalyst developed by Johnson Matthey. The reforming monolith catalyst consists of a high cell-density cordierite substrate (900 cells per square inch) which has been coated with 2%Pt-1%Rh (by mass) dispersed on a support containing 30% (by mass) ceria-zirconia (3:1 mole ratio) on 70% γ-alumina. The reforming catalysts used in this research were cored from large monolith substrates into the desired diameter and length for the reforming reactor. Reforming catalyst with aspect ratios (AR = length/diameter) of 3.75 and 3 were being used in this research. Figure 3.2 shows a fresh monolith catalyst and a central hole is to be drilled through the catalyst, representing the available movement of the thermocouple for temperature monitoring purposes along the monolith catalyst.

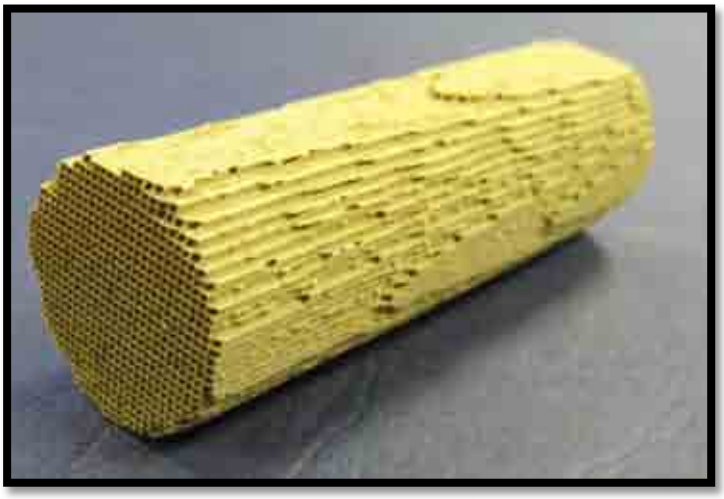

Figure 3.2: Monolith type reforming catalyst with 25 mm in diameter and 75 mm in length.

### 3.2.2 Mini Reactor Design

The mini reactor used in this study is a two phase system, involving gas phase (air, engine exhaust gas and biogas) and solid phase (monolith catalyst) as shown in Figure 3.3. The reactor was placed in a tubular furnace in which the reactor temperature was controlled by means of a temperature controller. The desired amount of air or exhaust gas is fed through a heated line to avoid any condensation and into a 1/4" outer diameter (o.d.) stainless steel tube to the reactor. The volumetric flow rate of the air and exhaust gas was controlled using a glass tube flowmeter. Moreover, for exhaust gas fuel reforming experiments, the temperature of the exhaust gas entering the reactor was monitored using a K-type thermocouple and external heat was provided by the furnace as a means of maintaining the temperature level similar to that of actual engine exhaust.

Biogas from a pressurised bottle was supplied directly into the reactor and mixed with the air or exhaust gas using a union tee at a distance above the top of the catalyst bed (Figure 3.3). This allows sufficient time for the biogas and exhaust to mix well before getting in contact with the reforming catalyst. The volumetric flow rate of biogas entering the reactor is again controlled using a glass tube flowmeter. The position of the catalyst is maintained throughout the test by placing a hard spring coil underneath it. As mentioned earlier, another K-type thermocouple was used to record the temperature profile along the catalyst by inserting it inside a stainless steel tube (o.d. 3.175mm) fitted in the centre of the reactor. Downstream the reactor, the reforming reactor product gas was condensed and the water was removed using a water trap; allowing the dry based analysis of reforming reactor product gas.

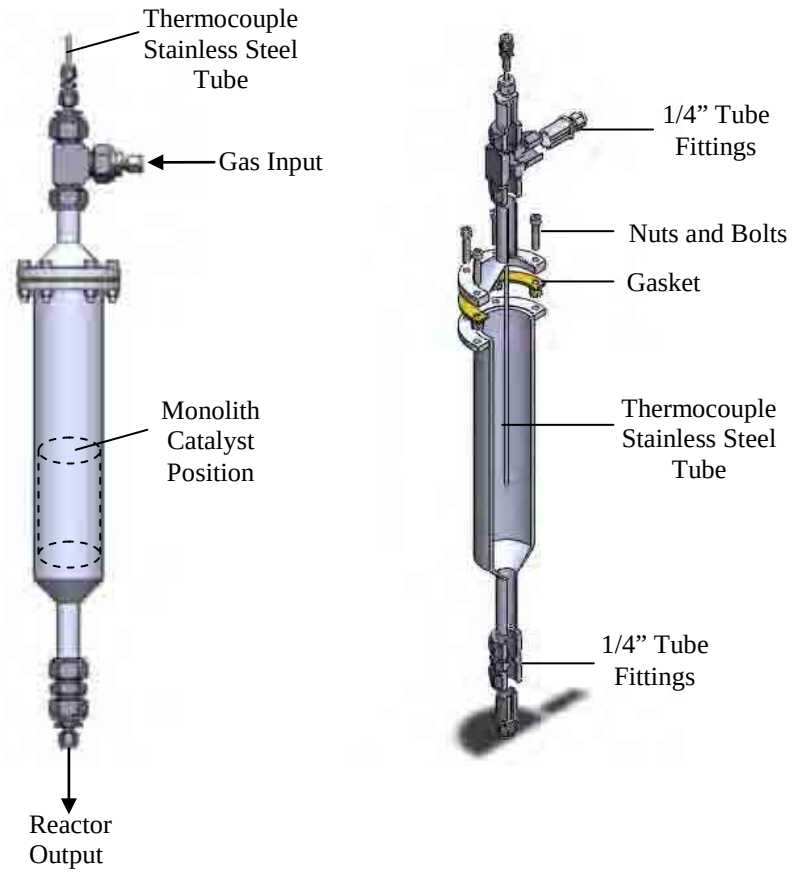


Figure 3.3: The front view (left) and isometric exploded cross-sectional view (right) of the CAD drawing for the reforming reactor.

### 3.2.3 Engine – Reactor System

For the engine – reactor system tests, reforming monolith catalysts with 25 mm in diameter and 75 mm in length (i.e. AR = 3) were situated inside the reforming reactor as shown in Figure 3.4. The reforming reactor is then placed in the same tubular furnace and the temperature was again controlled using a temperature controller to simulate the actual engine exhaust temperature. As biogas is combustible, a one way valve was used to prevent the back propagation of flame from the reactor into the pressurised bottle. The biogas flow rate into the reactor was controlled as described in the previous section. At the reactor outlet, the flow rate of the total product gas was controlled using a pump and another glass tube flowmeter. The total product gas is then being directed back into the engine intake and a portion of it was

directed to different analyzers using a two-way valve. The temperature profile along the monolith catalyst was measured as described in the previous section.

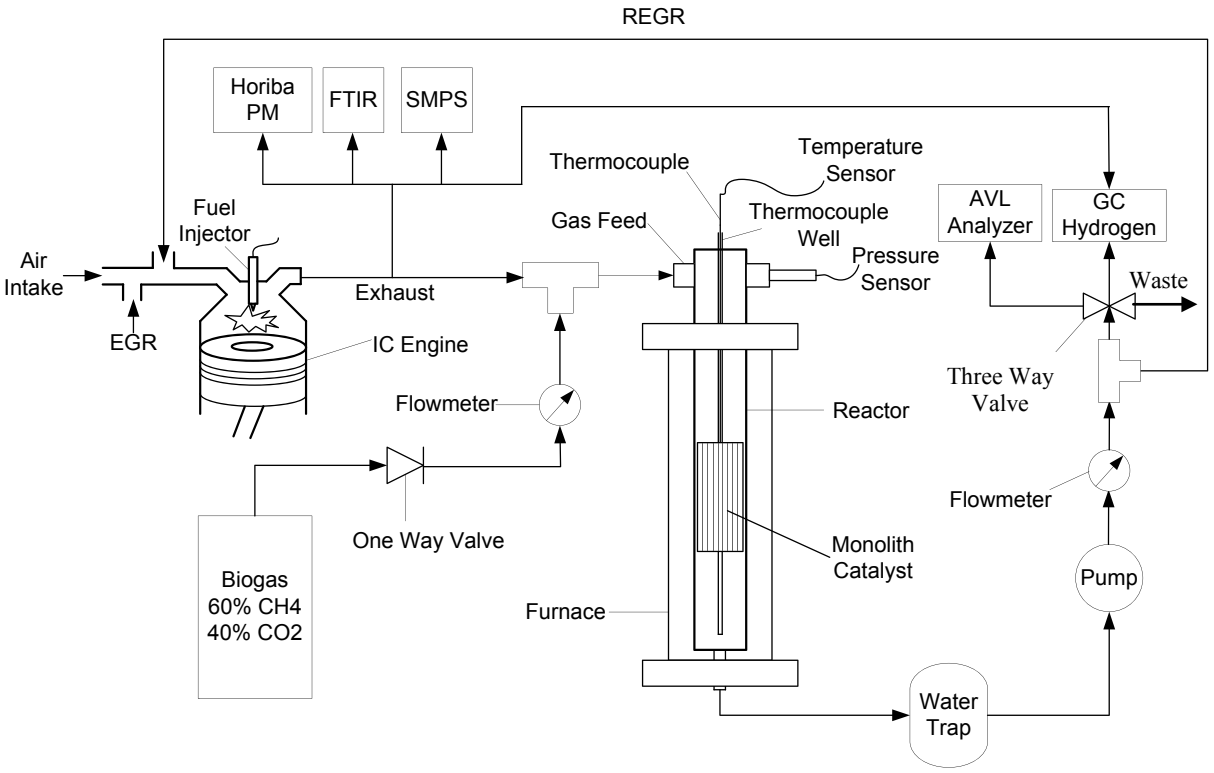


Figure 3.4: Schematic diagram for the engine – reactor closed loop system.

## 3.3 Fuels

The two main fuels used in this research are Ultra Low Sulphur Diesel (ULSD) and dry-based simulated biogas. The fuel properties of ULSD are shown in Table 3.2 and it is supplied by Shell Global Solutions UK. The simulated biogas used in this research work consists of 60 % volume methane and 40 % volume carbon dioxide supplied in a pressurised bottle by BOC.

Table 3.2: Fuel properties for ultra low sulphur diesel provided by Shell Global Solutions UK.

| **Fuel Analysis** | | **Method** |
|---|---|---|
| Cetane number | 53.9 | ASTM D613 |
| Density at 15°C (kg $m^{-3}$) | 827.1 | ASTM D4052 |
| Viscosity at 40°C (cSt) | 2.467 | ASTM D445 |
| 50% distillation (°C) | 264 | ASTM D86 |
| 90% distillation (°C) | 329 | ASTM D86 |
| LCV (MJ $kg^{-1}$) | 42.6 | |
| Sulphur (mg $kg^{-1}$) | 46 | ASTM D2622 |
| Carbon (wt. %) | 85.3 | |
| Hydrogen (wt. %) | 13.9 | |
| Oxygen (wt. %) | - | |
| Aromatics (wt. %) | 25.6 | |

## 3.4 Exhaust Gas Monitoring and Analysis

### 3.4.1 MKS Multigas and AVL Emissions Analyzers

The MKS MultiGas 2030 is a Fourier-transform infrared (FT-IR) based gas analyzer for measuring multiple gases. It was used to analyze the concentration of the engine exhaust emissions including: NOx (NO + $NO_2$), CO, $CO_2$, $H_2O$, UHC and $CH_4$. An AVL Digas 440 Analyzer was used for measuring UHC, CO and $CO_2$ by non-dispersive infrared (ND-IR) and $O_2$ in the reforming reactor product gas through an electrochemical method. The main reason for utilizing two analyzers was to avoid contamination between sampling of the engine exhaust gas and sampling of reforming product gas.

### 3.4.2 Gas Chromatograph

A Hewlett Packard (HP) gas chromatograph (GC), integrated with a thermal conductivity detector (TCD) and a HP integrator model 3395 was used to measure the hydrogen concentration. The oven for the GC is temperature controlled and it is installed with

two packed columns for hydrogen detection. Argon, which has a low thermal conductivity (0.024W/m/K) compared to that of hydrogen (0.223 W/m/K) was introduced into the GC as a carrier gas.

Certified span gas containing 30% hydrogen in nitrogen was used for GC calibration in this research work. To measure the amount of hydrogen present in the analyzing gas, the apparatus was first calibrated with the span gas to obtain a representative plot area for 300000 ppm hydrogen (i.e. 30 % by volume) plotted by the integrator. On sampling the analysis gas, another plot area corresponding to the hydrogen peak is obtained and the actual hydrogen concentration (ppm) is calculated by interpolation from the known certified span gas. For all tests, four measurements were taken and the calculated average value of hydrogen was used.

### 3.4.3 Horiba Mexa 1230PM

A Horiba Mexa 1230PM was used for continuous measurement of soot by a diffusion charging (DC) method and soluble organic fraction (SOF) by dual flame ionisation detection (FID) method. A heated dilution was implemented to prevent nucleation of particles and a dilution ratio of approximately 40 was set for the soot diluter.

### 3.4.4 Scanning Mobility Particle Sizer (SMPS)

A TSI SMPS 3080 Spectrometer was used to measure the total particle mass and number concentrations. The SMPS is comprised of an electrostatic classifier series 3080, a 3081 Differential Mobility Analyzer (DMA) and a model 3775 Condensation Particle Counter (CPC). The particle distributions were measured in the range of 10 – 500 nm with the exhaust gas dilution ratio preset to 200:1 at 150°C using a calibrated dilutor (Rotating Disk). Some of the other parameters used for the SMPS are as follow:

Table 3.3: Operating parameters for SMPS.

| **Parameter** | **Value** |
|---|---|
| Sheath Flow rate (L/min) | 5.00 |
| Aerosol Flow Rate (L/min) | 0.50 |
| Lower Size (nm) | 10.746 |
| Upper Size (nm) | 486.968 |
| D50 (nm) | 978.876 |
| Scan Time (sec) | 90 |

# CHAPTER 4

# BIOGAS UPGRADE TO SYNGAS VIA DRY AND OXIDATIVE REFORMING

## 4.1 Introduction

There are two main approaches to improve the usability of biogas for vehicular engine operations, (i) to reduce the amount of carbon dioxide and (ii) to upgrade it into fuels with higher energy content. As shown in Eq. 2.5, it is clear that the endothermic DRR reaction is capable of achieving both the above mentioned upgrading methods by producing high quality syngas (i.e. gas mixture of hydrogen and carbon monoxide) from the methane and carbon dioxide present in biogas.

The first objective of this chapter is to investigate the reaction profiles and reactor product distribution for the catalytic DRR reforming process of biogas. The basic process parameters affecting the reforming activity of DRR are the reformer operating temperatures, the gas hourly space velocity (GHSV) and the carbon dioxide-to-methane ($CO_2/CH_4$) molar ratio. Nonetheless, since the composition of biogas remains constant throughout this research work (i.e. 60% methane with 40% carbon dioxide), consequently the $CO_2/CH_4$ molar ratio is fixed for the work in this chapter as no external carbon dioxide is being fed into the reactor. A reforming catalyst with an aspect ratio of 3.75 was used. The temperatures implemented in these test range from 400 to 980 °C and this is used to represent the temperature ranges that occurred in the exhaust gas fuel reforming process. The GHSV is defined as the ratio of the reactor gas feed rate to the volume of the reforming catalyst bed as shown in Eq. 4.1 and it

was fixed at 16,500 $h^{-1}$ and 27,500 $h^{-1}$ respectively. Both the space velocities were chosen as the maximum process efficiency that can be achieved in this GHSV range and the values are also representative for on-board vehicle applications.

$$\mathrm{GHSV}\,(\mathrm{h}^{-1}) = \frac{1}{\mathrm{Residence\,Time}} = \frac{\mathrm{Feed\,Rate}\,(\mathrm{m}^3\,\mathrm{h}^{-1})}{\mathrm{Catalyst\,Bed\,Volume}\,(\mathrm{m}^3)} \tag{4.1}$$

According to the stoichiometric chemical equation for the DRR process of biogas (Eq. 4.2), the use of the selected biogas composition in the DRR process will produce approximately 11% volume of unreacted methane in the reforming reactor product gas distribution. Therefore, if biogas were to be used in exhaust gas fuel reforming processes under low exhaust temperatures, the excess methane or part of it could potentially be used in the exothermic POX to produce additional hydrogen (Eq. 2.3) or in complete oxidation (Eq. 2.4) to raise the reactor temperature and promote the DRR and SRR reactions. Therefore, this forms the second objective of this chapter; to study the effect of adding oxygen into the biogas DRR process. The simultaneous DRR and POX reforming reactions of biogas is represented by Eq. 4.3.

$$0.6CH_4 + 0.4CO_2 \rightarrow 0.8H_2 + 0.8CO + 0.2CH_4 \tag{4.2}$$

$$0.6CH_4 + 0.4CO_2 + 0.15O_2 \rightarrow 0.9CO + 1.2H_2 + 0.1CO_2 \tag{4.3}$$

Apart from temperatures and GHSVs, the main process parameter for the POX reforming reaction is the oxygen-to-methane molar ratio ($O_2/CH_4$). The $O_2/CH_4$ molar ratio represents the oxygen availability in the reforming reactor and three values (i.e. 0.16, 0.25, and 0.57) were selected for this test. The $O_2/CH_4$ molar ratio at 0.16 was chosen to study the effect of oxygen at low oxygen concentration while the ratio of 0.25 was used to investigate the effect of oxygen at stoichiometric condition for the simultaneous DRR and POX reaction

(Eq. 4.3). Lastly, the $O_2/CH_4$ molar ratio of 0.57 was selected to study the effect of oxygen at excess oxygen composition present in the reforming reactor. Figure 4.1 shows the schematic diagram for the test setup in this chapter.

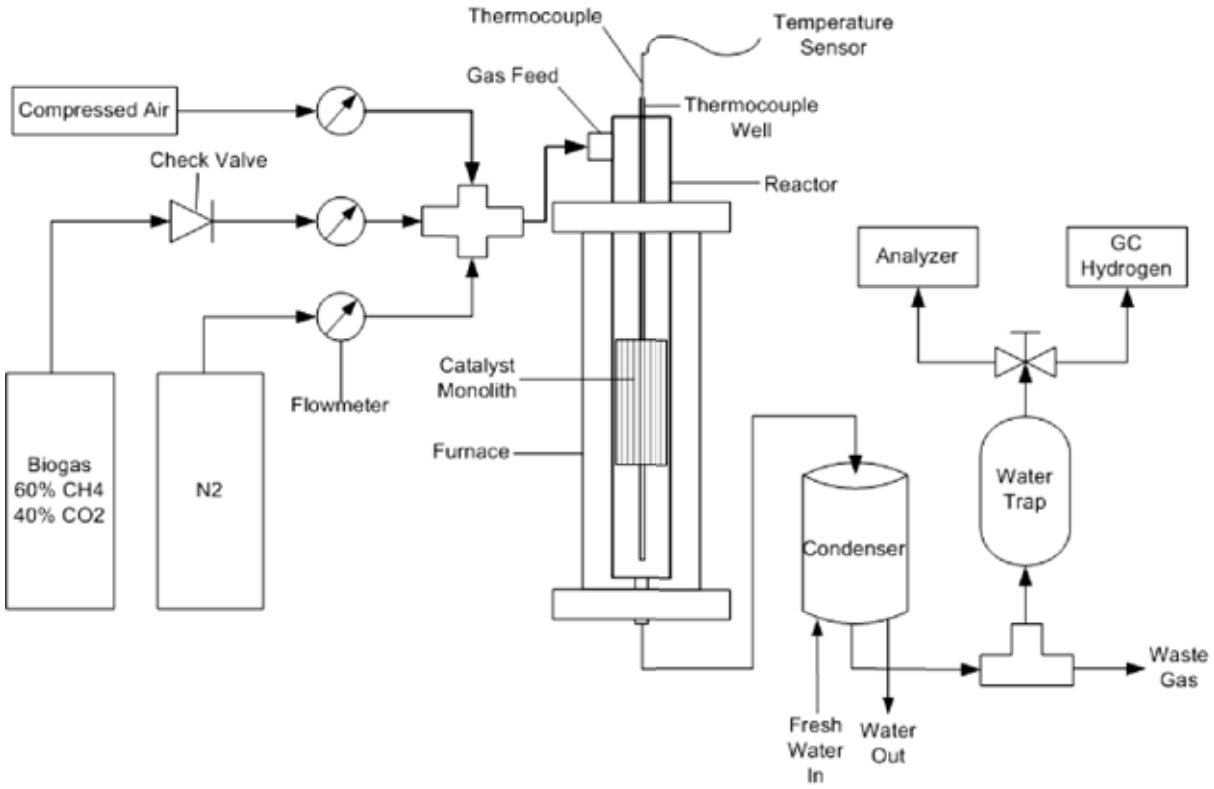


Figure 4.1: Test setup for biogas DRR and POX reforming reactions.

For both experimental studies, the temperature profile for the reforming reactor was first recorded with only nitrogen flow (inert gas), followed by the temperature profile under reaction conditions at each test point. Obtaining the temperature profile allowed the study of the sequence of the main reforming reactions along the catalyst bed (i.e. either exothermic or endothermic) and the overall nature of the reforming reactions.

### 4.1.1 Equilibrium Calculation

As a first step towards understanding the reforming processes of biogas, the STANJAN equilibrium model (v 3.91, Stanford University) was used to calculate the theoretical product gas distributions for (i) DRR and (ii) simultaneous POX and DRR process of biogas. STANJAN is a software for use in analysis of chemical equilibrium in single- or multi-phase systems whereby the input parameters are the output species, the atomic populations and reaction operation parameters (Reynolds, 1986). In this test, the equilibrium calculations were performed at a constant pressure of 1 bar and the stated temperature range from 300 – 980 °C. The temperature range not only includes temperatures that can be found in the engine exhaust (e.g. 300 – 700 °C), but also temperatures where completed reactants conversion can be achieved (i.e. promotion of an exothermic reaction to raise the reactor temperature). Using the predicted reactor product distribution, the reforming process efficiency was calculated as follow:

$$\text{Reforming Effciency}\,(\%) = \frac{\text{LCV}_{\text{fuel prod}}\ \dot{m}_{\text{fuel prod}}}{\text{LCV}_{\text{fuel in}}\ \dot{m}_{\text{fuel in}}} \times 100\% \tag{4.4}$$

where $\text{LCV}_{\text{fuel prod}}$ and $\text{LCV}_{\text{fuel in}}$ are the lower calorific values (LCV) of combustible gases in the reactor product distribution (i.e. $H_2$, $CH_4$, CO) and biogas while both $\dot{m}_{\text{fuel prod}}$ and $\dot{m}_{\text{fuel in}}$ are the mass flow rate of reactor product gas and reactor feed gas respectively.

## 4.2 Dry Reforming of Biogas

### 4.2.1 Equilibrium Predicted Results

According to the preliminary results from the predicted equilibrium calculations as shown in Figure 4.2, at low temperatures (i.e. below 400 °C) the DRR process shows very

little difference from the input composition with less than 10% of hydrogen produced. As the reforming reactor temperature increases, both hydrogen and carbon monoxide production are expected to increase significantly. As can be seen from Figure 4.2, starting at 600 °C, the equilibrium of the DRR process of biogas is predicted to increase and stoichiometric equilibrium is reached at approximately 800 °C reactor temperature with a maximum hydrogen production of 44.4% volume. In addition, as shown earlier in Eq. 4.2, the predicted unreacted methane remaining in the reforming product is approximately 11%.

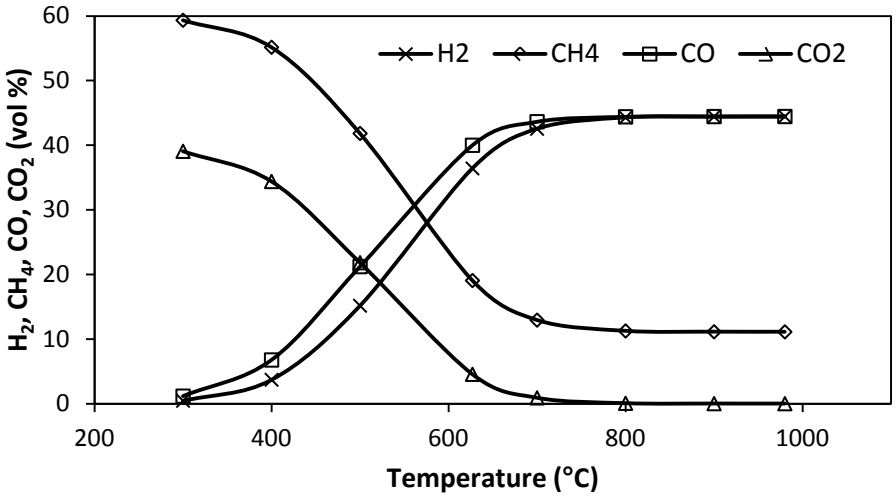


Figure 4.2: Equilibrium predicted product distribution for DRR of biogas.

Figure 4.3 shows the calculated reforming process efficiency for the DRR process of biogas. It should be noted that the heat energy supplied by the furnace for temperature control purposes was not taken into account during the process efficiency calculation as these heat energy will be provided by the exhaust gas and by burning part of the fuel in the exhaust gas fuel reforming process as explained in the Literature Review section. Hence, the calculated process efficiencies were always higher than 100% since the DRR process is highly endothermic. The increasing hydrogen production (the LCV of hydrogen is approximately three times higher than that of methane) and the continuous reduction in carbon dioxide

(which is a non-combustible diluents gas) give rise to the increasing process efficiency at higher temperatures. The maximum predicted process efficiency for the DRR of biogas is at 146% and it is reached at 800 °C.

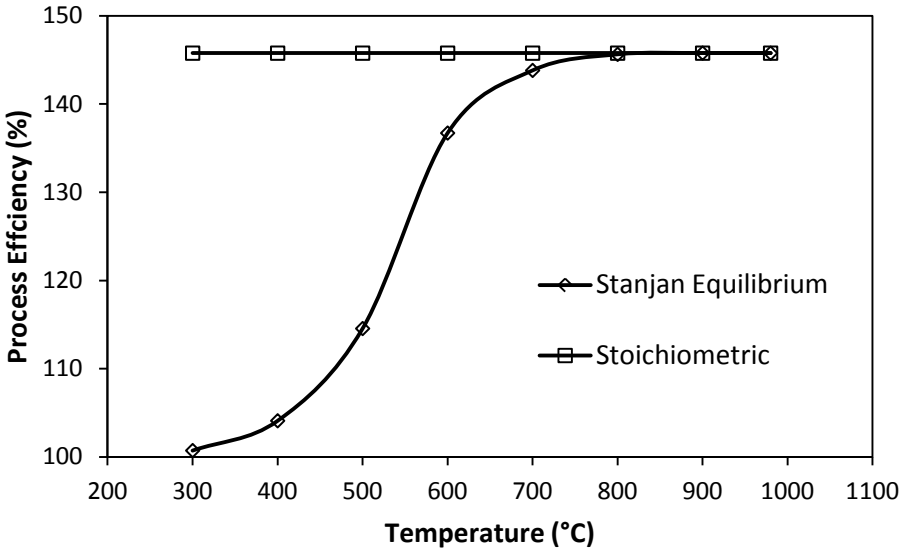


Figure 4.3: Process efficiency predicted for DRR of biogas.

### 4.2.2 Experimental Results

Similar to the results trend predicted by the equilibrium calculations, the DRR process activity of biogas increases with increasing temperature for both GHSVs, as shown in both Figure 4.4 and 4.5. At high reactor temperature of approximately 900 °C and low GHSV of 16,500 $h^{-1}$, stoichiometric equilibrium is reached with approximately 44% volume of hydrogen production as shown in Figure 4.4. When both Figure 4.4 and 4.5 were being compared, it can be seen that the DRR process activity of biogas is higher at the low GHSV of 16,500 $h^{-1}$ compared to that at the higher GHSV of 27,500 $h^{-1}$. As explained in the literature review section, DRR is a slow reacting process. An increase in GHSV from 16,500 to 27,500 $h^{-1}$ corresponded to an overall decrease in residence time from 0.22 to 0.13 seconds

(Eq. 4.1), thus resulted in decreasing catalytic reaction between the gas feed and the catalyst active sites.

It can be observed that throughout all test conditions, the production of carbon monoxide remained slightly higher than that of hydrogen. As shown by Bradford and Vannice (1996), the apparent activation energy barriers for hydrogen formation is higher compared to that of carbon monoxide, hence giving rise to the observed product distribution trend. In addition, the large activation barrier associated with the endothermic DRR process also resulted in the low initial methane conversion at low temperatures region, as shown in Figure 4.16.

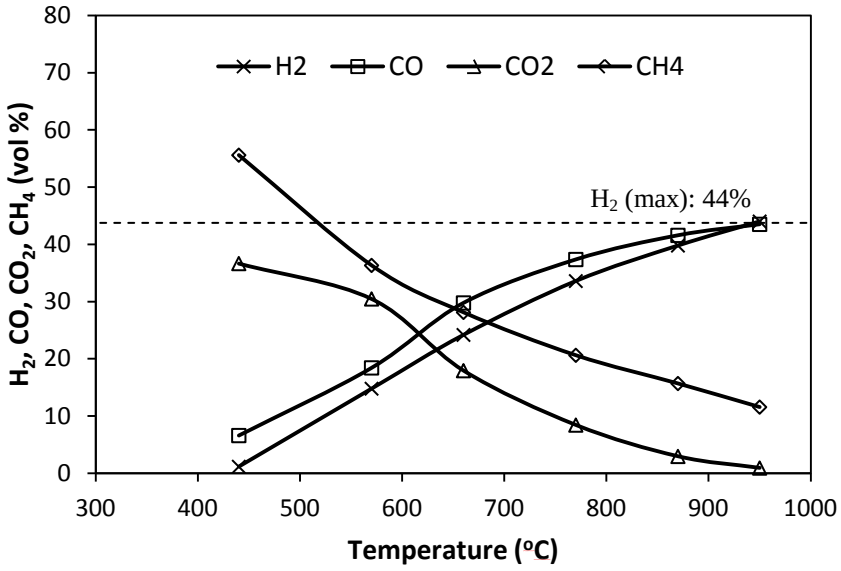


Figure 4.4: Experimental values of reactor product gas composition for DRR of biogas at GHSV: 16,500 $h^{-1}$.

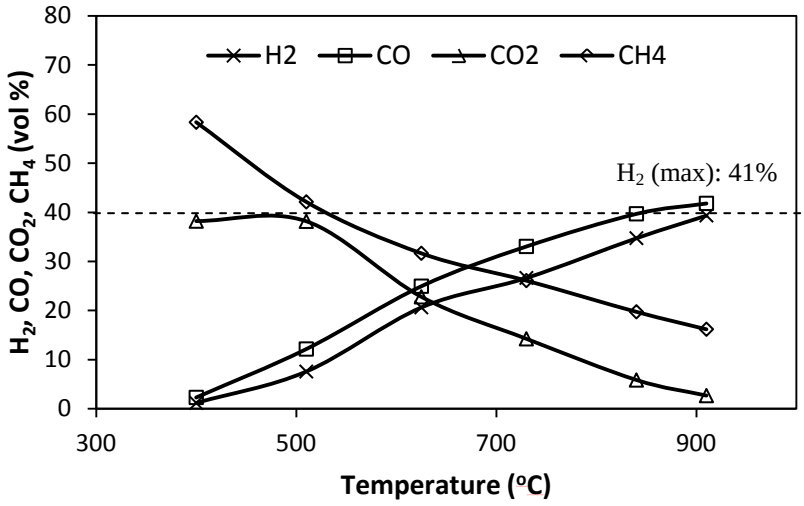


Figure 4.5: Experimental values of reactor product gas distribution for DRR of biogas at GHSV: 27,500 $h^{-1}$.

Figure 4.6 shows the temperature profile for the DRR process of biogas at approximately 700 °C. The drop in temperature along the monolith catalyst at both GHSVs proves that an endothermic DRR process was occurring. Nevertheless, there is a rise in temperature starting at 50 mm from the monolith catalyst inlet, showing that the DRR process activity ceased at that point in the catalyst.

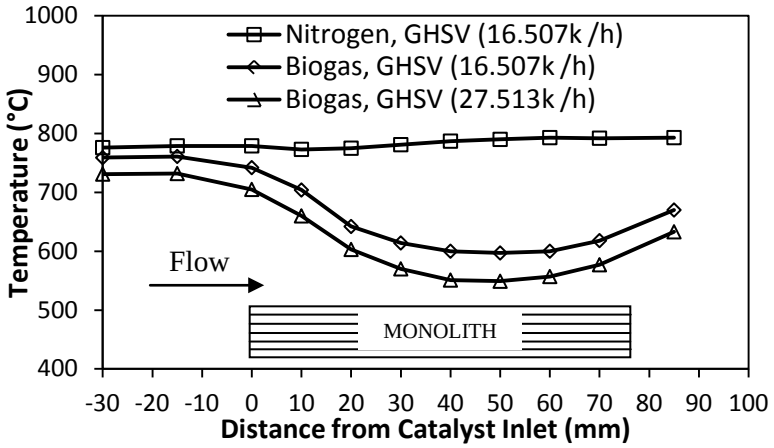


Figure 4.6: Effect of the GHSV on the reactor temperature profile for DRR of biogas at approximately 700 °C reactor inlet temperature.

## 4.3 Simultaneous Dry and Partial Oxidation Reforming of Biogas

### 4.3.1 Equilibrium Predicted Results

According to the product distribution predicted from equilibrium calculations, the overall reforming process efficiency dropped with the addition of oxygen, particularly with increasing $O_2/CH_4$ molar ratios. This is mainly due to the exothermic nature of the POX process where part of the fuel energy is released as heat energy which in turn increases reactor temperature (Figure 4.7). Nonetheless, the addition of oxygen into the reactor is expected to increase hydrogen production and the increment is more significant at the low temperature range, as shown in Figure 4.8. In comparison to Figure 4.2 (i.e. DRR of biogas), it can be seen that the addition of oxygen at the lowest $O_2/CH_4$ molar ratio of 0.16 increases the equilibrium hydrogen concentration from approximately 0% to 30% at the gas equilibrium temperature of 400 °C. At $O_2/CH_4$ molar ratio of 0.57, the hydrogen production is predicted to be almost constant at approximately 50% throughout all the temperature ranges.

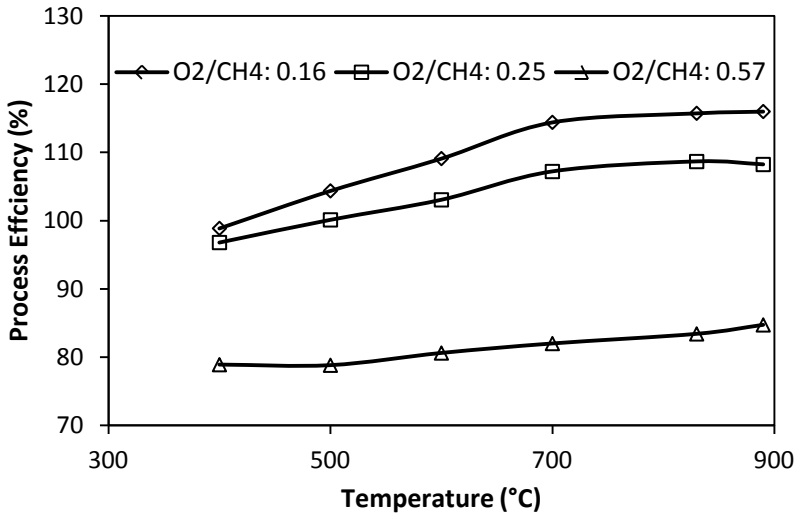


Figure 4.7: Process efficiency predicted for simultaneous DRR and POX of biogas.

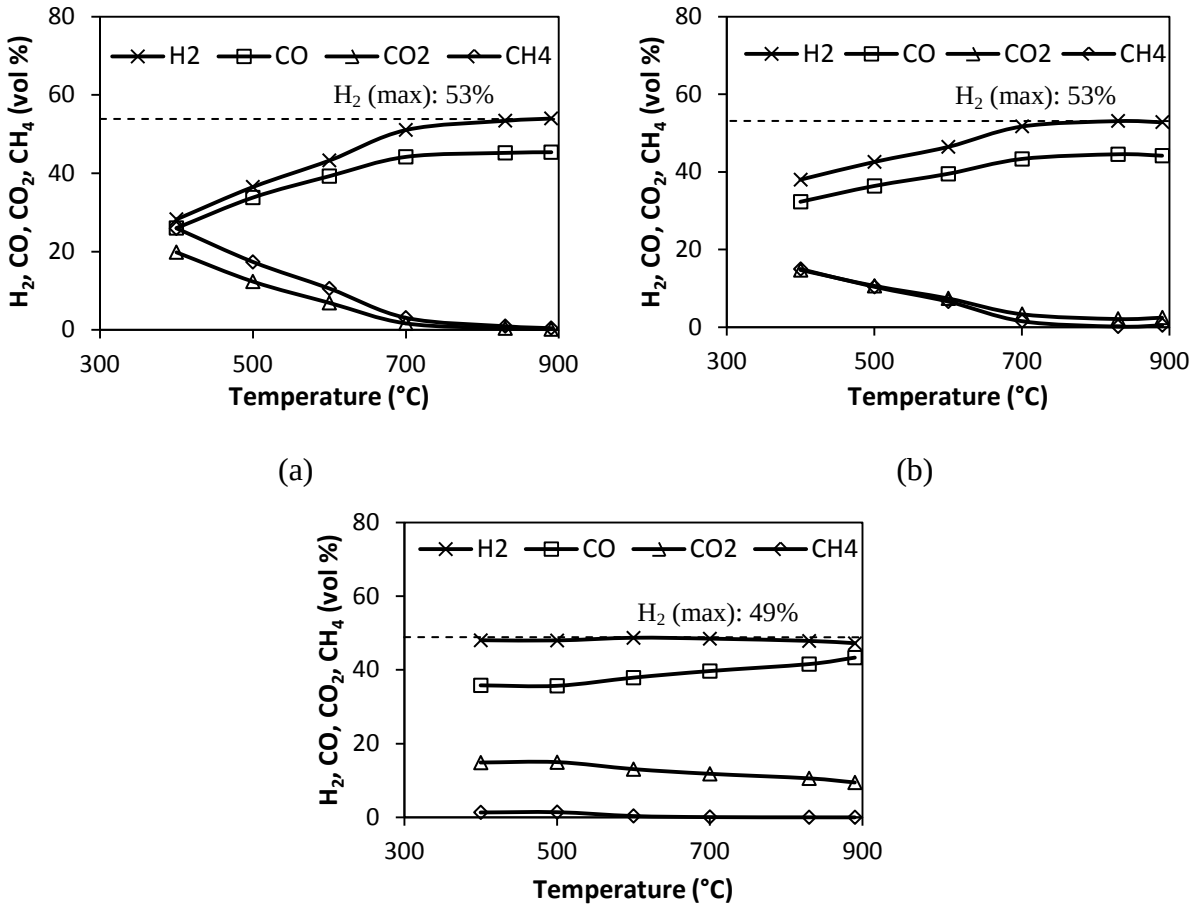


Figure 4.8: Equilibrium predicted product distribution for simultaneous DRR and POX of biogas at $O_2/CH_4$ molar ratio: (a) 0.16 (b) 0.25 (c) 0.57.

### 4.3.2 Experimental Temperature Profile

The addition of oxygen into the reforming reactor gives rise to a temperature profile which is different from the DRR process of biogas in Figure 4.6. As shown in Figure 4.9, there is a steep rise in temperature to a peak which is close to the catalyst inlet face before declining much more gradually downstream the monolith catalyst. The rise and peak in the temperature profile is associated with the exothermic POX or even possibly the complete combustion of the methane gas component of the biogas, depending on the availability of oxygen in the reforming reactor. On the contrary, the decline in temperature is corresponded

to the endothermic DRR process of biogas. The trend of rise followed by gradual decrease in temperature profile is mainly due to the fact that the exothermic POX process or combustion of methane proceed much faster compared to that of the DRR process (Tomishige et al., 2001).

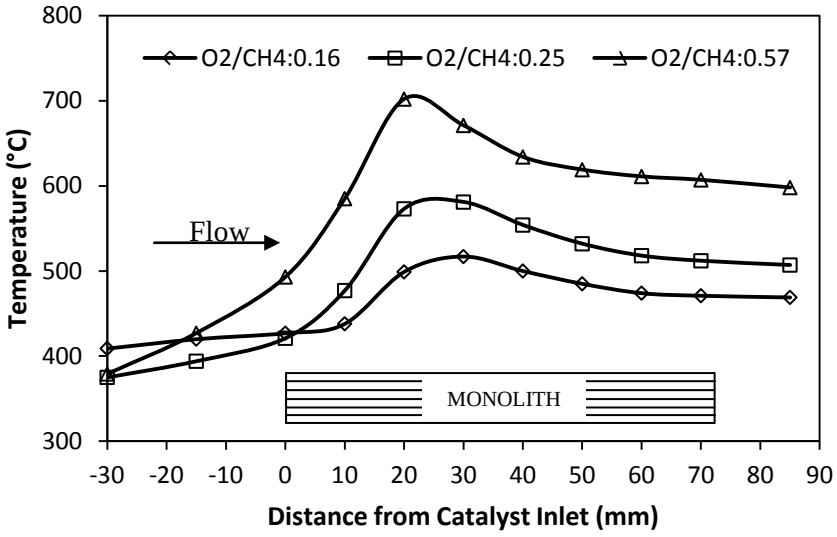


Figure 4.9: Reactor temperature profile at GHSV 27,500 $h^{-1}$ at approximately 400 °C reactor temperature.

The position, height and width of the temperature peak responded to the changes in the reactor gas feed. Figure 4.9 shows the temperature profile along the monolith catalyst at inlet gas temperature of approximately 400 °C and GHSV of 27,500 $h^{-1}$. It can be seen that with an increase in $O_2/CH_4$ molar ratio from 0.16 to 0.57, the maximum peak temperature rose from approximately 500 °C to 700 °C, mainly due to the increase in availability of oxygen for the POX process to occur. It should also be noted that throughout all the test conditions, the conversion of oxygen remained 100%. Figure 4.10 shows the temperature profile at approximately 700 °C and 27,500 $h^{-1}$. When comparing both Figure 4.9 (inlet temperature 400 °C) with Figure 4.10 (inlet temperature 700 °C), it can be observed that at the higher temperature range, the overall maximum rise in the temperature peak decreased and it was followed by a more drastic drop in the temperature profile at approximately 20 mm from the

catalyst inlet face. This signifies that the high temperature condition demotes the POX process of biogas, with no temperature peak observed at low $O_2/CH_4$ molar ratio of 0.16 (Figure 4.10). On the contrary, the high temperature range promotes the endothermic DRR process of biogas, as explained earlier in the Literature Review section. Hence, this contributed to the rapid decline in temperature profile starting at the peak of approximately 800 °C. Overall, it can be concluded that the process exothermicity for simultaneous DRR and POX processes of biogas decreased with increasing reactor temperature.

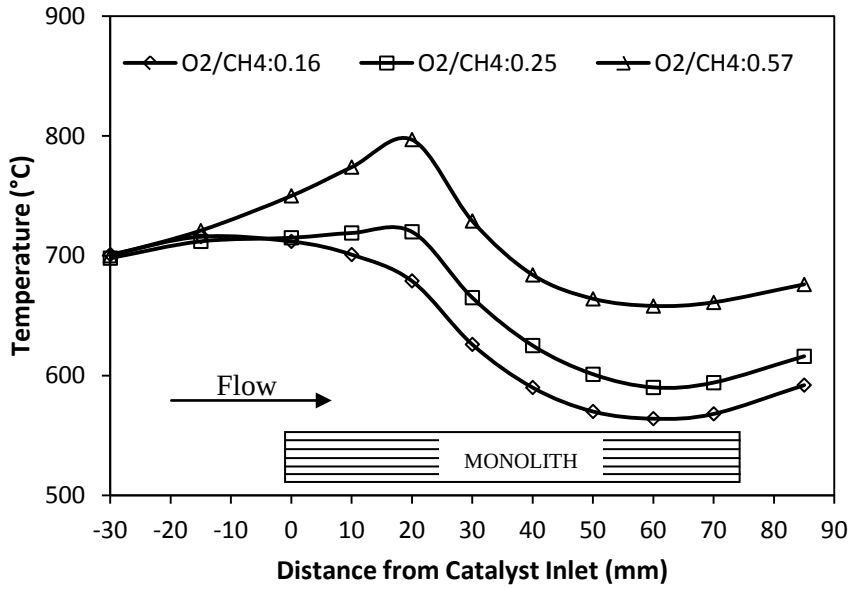


Figure 4.10: Reactor temperature profile at GHSV 27,500 $h^{-1}$ at approximately 700 °C reactor temperature.

In terms of comparison between the high and low GHSVs used, the effect on the profile peak temperature along the monolith catalyst is more profound at low temperature range whereby the POX process is dominant. As shown in Figure 4.11, an increase in GHSV at approximately 500 °C increased the peak temperature and shifted it towards downstream, causing the overall exothermic reaction to move further down the monolith catalyst bed. Unlike the DRR process, increasing the GHSV actually promotes the POX process of biogas

as it improves the transport of reactants to the active sites on the catalyst surface, resulting in higher rates of oxidation. This can be seen from the overall higher temperature readings along the monolith catalyst bed at GHSV of 27,500 $h^{-1}$. In addition, the larger amount of heat released at high GHSV generated a hot layer on top of the catalyst bed, indirectly allowing the DRR process that follows to proceed at higher temperatures.

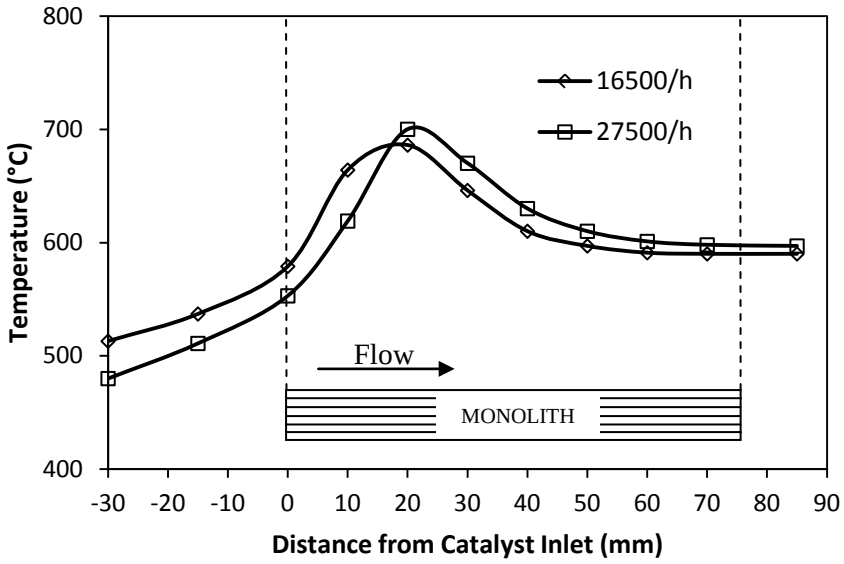


Figure 4.11: Effect of GHSV on catalyst temperature profile at gas inlet temperature of approximately 500 °C.

### 4.3.2 Experimental Reformer Product Distribution

According to the experimental results obtained, the positive effect of adding oxygen onto the reforming process of biogas is more pronounced at the lower temperature range (Figure 4.12 – 4.15). As shown in Figure 4.12 and 4.13, the addition of oxygen at $O_2/CH_4$ molar ratio of 0.16 shows that at low temperature range (i.e. 400 – 600 °C), the amount of leftover unreacted methane present in the reformer product gas is lower than that of carbon dioxide. This product distribution trend differs from that of the DRR process, indicating that methane is being used up for the POX process by oxygen at low temperature range.

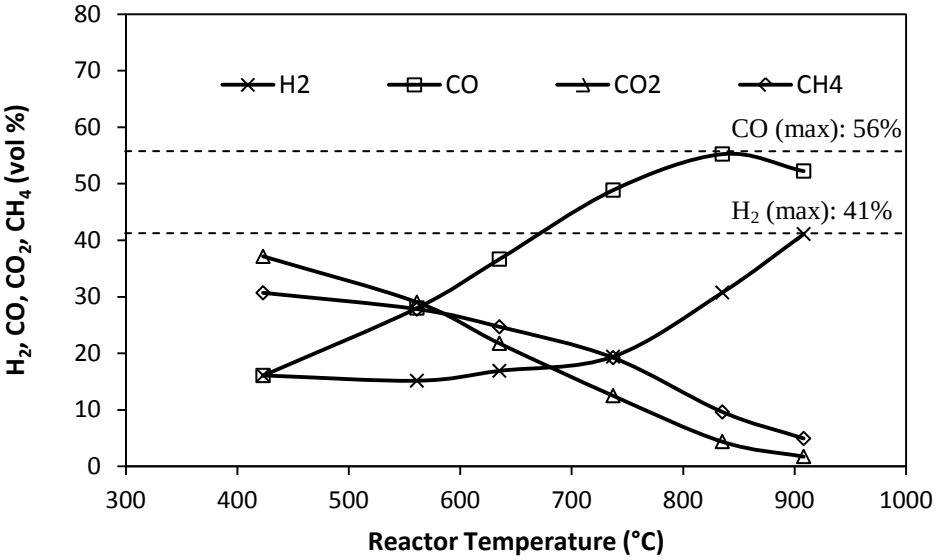


Figure 4.12: Experimental reactor product gas distribution for simultaneous DRR and POX of biogas at $O_2/CH_4$ molar ratio of 0.16 and GHSV 16,500 $h^{-1}$.

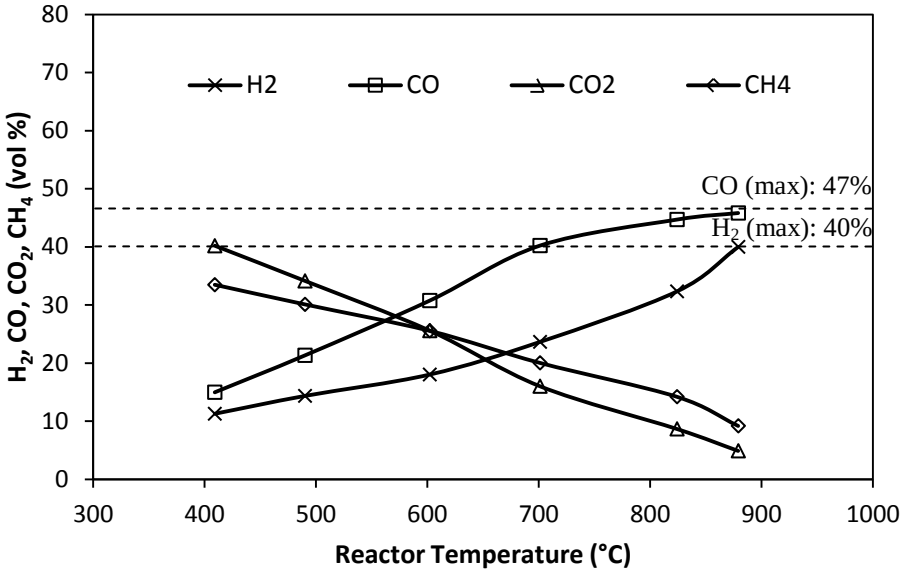


Figure 4.13: Experimental reactor product gas distribution for simultaneous DRR and POX of biogas at $O_2/CH_4$ molar ratio of 0.16 and GHSV 27,500 $h^{-1}$.

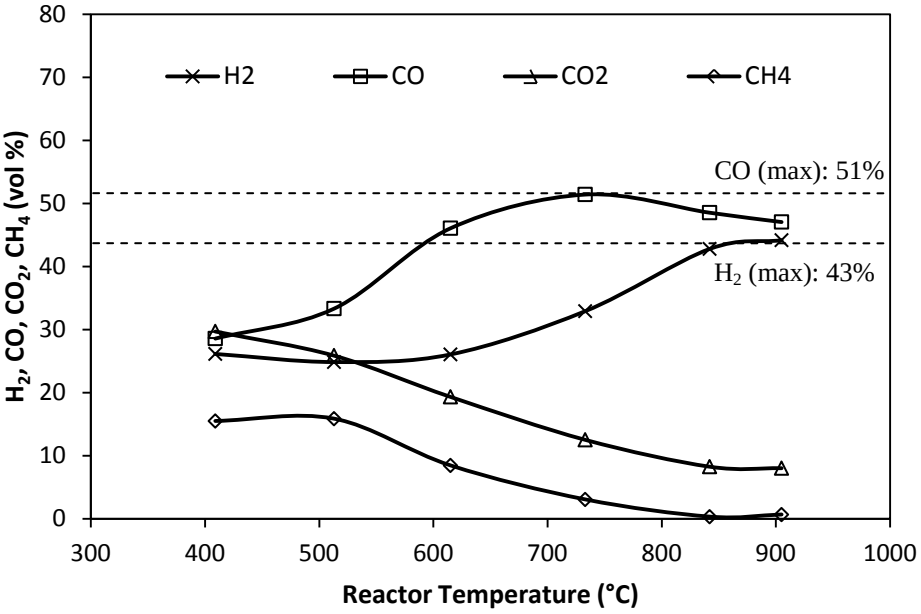


Figure 4.14: Experimental reactor product gas distribution for simultaneous DRR and POX of biogas at $O_2/CH_4$ molar ratio of 0.57 and GHSV 16,500 $h^{-1}$.

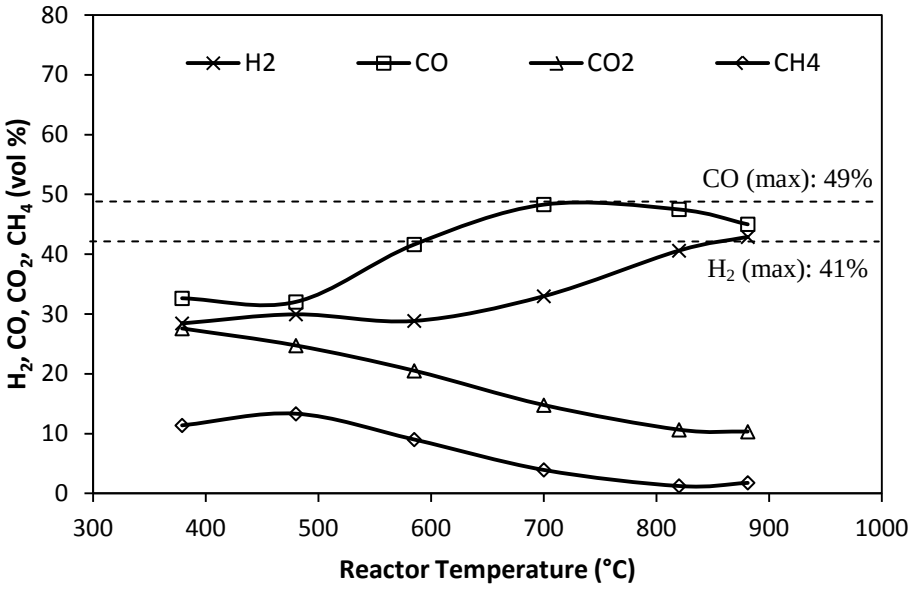


Figure 4.15: Experimental reactor product gas distribution for simultaneous DRR and POX of biogas at $O_2/CH_4$ molar ratio of 0.57 and GHSV 27,500 $h^{-1}$.

At $O_2/CH_4$ molar ratio of 0.57 as shown in Figure 4.14 and 4.15, the amount of methane present in the reformer product gas is always lower than carbon dioxide throughout the entire temperature range. This proves that at high $O_2/CH_4$ molar ratios, the increased availability of oxygen promotes the oxidative reforming processes and most probably increased the carbon dioxide content in the reactor gas product through complete combustion of methane at low reactor temperatures (Eq. 2.4). In addition, the high amount of carbon dioxide present at temperature range 600 – 700 °C could potentially be due to carbon dioxide formation through Eq. 4.5 at low hydrogen-to-carbon monoxide ($H_2/CO$) molar ratio (Figure 4.19) (Richardson and Paripatyadar, 1990).

$$2CO \rightarrow C + CO_2 \tag{4.5}$$

In parallel with Figure 4.16, the conversion of methane increased with the addition of oxygen throughout the temperature range with almost 100% conversion achieved at $O_2/CH_4$ molar ratio of 0.57 and approximately 900 °C. The conversion of methane is calculated as follow:

$$\text{Methane Conversion (\%)} = \frac{\dot{m}_{\text{methane biogas}} - \dot{m}_{\text{methane product}}}{\dot{m}_{\text{methane biogas}}} \text{ X } 100\% \tag{4.6}$$

where $\dot{m}_{\text{methane biogas}}$ and $\dot{m}_{\text{methane product}}$ are the respective methane mass flow rate for biogas input and the reformer product gas.

Regarding hydrogen production for the simultaneous DRR and POX process of biogas, it can be seen from Figure 4.17 and 4.18 that in general, when oxygen is being added into the reforming reactor, there is an increase in catalyst peak temperature along with an increase in the amount of hydrogen produced. At temperature range below 500 °C, the addition of oxygen at any $O_2/CH_4$ molar ratios and GHSVs increases the hydrogen production.

Nonetheless, starting from 500 °C at GHSV 16,500 $h^{-1}$ and 600 °C at GHSV 27,500 $h^{-1}$, the introduction of oxygen at low $O_2/CH_4$ molar ratio of 0.16 has negative effect on the hydrogen production even though the methane conversion is increased (Figure 4.16), as compared to the case when no oxygen is being added into the reactor (DRR process of biogas). This could be because at this temperature range and low $O_2/CH_4$ conditions, the added oxygen caused part of the methane in biogas to be fully combusted without any significant rise in the reforming reactor temperature profile, hence consuming methane while forming steam and carbon dioxide instead of hydrogen (Eq. 2.4).

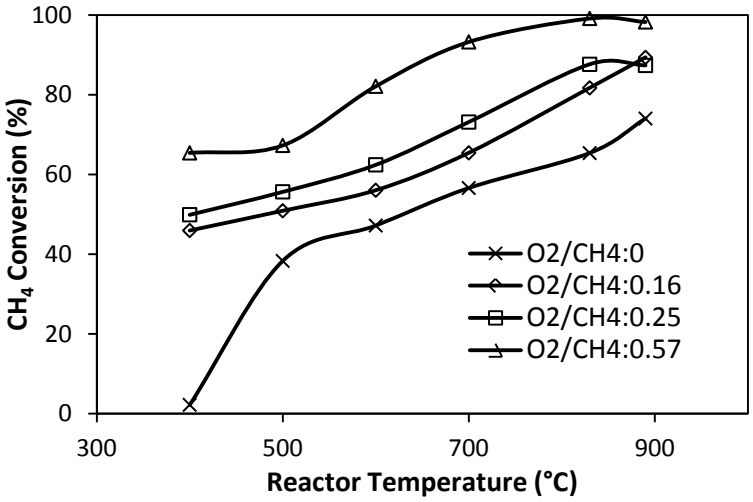


Figure 4.16: Effect of $O_2/CH_4$ molar ratio on the methane conversion at GHSV: 16,500 $h^{-1}$.

At the low GHSV value of 16,500 $h^{-1}$ as shown in Figure 4.17, the addition of oxygen into the reforming reactor at $O_2/CH_4$ molar ratios of 0.25 and 0.57 resulted in significant increase in hydrogen production at low temperature range (below 600 °C), but with an adverse effect on hydrogen production at high temperatures. On the contrary, at 27,500 $h^{-1}$ the introduction of oxygen at $O_2/CH_4$ molar ratios of 0.25 and 0.57 increases hydrogen production throughout the entire temperature range. This is thought to be mainly due to the generation of hot layer on the catalyst bed at high GHSV as explained earlier (overall

increment in the temperatures along catalyst bed in Figure 4.11), which promotes the endothermic DRR process of biogas downstream the catalyst.

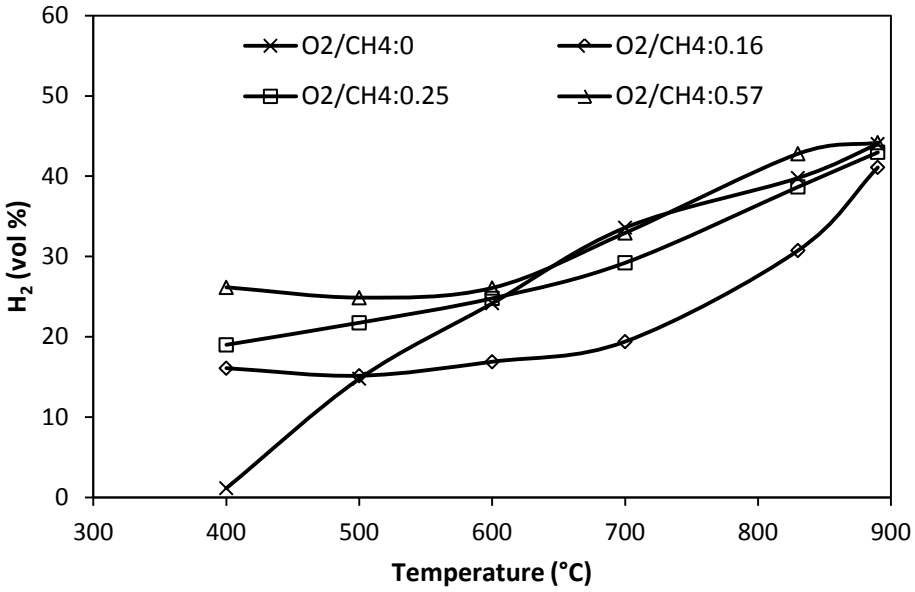


Figure 4.17: Reactor product hydrogen for the different $O_2/CH_4$ molar ratios at 16,500 $h^{-1}$.

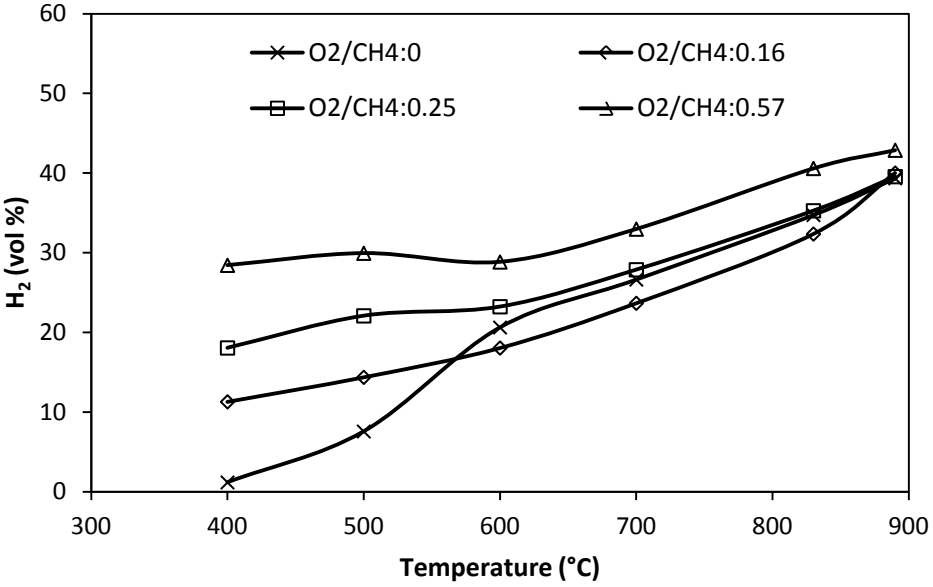


Figure 4.18: Reactor product hydrogen for the different $O_2/CH_4$ molar ratios at 27,500 $h^{-1}$.

The $H_2$/CO reactor product molar ratio is derived based on the reactor product gas distribution (Figure 4.12 – 4.15) and it allows the study of each individual reforming reactions. Based on Eq. 2.3 and Eq. 2.5 for the chemical equation of POX and DRR respectively, the stoichiometric $H_2$/CO product molar ratio for POX process is 2, which is higher than that of the DRR process at 1. Therefore, it can be deduced from Figure 4.19 that at low temperature range of 500 °C, the higher $H_2$/CO product molar ratio and the larger increment in peak temperature of 220 °C at 27,500 $h^{-1}$ (compared to only 173 °C at 16,500 $h^{-1}$) signifies that the exothermic POX process of biogas is being favoured at high GHSVs. Despite that, there is a drop in $H_2$/CO product molar ratios with increasing temperatures, showing that the exothermic POX process of biogas becomes less significant at high temperatures, consistent with the temperature profile plot in Figure 4.10. Further increasing the reactor temperatures causes the $H_2$/CO product molar ratio to rise back starting at 700 °C and it reached approximately 1 at 900 °C. This shows that at high temperatures, DRR process of biogas is the dominating reforming reaction and the reaction is complete.

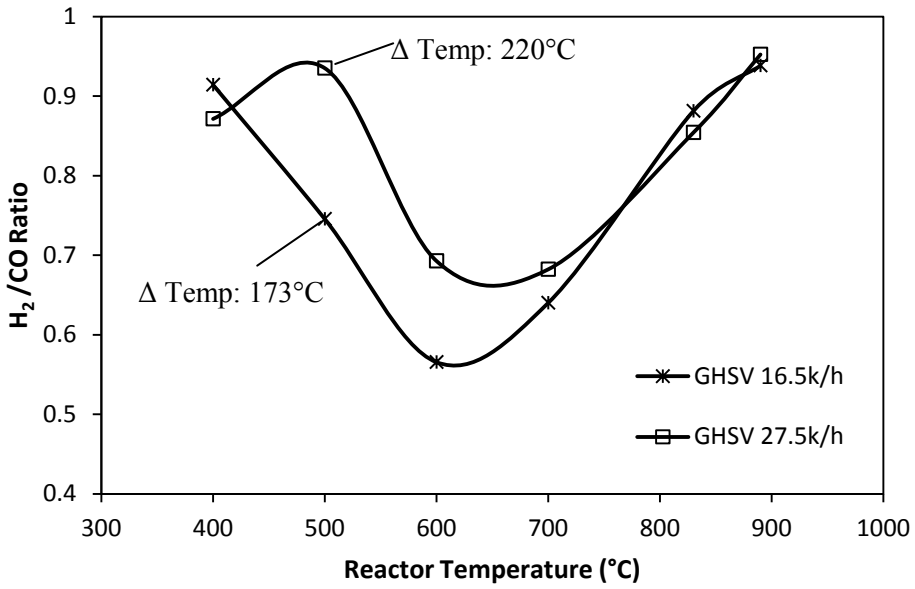


Figure 4.19: $H_2$/CO product molar ratio at both GHSVs and $O_2/CH_4$ molar ratio of 0.57

## 4.4 Summary

The DRR process of biogas, followed by the simultaneous DRR and POX process of biogas were investigated at various temperature range and GHSVs. The main findings are summarized as follow:

- For upgrading biogas into high quality syngas, biogas can be reformed through the DRR reforming process and high hydrogen yield is achieved at high temperatures and low GHSVs conditions.
- The addition of oxygen into the reforming reactor which promotes the oxidative reforming reactions within the reforming reactor improves the hydrogen yield, especially at low temperatures and the beneficial effects were more significant at high GHSVs.
- Based on the reactor gas composition acquired and the temperature profile along the monolith catalyst, it can be concluded that at low temperatures below 600 °C and high GHSVs, the exothermic POX process of biogas is the dominating reforming reaction. The heat generated in turn promoted the DRR process of biogas downstream the monolith catalyst.
- The effect of oxygen availability in the reforming reactor (i.e. the $O_2/CH_4$ molar ratios) on the hydrogen production had been investigated. At low $O_2/CH_4$ molar ratio of 0.16, increase in reactor temperatures reduces the hydrogen production irrespective of GHSVs. At high $O_2/CH_4$ molar ratios, increasing temperature promotes hydrogen yield at high GHSV but has an adverse effect on hydrogen production at low GHSV.
- Simultaneous DRR and POX process of biogas has the potential for use in vehicular or power generation applications as it improves syngas production at low temperature range (400-600 °C), which represents the typical engine exhaust gas temperature level.

# CHAPTER 5

# BIOGAS UPGRADE THROUGH EXHAUST GAS FUEL REFORMING PROCESS WITH ENGINE EXHAUST WASTE HEAT RECOVERY

## 5.1 Introduction

This chapter presents the experimental findings on the exhaust gas fuel reforming process using biogas to achieve on-demand generation of high quality hydrogen-enriched gaseous fuels for vehicular applications.

As shown in Chapter 4, biogas has the potential to be upgraded through catalytic reforming at a low temperature range with the utilization of oxygen into the reforming reactor. The use of engine exhaust gas from diesel operation is beneficial for the exhaust gas fuel reforming process as diesel engines, which operate under lean conditions (i.e. $\lambda>1$) always contain excessive oxygen in the engine exhaust. Nonetheless, based on Eq. 2.7 and 2.8, it is clear that the engine exhaust compositions (i.e. % volume of oxygen, steam and carbon dioxide present) is largely dependent on the engine operating conditions (differing $\lambda$ value) which then in turn affects the performance of the biogas exhaust fuel reforming process. The main objective of this chapter is to investigate the effects of various engine operating conditions (i.e. engine load and % EGR implemented) and GHSVs on the reaction profiles and reactor product distribution of the biogas exhaust fuel reforming process at low exhaust temperatures. Figure 5.1 illustrates the experimental setup for the biogas exhaust gas fuel reforming process.

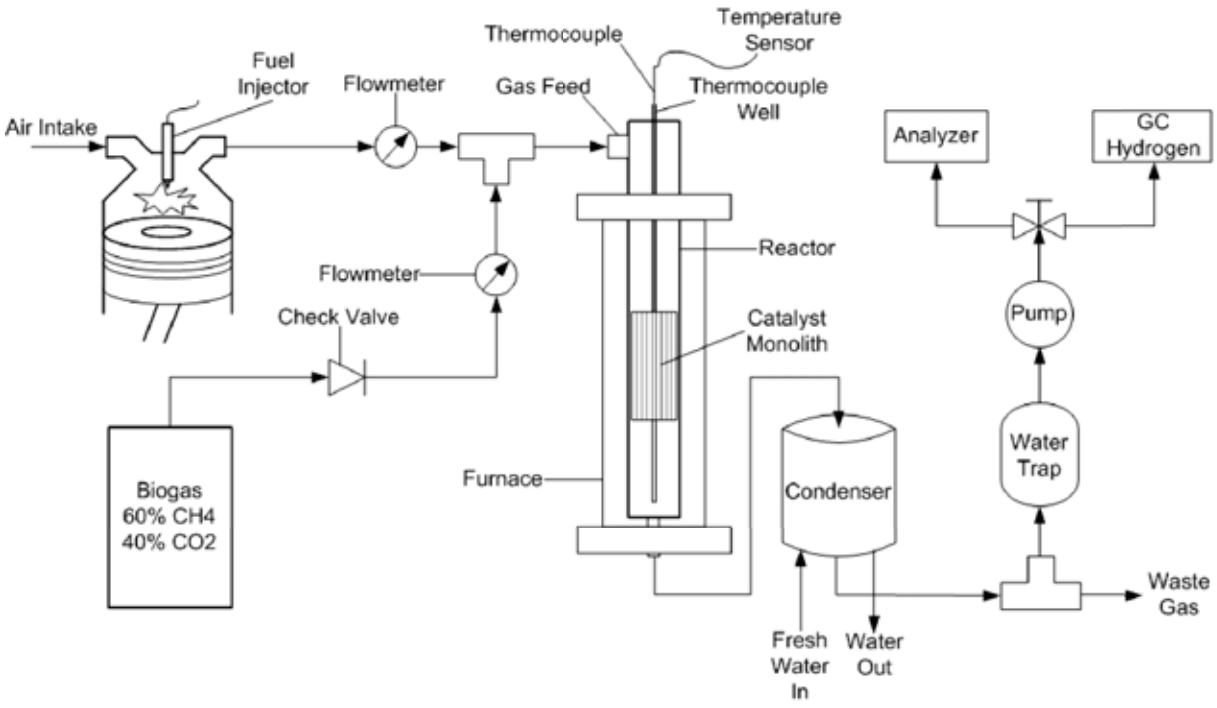


Figure 5.1: Schematic diagram for the exhaust gas fuel reforming process of biogas.

Three engine test conditions were chosen and the engine exhaust gas compositions at each operating condition were summarized in Table 5.1. The engine exhaust gas is fed directly into the reformer reactor loaded with a monolith catalyst with an aspect ratio of 3. In addition, the actual exhaust gas temperature at each engine operating point is maintained through the use of an external furnace, as shown in Figure 5.1. The IMEP values of 2 and 4 bar represented “low” and “medium” engine load conditions respectively. Calculations for the various engine operating parameters are as follow:

$$\text{Indicated Mean Effective Pressure (IMEP)} = \frac{\text{Indicated work per cycle}}{\text{Displaced volume}} = \frac{\oint p dV}{V_d} \quad (5.1)$$

where p and V are both the in-cylinder pressure and the corresponding cylinder volume

$$\text{Percentage of cooled EGR (\% vol)} = \frac{\dot{V}_o - \dot{V}_i}{\dot{V}_o} \times 100 \quad (5.2)$$

where $\dot{V}_o$ and $\dot{V}_i$ are the measured intake air volumetric flow rates without and with EGR, respectively.

Table 5.1: Exhaust gas composition for the three engine operating conditions.

| **Engine exhaust gas composition (wet)** | **Condition 1 Speed: 1500 rpm IMEP: 2 bar EGR: 0%** | **Condition 2 Speed: 1500 rpm IMEP: 4 bar EGR: 0%** | **Condition 3 Speed: 1500 rpm IMEP: 4 bar EGR: 20%** |
|---|---|---|---|
| $O_2$ (vol%) | 16.57 | 13.47 | 11.06 |
| $H_2O$ * (vol %) | 3.02 | 5.23 | 6.63 |
| CO (vol %) | 0.015 | < 0.01 | < 0.01 |
| $CO_2$ (vol %) | 3.21 | 5.56 | 7.05 |
| Exhaust Temperature (°C) | 186 | 295 | 300 |

* $H_2O$ contents are calculated values.

As explained in the literature review section, the exhaust gas fuel reforming process is a combination of the basic reforming reactions (Eq. 2.1 – 2.5) in a single reformer reactor. Hence, the basic operating parameters affecting the reforming process are the (i) steam-to-methane ($H_2O/CH_4$) molar ratio, (ii) $O_2/CH_4$ molar ratio and (iii) $CO_2/CH_4$ molar ratio of the reactor gas feed inlet. Based on the discussions in Chapter 4, it was concluded that at low temperatures the production of hydrogen enriched gaseous product from biogas is highly dependent on the $O_2/CH_4$ molar ratios. Therefore, four values of $O_2/CH_4$ molar ratios at 0.16, 0.25, 0.50 and 0.75 were selectively used in this test.

The GHSV was fixed at 16,500 $h^{-1}$ and 25,500 $h^{-1}$ and according to Eq. 4.1, these GHSV values correspond to the total reactor gas feed volumetric flow rate of 10 and 15 L/min respectively. Based on Table 5.2, the individual feed rate of the engine exhaust and biogas

into the reactor was altered accordingly at each test point (there are 24 test points in total). Table 5.3 summarizes the corresponding reactor gas feed $H_2O/CH_4$ and $CO_2/CH_4$ molar ratios at each test points.

Table 5.2: Individual exhaust and biogas feed gas flow rates for all reforming test conditions measured at 100 °C and atmospheric pressure (1 bar).

| Engine Condition | $O_2/CH_4$ | GHSV: 16,500 $h^{-1}$ | | GHSV: 25,500 $h^{-1}$ | |
|---|---|---|---|---|---|
| | | Exhaust (L/min) | Biogas (L/min) | Exhaust (L/min) | Biogas (L/min) |
| 1 | 0.16 | 3.5 | 6.5 | 5.0 | 10.0 |
| | 0.25 | 4.5 | 5.5 | 7.0 | 8.0 |
| | 0.50 | 6.0 | 4.0 | 9.0 | 6.0 |
| | 0.75 | 7.0 | 3.0 | 10.5 | 4.5 |
| 2 | 0.16 | 4.0 | 6.0 | 6.0 | 9.0 |
| | 0.25 | 5.0 | 5.0 | 7.5 | 7.5 |
| | 0.50 | 6.5 | 3.5 | 10.0 | 5.0 |
| | 0.75 | 7.5 | 2.5 | 11.0 | 4.0 |
| 3 | 0.16 | 4.5 | 5.5 | 6.5 | 8.5 |
| | 0.25 | 5.5 | 4.5 | 8.5 | 6.5 |
| | 0.50 | 7.0 | 3.0 | 10.5 | 4.5 |
| | 0.75 | 8.0 | 2.0 | 12.0 | 3.0 |

Table 5.3: $H_2O/CH_4$ and $CO_2/CH_4$ molar ratios at specified $O_2/CH_4$ molar ratios for the three engine conditions.

| Engine Condition | $O_2/CH_4$: 0.16 | | $O_2/CH_4$: 0.25 | | $O_2/CH_4$: 0.50 | | $O_2/CH_4$: 0.75 | |
|---|---|---|---|---|---|---|---|---|
| | $H_2O/CH_4$ | $CO_2/CH_4$ | $H_2O/CH_4$ | $CO_2/CH_4$ | $H_2O/CH_4$ | $CO_2/CH_4$ | $H_2O/CH_4$ | $CO_2/CH_4$ |
| 1 | 0.021 | 0.76 | 0.034 | 0.78 | 0.060 | 0.82 | 0.094 | 0.87 |
| 2 | 0.027 | 0.80 | 0.040 | 0.83 | 0.078 | 0.92 | 0.12 | 1.04 |
| 3 | 0.032 | 0.84 | 0.051 | 0.89 | 0.094 | 1.03 | 0.16 | 1.25 |

## 5.2 Temperature Profile for Biogas Exhaust Fuel Reforming

### 5.2.1 Effects of Engine Conditions on Temperature Profile

At engine condition 1 (i.e. low engine load operation), no reforming activity was observed when the engine exhaust gas was fed into the reactor together with biogas, hence the temperature profile along the catalyst was flat and was not shown. This is mainly due to the low exhaust temperature (i.e. approximately 186 °C) at this engine condition being insufficient to achieve the light-off temperature of the monolith catalyst used in this test.

When the engine operating load was increased from low (2 bar IMEP) to medium (4 bar IMEP), a non-uniform temperature profile was observed along the length of the catalyst bed. Figure 5.2 shows the different reactor temperature profiles varying the with $O_2/CH_4$ molar ratios at engine condition 2 and at GHSV of 25,500 $h^{-1}$. It can be observed that the trend for the temperature profile was similar to that of simultaneous DRR and POX process of biogas, with the temperature rising steeply close to the catalyst inlet face, before gradually declining along the length of the catalyst. The peak in the temperature profile is associated with the oxidation of the methane component of biogas either through the POX process or by catalytic combustion. In contrast, the decline is mainly associated with the endothermic SRR or DRR of biogas. It was also worth noting that some of the heat generated at the catalyst inlet was back-radiated, resulting in a 100 – 200 °C temperature increment at 10 mm distance upstream the catalyst bed (Figure 5.2).

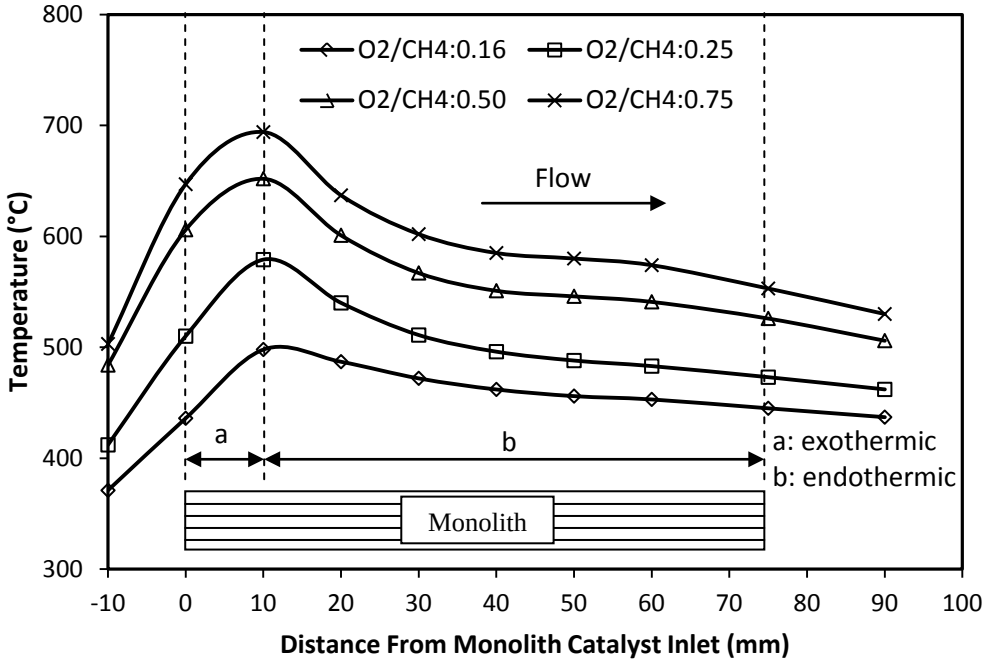


Figure 5.2: Reactor temperature profile at engine condition 2 at GHSV 25,500 $h^{-1}$.

In exhaust gas fuel reforming, the height, width and position of the temperature peak reflects the condition of each of the main reforming reactions and to the changes in the reactor gas feed (Tsolakis and Golunski, 2006). From Figure 5.2, it was shown that the peak temperature increases with increasing $O_2/CH_4$ molar ratios due to the higher availability of oxygen for exothermic reforming reactions. In addition, the higher temperature peak provides the enthalpy required and increases the reaction rate for the SRR and DRR downstream, hence increasing the hydrogen yield. Nonetheless, it should be noted that increasing $O_2/CH_4$ molar ratios could potentially impose a penalty on the overall reforming process efficiency as more chemical energy from the feed gas is being converted into waste heat energy.

Figure 5.3 shows the effect of implementing 20% EGR in the engine on the reactor temperature profile at the $O_2/CH_4$ molar ratio of 0.75 and the GHSV of 16,500 $h^{-1}$. The fuel reforming reaction with exhaust from the engine operating with EGR increases the temperature peak slightly at the constant GHSV and $O_2/CH_4$ molar ratios. As shown in Table

5.1, introducing EGR into the engine decreases the oxygen content inside the engine exhaust due to the displacement of fresh air intake by EGR. Therefore, in order to maintain the similar $O_2/CH_4$ molar ratios for both engine conditions (i.e. 0 and 20% EGR), less biogas and more hot exhaust gas has to be fed into the reforming reactor when 20% EGR was implemented (refer to values in Table 5.2). The larger proportion of hot exhaust gas entering the reforming reactor was believed to have increased the catalyst bed temperature due to the formation of hot spots (Li et al., 2006, Mukainakano et al., 2007). In addition, applying EGR also increases the amount of steam and carbon dioxide present in the engine exhaust, promoting SRR and DRR downstream, as can be seen from the larger temperature drop along the monolith catalyst.

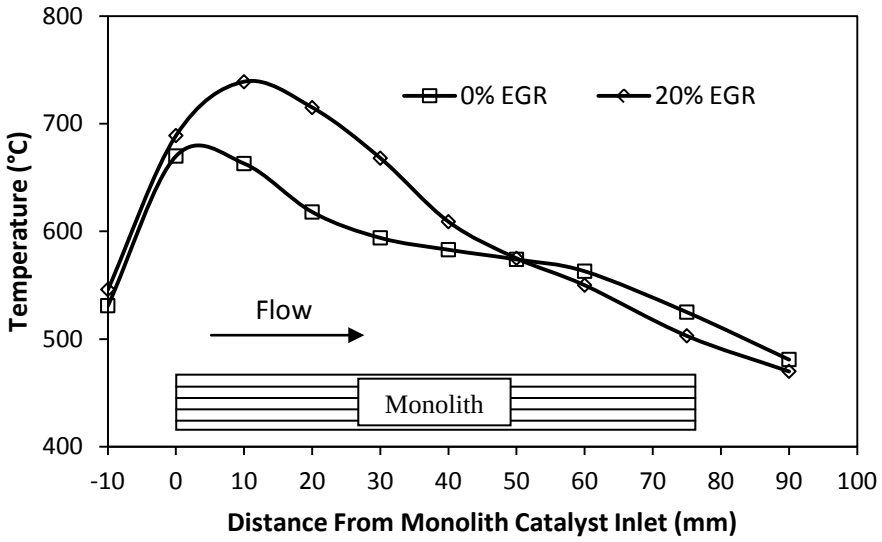


Figure 5.3: Effect of EGR on the reactor temperature profile at $O_2/CH_4$: 0.75 and GHSV: 16,500 $h^{-1}$.

### 5.2.2 GHSV Effects on Temperature Profile

The effect of GHSV on the temperature peak in the catalyst bed was more pronounced when exhaust gas from the engine without EGR was used, as can be observed from Figure 5.4. At 0% EGR (Figure 5.4(a)), the increase in GHSV from 16,500 $h^{-1}$ to 25,500 $h^{-1}$ increased the peak temperature and shifted it downstream, similar to that observed in simultaneous DRR and POX reforming of biogas. The more drastic decrease in the temperature immediately after the peak at high GHSV indicates that the endothermic SRR and DRR process of biogas was promoted at the temperature range in the vicinity of the profile peak. By contrast, the effect of GHSV on the temperature profile along the catalyst was less significant with 20% EGR to the engine. As can be observed from Figure 5.4(b), the peak temperature at engine condition 3 is almost consistent for both the GHSVs implemented. However, the temperature drop downstream is significantly larger at the low GHSV of 16,500 $h^{-1}$, with a temperature drop of approximately 250 °C compared to only 170 °C at 25,500 $h^{-1}$. This is mainly because the high GHSV decreases the residence time and significantly reduces the endothermic reaction rates for both the SRR and DRR process further downstream, hence recovering less heat.

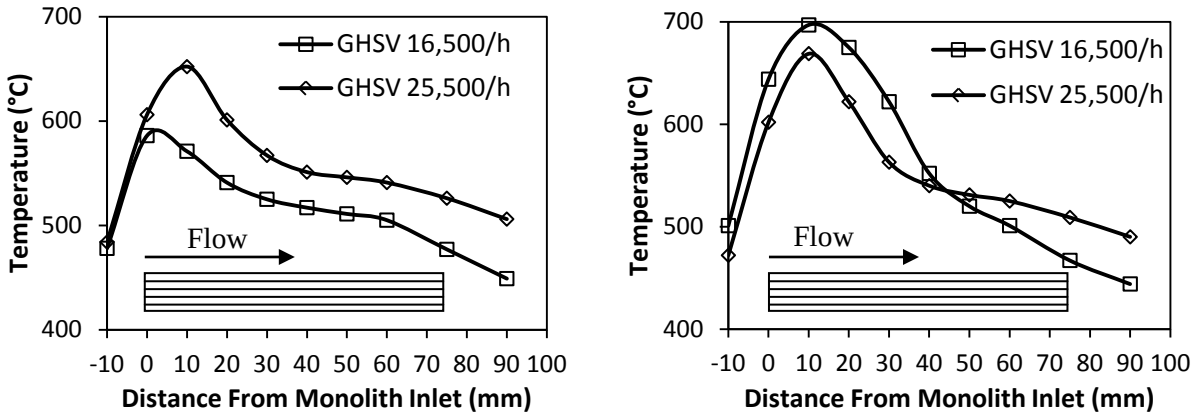


Figure 5.4: Effects of GHSV on the reactor temperature profile at $O_2/CH_4$ molar ratio 0.5 at: (a) engine condition 2 (b) engine condition 3

## 5.3 Reactor Product Distribution

### 5.3.1 Engine Condition Effects on Overall Reactor Product Distribution

As mentioned earlier, the reforming catalyst was inactive at the low exhaust temperatures in engine condition 1. This is confirmed in Figure 5.5 and 5.6 which shows that none of the oxygen fed into the reactor was consumed and the hydrogen and carbon monoxide yields remained 0 throughout all conditions used.

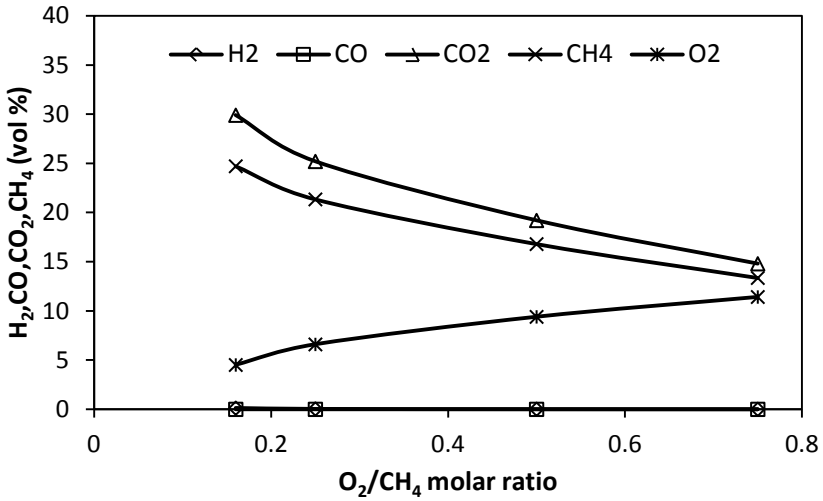


Figure 5.5: Reactor gas product distribution at engine condition 1 and 16,500 $h^{-1}$.

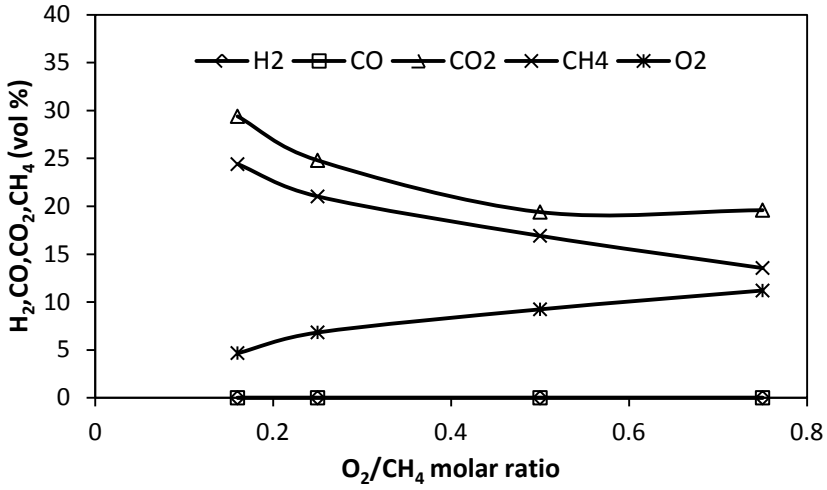


Figure 5.6: Reactor gas product distribution at engine condition 1 and 25,500 $h^{-1}$.

Upon increasing the engine operating load from low to medium and thus raising the exhaust gas temperature from approximately 186 to 295 °C, exhaust gas fuel reforming activity was observed for both engine conditions 2 and 3, with all the oxygen content being consumed and hydrogen being formed (Figure 5.7 – 5.10). As mentioned earlier, an increase in the $O_2/CH_4$ molar ratio increases the oxidative reforming activities (POX process and complete combustion) which raised the temperature along the catalyst bed and hence, increased hydrogen and carbon monoxide production through the promotion of endothermic reforming reactions for all test conditions.

At engine condition 2 (i.e. 0% EGR), by comparing Figure 5.7 and 5.8, it can be deduced that the POX process of biogas was promoted at high GHSV of 25,500 $h^{-1}$ whereby higher hydrogen and carbon monoxide yields were observed at high $O_2/CH_4$ molar ratios. Nonetheless, the effect of GHSV on the hydrogen production was much less significant at engine condition 3 (20% EGR) as shown in Figure 5.9 and 5.10. The effect of using the exhaust gas from the engine operated with EGR on the hydrogen production can be seen by comparing Figures 5.7 and 5.8 to Figures 5.9 and 5.10. It was observed that the addition of EGR at low GHSV and low $O_2/CH_4$ molar ratios benefits hydrogen production, due to increase in SRR process of biogas. In addition, despite producing more hydrogen with the introduction of EGR into the engine system, the methane conversion at low GHSV remained lower for all the $O_2/CH_4$ molar ratios implemented (Figure 5.11). This is beneficial for the overall exhaust gas reforming process efficiency as there will be more combustible product gas present in the reformate.

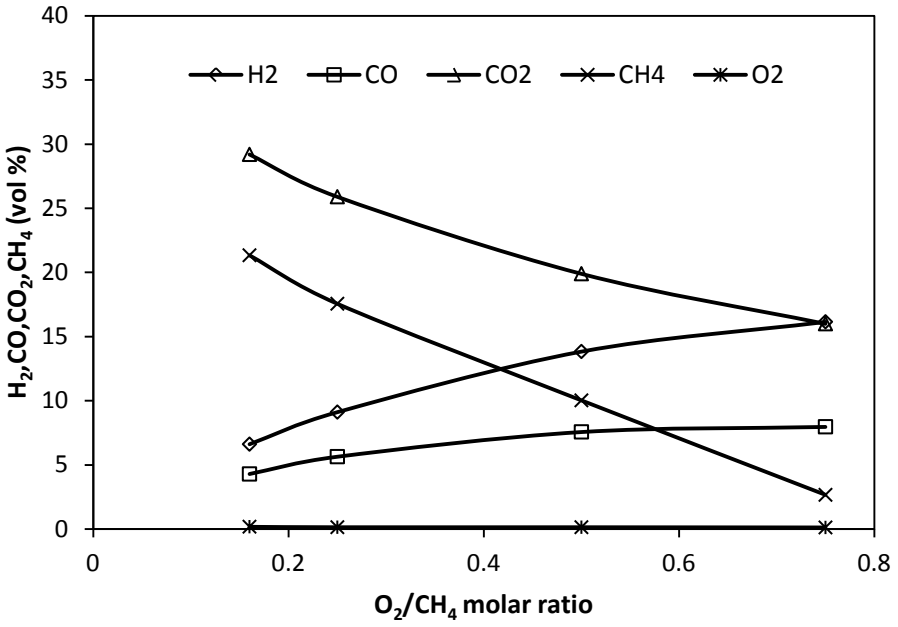


Figure 5.7: Reactor gas product distribution at engine condition 2 and 16,500 $h^{-1}$.

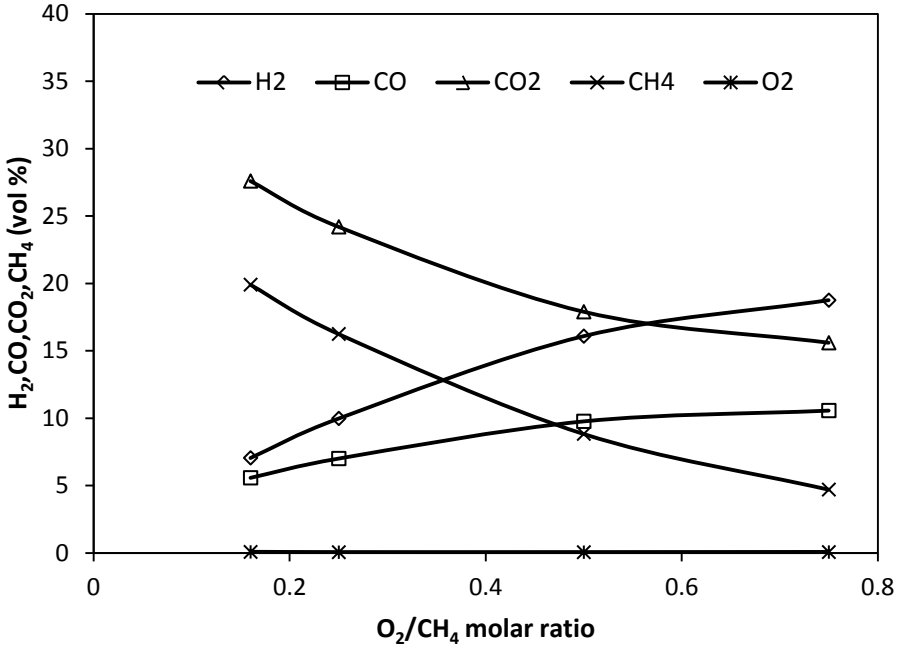


Figure 5.8: Reactor gas product distribution at engine condition 2 and 25,500 $h^{-1}$.

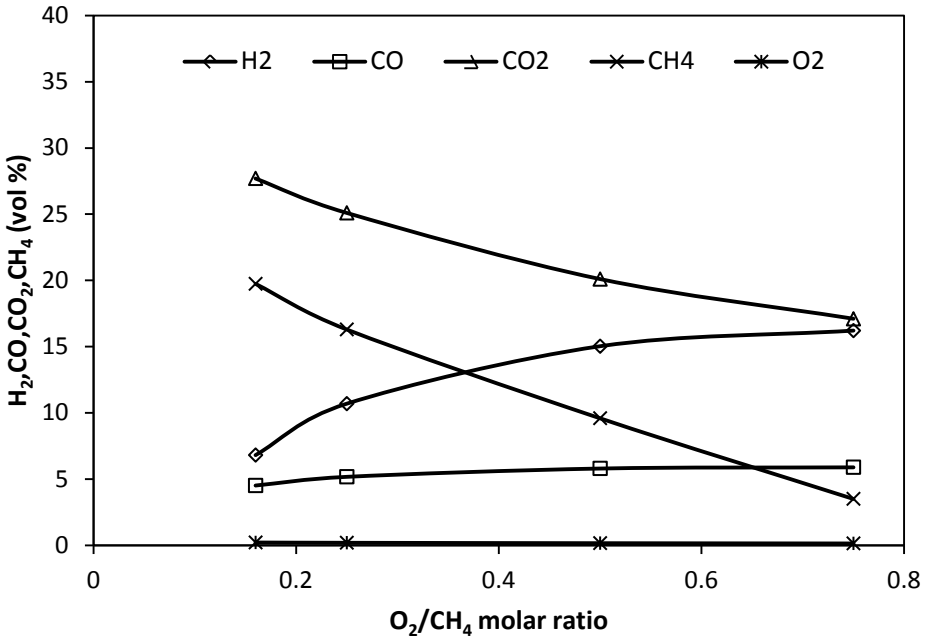


Figure 5.9: Reactor gas product distribution at engine condition 3 (20% EGR) and 16,500 $h^{-1}$.

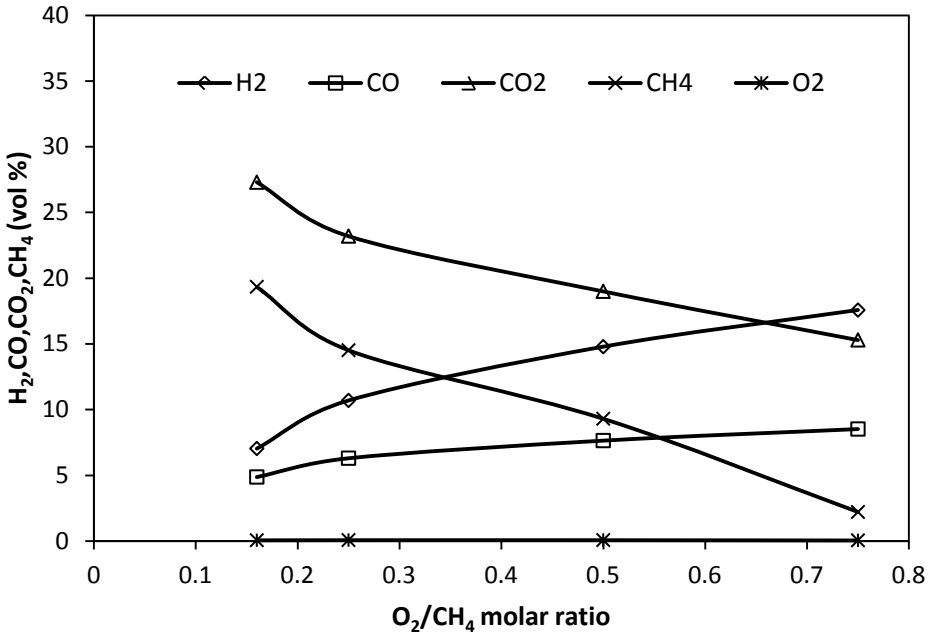


Figure 5.10: Reactor gas product distribution at engine condition 3 (20% EGR) and 25,500 $h^{-1}$.

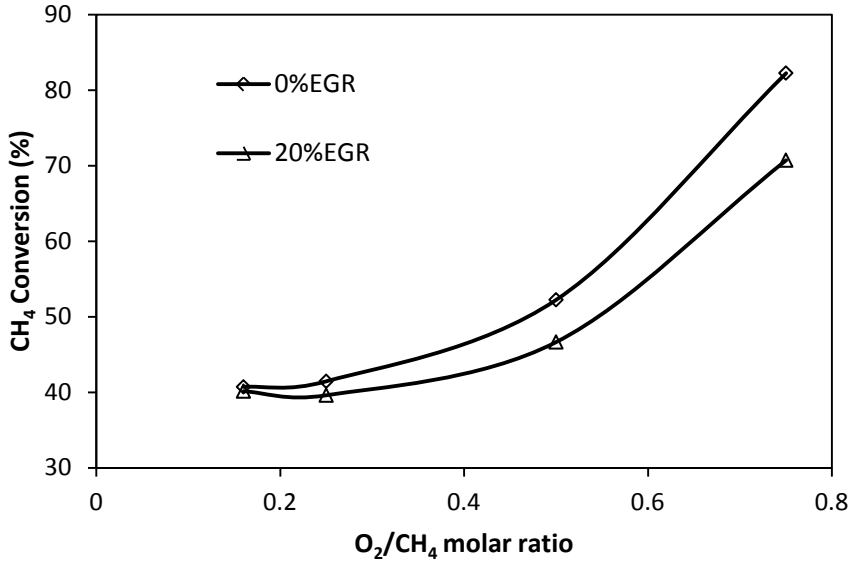


Figure 5.11: Methane conversion at GHSV: 16,500 $h^{-1}$ at engine condition 2 (0% EGR) and engine condition 3 (20% EGR).

### 5.3.2 Engine Condition Effects on Individual Reforming Reactions

According to Table 5.1, the introduction of EGR (i.e. engine condition 3) increases the steam and carbon dioxide content in the engine exhaust, resulting in higher $H_2O/CH_4$ and $CO_2/CH_4$ molar ratios in the reactor gas feed at each test point (Table 5.3). It was shown by Simeone et al. (2008) that the positive effect of increasing $H_2O/CH_4$ molar ratio was more pronounced at the low $O_2/CH_4$ molar ratio test conditions, which is consistent with the experimental results obtained in Figure 5.7 – 5.10 at $O_2/CH_4$ of 0.16 and 0.25.

Based on Eq. 2.1, 2.3 and 2.5, the stoichiometric $H_2/CO$ product molar ratios for the SRR, POX and DRR processes are 3, 2 and 1 respectively. At 0% EGR (engine condition 2) in Figure 5.12(a), the increase in $H_2/CO$ molar ratio in the reactor product gas ran parallel for both GHSVs throughout the different $O_2/CH_4$ molar ratios used, reaching a maximum value of approximately 1.8, reflecting the high CO yield at this operating condition. Therefore, it

could be concluded that the SRR process of biogas is less reactive at 0% EGR. In this condition, oxidative reforming reactions predominate, with the POX process of biogas occurring at the low $O_2/CH_4$ molar ratios and catalytic combustion of biogas being favourable under high $O_2/CH_4$ molar ratios (Horn et al., 2007). This is proven from the result trend involving higher methane conversion (Figure 5.11) with lower hydrogen yield (Figure 5.7 – 5.8) at engine condition 2.

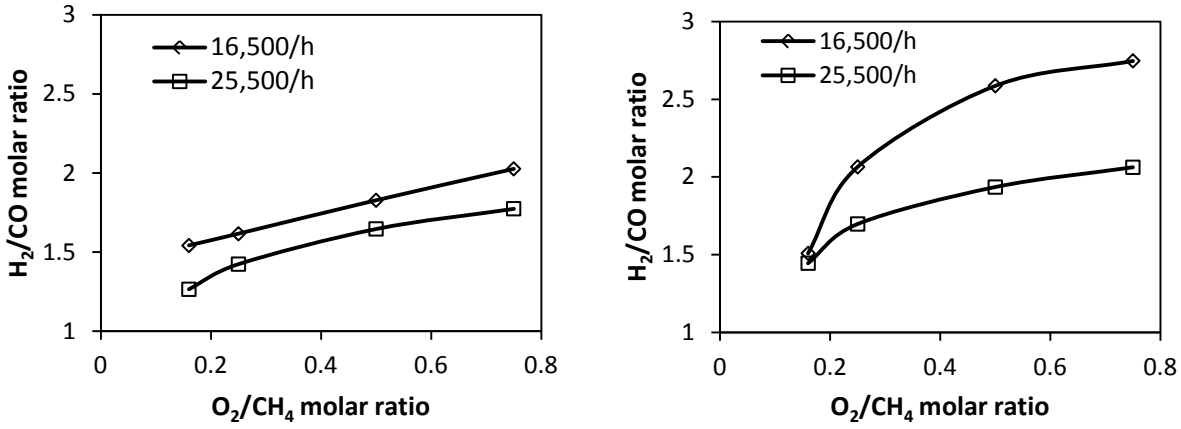


(a) (b)

Figure 5.12: Effect of different GHSVs on the $H_2/CO$ product molar ratio at: (a) engine condition 2 (b) engine condition 3.

With the application of 20% EGR at engine condition 3, a large increase in the $H_2/CO$ product molar ratios was observed, especially at the low GHSV level (Figure 5.12(b)). The maximum value reached is approximately 2.7 at the highest $O_2/CH_4$ molar ratio, compared to that of only 1.8 at engine condition 2. This shows that the SRR process of biogas is significant at 20% EGR ratio and the low GHSV condition helps promote that endothermic activity. In addition, as shown in Table 5.1 the application of EGR on the engine system not only increases the steam content but the carbon dioxide content as well. Hence, it can be said that the increase in $H_2O/CH_4$ and $CO_2/CH_4$ molar ratios comes in tandem (by comparing engine condition 2 and 3 in Table 5.3). This increase in $CO_2/CH_4$ molar ratio at high $O_2/CH_4$ molar

ratio test conditions promotes the DRR process of biogas, especially at the low GHSV due to the slow reacting nature of the endothermic process as explained earlier in Chapter 4.

As mentioned earlier, the stoichiometric $H_2$/CO product molar ratios for the DRR and SRR processes are 1 and 3 respectively. Hence, from the rapid decline in the incremental rate for the $H_2$/CO product molar ratios at 16,500 $h^{-1}$ with EGR (Figure 5.12(b)), it can be deduced that there is a shifting trend in reforming reactions from SRR to DRR processes at this condition. This increase in the DRR process activity not only reduces the carbon dioxide content in the reformate, it is also beneficial to the overall exhaust gas reforming process as DRR has been reported to have potential benefits in reducing the formation of carbon depositions that can occur through methane dissociation from biogas (Nagai et al., 2007).

Apart from the SRR process of biogas, implementing EGR in the engine system also promotes the secondary WGSR process due to the excess steam from the engine exhaust, as explained in the Literature Review section. In general, the WGSR process can be constrained either kinetically by the low residence time between biogas and the catalyst active sites or thermodynamically by the high temperature environment inside the reforming reactor. Since based on Figure 5.2 it can be seen that the peak temperatures inside the reforming reactor ranges from approximately 500 °C to 700 °C, which is the optimum range for the WGSR over the Pt-Rh based reforming catalyst (Tsolakis and Golunski, 2006), the kinetic effect seems more significant for the study in this chapter. This is shown by the relatively low carbon monoxide level in the reactor product gas at low GHSV of 16,500 $h^{-1}$ and engine condition 3, showing that part of the carbon monoxide produced from the other primary reforming processes was consumed in the WGSR process to produce more hydrogen.

Figure 5.13 summarizes the overall hydrogen production distribution at engine conditions 2 and 3. In general, the implementation of 20% EGR onto the engine system improves hydrogen production due to the promotion of SRR process of biogas (i.e. the highest hydrogen yield reforming reaction) and WGSR side reaction with increased steam content in the engine exhaust. Nonetheless, the hydrogen production peaked at the $O_2/CH_4$ molar ratio of 0.75 with 0% EGR and 25,500 $h^{-1}$ in GHSV. This could mainly be explained from the fact that the complete combustion of methane was favourable at such reactor conditions, hence providing the excess heat and suitable temperature range (Figure 5.2) which activates the SRR and DRR processes of biogas. However, it should be noted that the high hydrogen yield might come with a price of increased fuel penalty on the overall reforming process efficiency as more non-combustible carbon dioxide and steam were produced from complete oxidation of biogas. This is further discussed in the following section.

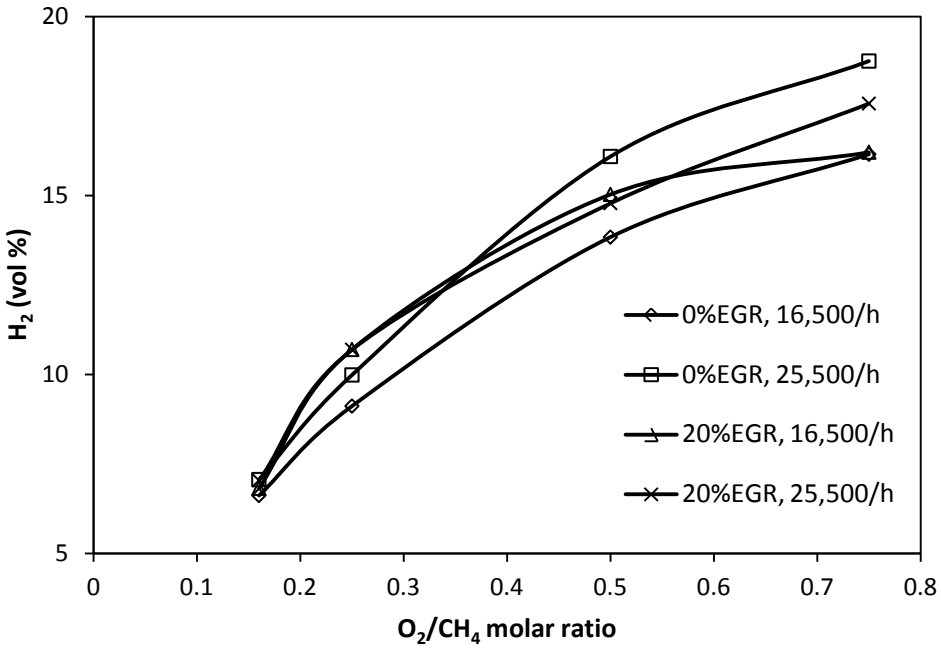


Figure 5.13: Reactor hydrogen product distribution at GHSV 16,500 $h^{-1}$ and 25,500 $h^{-1}$ and engine condition 2 and 3.

## 5.4 Exhaust Reforming Process Efficiency

As defined earlier in Eq. 4.4, reforming process efficiency is the ratio of the total chemical energy associated with the reformer gaseous product to the reactor energy input. Since the aim of this thesis is to investigate the upgrading of biogas for use in vehicular applications, the output energy for the biogas exhaust fuel reforming process includes the chemical energy associated with all the reactor gaseous products which are combustible in the dual fuel operation (i.e. hydrogen, carbon monoxide and unreacted methane). On the contrary, the energy input is simply defined as the chemical energy of the biogas being fed into the reactor. Nonetheless, from Table 5.1 it can be seen that even though there are some gases present in the engine exhaust that could potentially be used in the reforming process (e.g. carbon monoxide and unburned hydrocarbons from diesel combustion), these gases are present in small amount and so is not being taken into account.

In general, it can be observed from Figure 5.14 that increasing $O_2/CH_4$ molar ratio at 0% EGR engine condition improves the reforming process efficiency at the high GHSV, with a drop in efficiency at the maximum $O_2/CH_4$ molar ratio at low GHSV conditions. This is mainly because the high GHSV promotes the POX process of biogas which produces more hydrogen with higher calorific value and hence, increases the overall process efficiency. Nonetheless, the reforming process efficiency was improved throughout all test conditions with the introduction of 20% EGR onto the engine system. There are two main factors contributing to this beneficial effect. Firstly, it was shown in Figure 5.3 that with EGR, the overall temperature along the catalyst bed was partly increased. Thus, the combination of high catalyst bed temperature and high steam content in the reactor promotes the endothermic SRR activity which helps reduce the generation of waste heat energy. The second factor is mainly

due to the volumetric flow rate of reactor biogas feeds. As shown in Table 5.2, in order to compensate for the lower exhaust oxygen content at 20% EGR condition, higher amounts of engine exhaust gas and hence less biogas were being fed into the reforming reactor. Since there was no energy contribution from the engine exhaust, this simply reduces the energy input into the reforming reactor and therefore increasing the overall process efficiency.

The maximum process efficiency achieved by the biogas exhaust reforming is approximately 95% with engine condition 3 (20% EGR) at 25,500 $h^{-1}$ GHSV and the $O_2/CH_4$ molar ratio of 0.5, which corresponds to the $O_2/CH_4$ molar ratio for the stoichiometric POX process (Eq. 2.3). Further increasing the $O_2/CH_4$ molar ratios causes complete oxidation (Eq. 2.4) to occur which increases the generation of waste heat energy, thus decreasing the reforming process efficiency. Therefore, by optimizing the biogas and engine exhaust gas feed ratios, biogas could be upgraded with a minimal loss in the energy content.

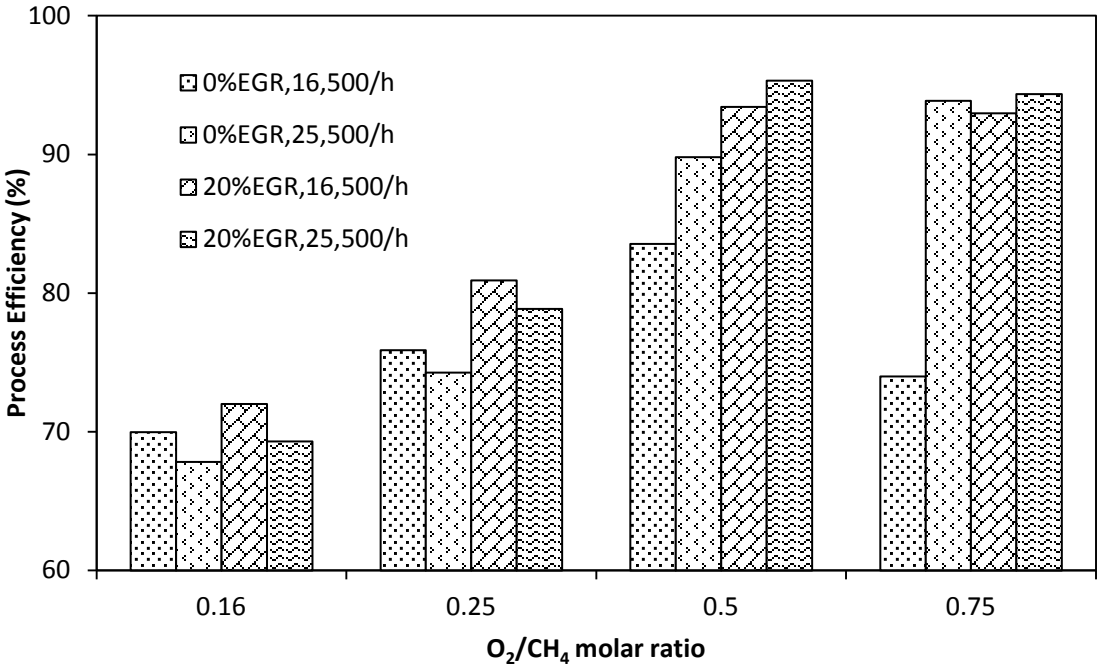


Figure 5.14: Effect of $O_2/CH_4$ molar ratios on the overall exhaust reforming process efficiency.

## 5.5 Summary

The upgrading of biogas through the exhaust gas fuel reforming process was performed at various engine conditions, $O_2/CH_4$ molar ratios and GHSVs. The main findings are summarized as follow:

- At low engine load, the extremely low engine exhaust temperature at approximately 186 °C was insufficient to achieve the light-off temperature of the reforming catalyst. Hence, no reforming activities were observed in this engine condition.
- At medium engine load (engine condition 2 and 3), it was shown that reactor product gas with up to 20% volume hydrogen production is achieved. In general, the increase in $O_2/CH_4$ molar ratios improves the hydrogen yield at both low and high GHSV conditions due to the increased temperatures along the catalyst bed.
- When no EGR was applied onto the engine system, the fast reacting exothermic POX process of biogas proves to be dominant and this reforming process was further enhanced at high GHSV condition.
- With the introduction of 20% EGR (i.e. engine condition 3), both SRR process of biogas and the WGSR side reactions become increasingly active due to the high steam content present in the engine exhaust gas which promotes the forward reaction for the two endothermic reforming processes. In contrast to POX process, SRR process of biogas and WGSR was enhanced at low GHSV, with higher hydrogen yield at 16,500 $h^{-1}$.
- In addition, it was also shown that the overall exhaust gas fuel reforming process efficiency was improved resulting from the higher reactivity of the endothermic reforming processes at engine condition 3. The maximum process efficiency reached was approximately 95%, showing that at optimum conditions biogas could be upgraded into

higher quality syngas with a minimal loss in the energy content at low exhaust temperatures.

# CHAPTER 6

# PERFORMANCE OF THE BIOGAS EXHAUST GAS FUEL REFORMING PROCESS AND THE GAS – DIESEL DUAL FUEL OPERATION WITH REGR

## 6.1 Introduction

This chapter investigates the performance of the exhaust gas fuel reforming process for upgrading biogas in the engine – reactor system and the effect of adding reformate gaseous fuel through REGR on the combustion efficiency and emissions of the gas-diesel dual fuel operation. As shown in the Literature Review section (Figure 2.10), the REGR operation was achieved by coupling the exhaust gas fuel reforming process with the diesel engine operation, directly feeding the reformer product gas into the engine air intake and hence forming the engine – reactor system. Figure 3.4 illustrates the experimental setup for the engine – reactor system described in this chapter.

For the experiments conducted in this chapter, the engine operating condition used was 1500 rpm engine speed with 3.5 bar IMEP (representing 45% engine load). In addition, based on the findings from Chapter 5, it was shown that the amount of EGR implemented on the engine system has a significant effect on the overall reforming process efficiency. Hence 0%, 10% and 20% EGR were applied to the engine operating condition and the corresponding engine exhaust gas was fed directly into the reforming reactor. For the exhaust gas fuel reforming process, the GHSV was fixed at 25,500 $h^{-1}$ and the corresponding total reactor product outflow of 15 L/min representing 3% of the total engine air intake volumetric flow

was fed back into the engine (i.e. engine – reactor system). Hence, 3% REGR ratio is used throughout all the tests. The calculation of % REGR was done based on Eq. 5.2, similar to that of % EGR. The $O_2/CH_4$ molar ratios of 0.35 and 0.5 were implemented to study the effect of two different engine exhaust to biogas feed ratios on the reactor product composition and the overall reforming process efficiency. As explained in Chapter 5, the individual volumetric flow rate for both the biogas and engine exhaust gas being fed into the reforming reactor were altered for each test condition, maintaining a total reactor volumetric flow rate of 15 L/min (Table 6.1) corresponding to GHSV of 25,500 $h^{-1}$. In addition, Table 6.2 shows the respective $H_2O/CH_4$ and $CO_2/CH_4$ molar ratios at each test point.

Table 6.1: Measured individual exhaust and biogas reactor feed rate for each engine % EGR at 100 °C and atmospheric pressure (1 bar).

| Engine % EGR | $O_2/CH_4$ Molar Ratio | GHSV: 25,500 $h^{-1}$ | |
|---|---|---|---|
| | | Exhaust Flow (L/min) | Biogas Flow (L/min) |
| 0 | 0.35 | 10 | 5 |
| | 0.5 | 11 | 4 |
| 10 | 0.35 | 10.3 | 4.7 |
| | 0.5 | 11.4 | 3.6 |
| 20 | 0.35 | 10.5 | 4.5 |
| | 0.5 | 12 | 3 |

Table 6.2: $H_2O/CH_4$ and $CO_2/CH_4$ molar ratios at specified $O_2/CH_4$ molar ratio and EGR ratio.

| Engine % EGR | $O_2/CH_4$: 0.35 | | $O_2/CH_4$: 0.5 | |
|---|---|---|---|---|
| | $H_2O/CH_4$ | $CO_2/CH_4$ | $H_2O/CH_4$ | $CO_2/CH_4$ |
| 0 | 0.080 | 0.853 | 0.114 | 0.904 |
| 10 | 0.106 | 0.898 | 0.142 | 0.955 |
| 20 | 0.125 | 0.915 | 0.184 | 1.021 |

Comparison studies on the engine indicated thermal efficiency and emission analysis were performed for the 3 engine operations (i) pure diesel operation (ii) biogas-diesel dual fuel operation and (iii) reformate gas-diesel dual fuel operation (i.e. engine – reactor system).

The pure diesel operation was done by running the engine with ULSD at the start of each test. For the biogas-diesel dual fuel operation, the same amount of biogas used in the exhaust reforming process (Table 6.1) was fed directly into the engine air intake at each test point. It should be noted that during the dual fuel operations, the diesel fuel intake was reduced in order to maintain constant engine power. The engine indicated thermal efficiency was calculated as follow:

$$\text{Engine Indicated Thermal Effciency } (\eta_{th}),\ \% = \frac{\text{Indicated Power}}{\sum[\dot{m}_{\text{fuel in}} \times \text{LCV}_{\text{fuel in}}]} \tag{6.1}$$

$$\text{Indicated Power (IP)} = \frac{\text{IMEP} \times \text{Displaced volume} \times n \times K}{60000} \tag{6.2}$$

where $\dot{m}_{\text{fuel in}}$ and $\text{LCV}_{\text{fuel in}}$ are the total mass flow rate and lower calorific value for the diesel fuel and biogas respectively. n represents the number of power strokes per minute while K is the number of cylinders in the engine (i.e. K=1 for this thesis).

In calculating the engine indicated thermal efficiency for the reformate gas-diesel dual fuel operation, the biogas mass flow rate into the reforming reactor and not the mass flow rate of the combustible reactor gaseous products (i.e. hydrogen, carbon monoxide and unreacted methane) was considered. This is due to the fact that the engine – reactor system (Figure 2.10) starts with the input chemical energy for the reforming reactor (i.e. biogas) and ends with the engine power output. It was assumed that the biogas was upgraded into high quality syngas through the exhaust gas fuel reforming process by recovering the engine exhaust waste heat. Hence, the biogas energy input for both the reformate gas-diesel and biogas-diesel dual fuel operations are similar. Nonetheless, since the LCV of reformate gas differs from that of pure biogas, the liquid diesel fuel substitution level would be different, hence giving rise to

different values in engine indicated thermal efficiency obtained for both reformate gas-diesel and biogas-diesel dual fuel operations.

## 6.2 REGR Effects on Exhaust Gas Fuel Reforming Process

### 6.2.1 Reactor Product Distribution

The reactor gas product distribution shown in Figures 6.1 and 6.2 represents the REGR composition for the engine – reactor system. It was observed that there are two beneficial effects in increasing the $O_2/CH_4$ molar ratios. Firstly, there was an increase in hydrogen production from 20% at $O_2/CH_4$ molar ratio of 0.35 to 24% at 0.50. This increasing trend is consistent with the experimental results observed in chapter 4 and 5. In addition, compared to the maximum hydrogen production of only 20% for the biogas exhaust fuel reforming process in Chapter 5, it can be deduced that the implementation of REGR benefits hydrogen production with an increase in maximum hydrogen yield to 24%. It has been shown earlier that increasing steam content in the engine exhaust promotes the endothermic SRR process of biogas, resulting in high hydrogen yield. The engine – reactor system further increases the steam content in the engine exhaust through the combustion of the hydrogen present in the reformate, subsequently increasing hydrogen yield in the exhaust gas fuel reforming process.

The second beneficial effect of increasing the $O_2/CH_4$ molar ratios is the significant reduction in unreacted methane in the reactor gas product. As can be seen in Table 6.1, less amount of biogas was being fed into the reforming reactor at high $O_2/CH_4$ molar ratios and this simply reduces the amount of unreacted methane present. In addition, the increased $O_2/CH_4$ molar ratios in the reactor feed gas was shown to promote the oxidative reforming reactions, hence consuming more methane portion of biogas. As described in the Literature

Review section, unburned methane is the main constituent for biogas-diesel dual fuel emissions. The reduction of methane % volume present in reactor product gas (i.e. reformate) is crucial in reducing the UHC emissions and hence potentially improving the overall efficiency for the engine – reactor system. This is further discussed in the following sections in this chapter.

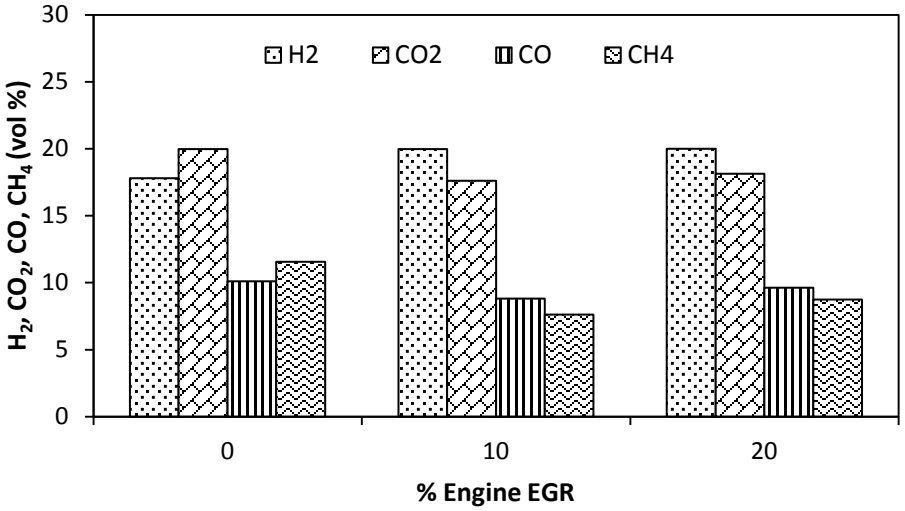


Figure 6.1: Reactor product gas distribution at $O_2/CH_4$ molar ratio of 0.35 and engine % EGR condition 0, 10 and 20.

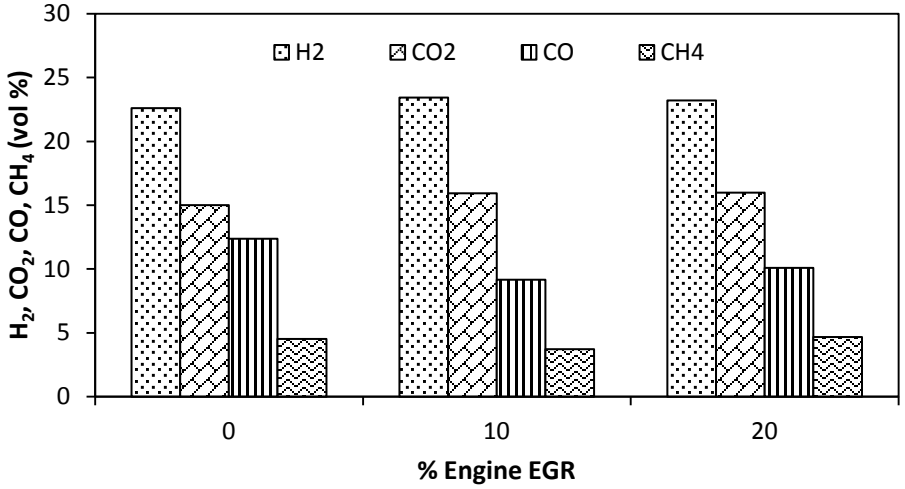


Figure 6.2: Reactor product gas distribution at $O_2/CH_4$ molar ratio of 0.5 and engine % EGR condition 0, 10 and 20.

### 6.2.2 Overall Reforming Process Efficiency

Figure 6.3 shows the overall reforming process efficiency for the engine – reactor system. By comparing Figure 6.3 to Figure 5.13, it was observed that the overall efficiency was improved with the implementation of the engine – reactor system, reaching a maximum value of 127% at $O_2/CH_4$ molar ratio of 0.5 and 20% EGR engine condition. This improvement in the process efficiency was mainly due to the increased hydrogen production from the higher $H_2O/CH_4$ molar ratio reactor gas feed conditions. At 0% EGR, the process efficiency drops when increasing the $O_2/CH_4$ molar ratio as the high oxidative reforming reactivity at that engine condition generates more waste heat. On the contrary, the significant increase in the endothermic SRR and DRR process of biogas due to the higher catalyst bed temperature at both 10% and 20% EGR engine conditions improves the overall process efficiency at high $O_2/CH_4$ molar ratio reactor gas feed conditions.

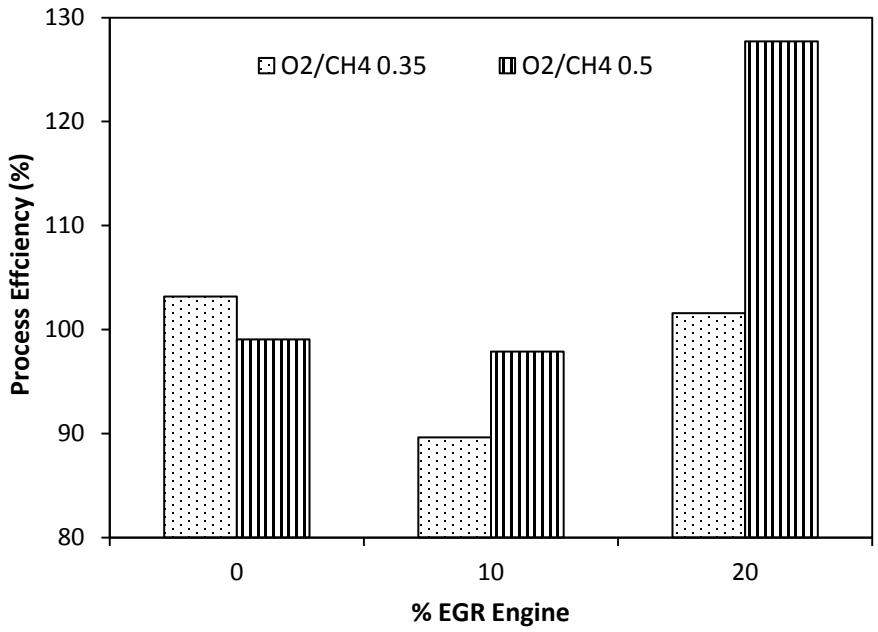


Figure 6.3: Effect of EGR application on the overall reforming process efficiency.

## 6.3 REGR Effects on Gas – Diesel Engine Performance

### 6.3.1 Engine Indicated Thermal Efficiency

Figure 6.4 presents the engine indicated thermal efficiency for the three engine operations, namely (i) pure diesel operation, (ii) biogas-diesel dual fuel operation and (iii) reformate gas-diesel dual fuel operation. It was clear that at engine part load operation (45% engine load) the induction of biogas into the engine (i.e. biogas-diesel operation) significantly reduces the engine thermal efficiency, with approximately 8% drop in engine indicated thermal efficiency compared to pure diesel operation (Figure 6.4). This is mainly due to the high amount of inert carbon dioxide present in biogas, which reduces the cylinder charge temperature and affects the burning velocity of the gaseous fuel-air mixture in the combustion chamber (Abd-Alla, 2002). This resulted in less gaseous fuel being effectively utilized in the dual fuel combustion process. Another factor contributing to the lower engine thermal efficiency is the displacement of a large volume of intake air by the biogas induction through the engine intake manifold due to the low heating value of biogas. The large volumetric flow rate of low energy content biogas reduces the air flow into the engine and in turn decreases the engine volumetric efficiency (Korakianitis et al., 2011).

The induction of reforming reactor product gas into the engine system proved to be superior in terms of engine thermal efficiency. From Figure 6.4, it can be seen that the engine thermal efficiency was significantly improved at all engine operating conditions, with a maximum increment value of almost 2%. In addition, a direct correlation is observed between Figure 6.3 and 6.4 whereby the increment trend in the engine thermal efficiency is directly affected by the overall efficiency of exhaust gas fuel reforming process, showing that the

exhaust reforming process and engine combustion characteristics within the engine - reactor system are closely coupled.

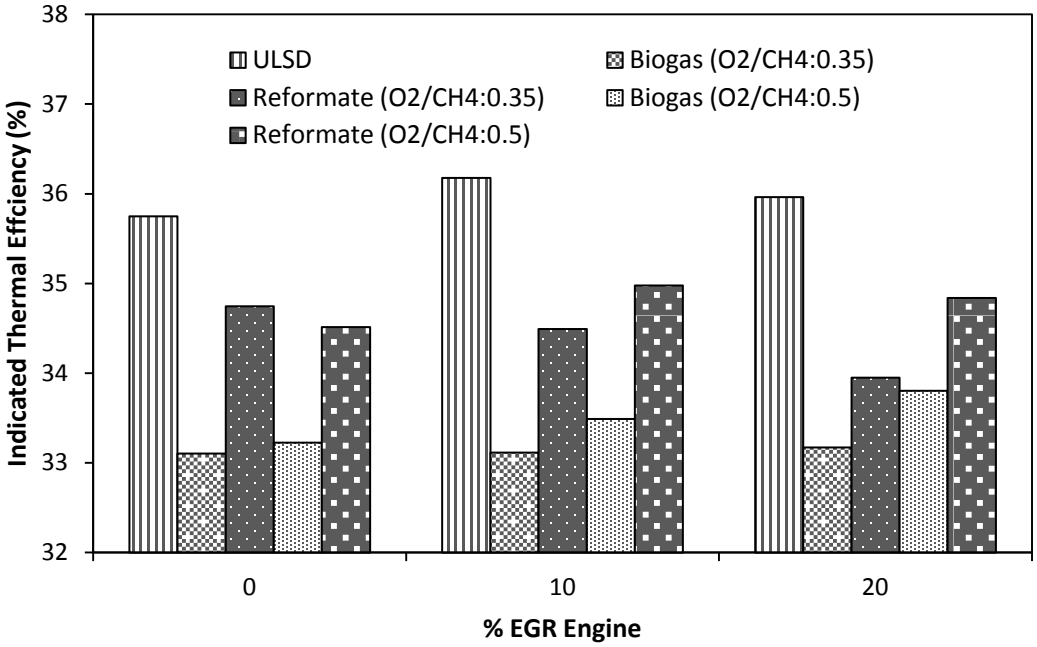


Figure 6.4: Engine indicated thermal efficiency for (i) pure diesel operation (ii) biogas-diesel operation (iii) reformate gas-diesel operation at % EGR condition: 0, 10 and 20.

There are two main reasons contributing to the higher engine thermal efficiency for the reformate gas-diesel operation, (i) the reduced amount of carbon dioxide in the reformate gas compared to biogas and (ii) the positive effects of inducting hydrogen and carbon monoxide into the combustion chamber. Based on the experimental findings in Chapter 4 and 5, it was shown that the carbon dioxide present in biogas was reformed into comparatively higher flammable hydrogen and carbon monoxide gaseous fuels through the biogas DRR process. This reduction in carbon dioxide improves the flame propagation from the diesel pilot ignition point to the surrounding gaseous fuel-air mixture, as explained in the Literature Review section.

Apart from the lower amount of inert carbon dioxide present in the cylinder charge, the hydrogen-air mixture has higher laminar burning velocity and lower minimum ignition energy (an order of magnitude lower) compared to that of the methane-air mixture (Ono et al., 2007). These superior properties of hydrogen-air mixture enhanced the flame propagation and improved the combustion process of the total gaseous fuel-air mixture; hence decreasing the amount of unburned methane in the exhaust and increases the engine thermal efficiency. It should also be noted that no hydrogen was detected in the engine exhaust throughout all the test conditions, showing that the combustion of hydrogen is complete. In addition, the higher energy content of hydrogen and carbon monoxide present in reformate also contributed to the higher engine thermal efficiency in the reformate gas-diesel operation. Nonetheless, it was shown in Figure 6.3 and 6.4 that the highest reforming process efficiency obtained at 20% EGR engine condition and $O_2/CH_4$ molar ratio of 0.5 does not correspond to the highest improvement in the engine thermal efficiency at that particular test condition. This is mainly due to the fact that at 20% EGR engine condition, the comparatively high amount of inert carbon dioxide being recirculated back into the combustion chamber through EGR adversely affects the flame propagation within the reformate gas-air mixture (Chigier, 1981).

### 6.3.2 Engine Cylinder Pressure and Heat Release Rate

Figure 6.5 shows the in cylinder pressure and rate of heat release (ROHR) diagram for both pure diesel and reformate gas-diesel operations at 0% EGR engine condition. Due to the small quantity of REGR used (3% volume of the total air intake), it can be seen that the introduction of reformate gaseous fuel into the combustion chamber does not significantly affect the overall trend of the combustion process. Nonetheless, the ignition delay was prolonged and the cylinder peak pressure was slightly reduced compared to the pure diesel

operation. The increase in ignition delay was mainly due to the reduced oxygen content (replacement by REGR) in the cylinder charge mixture which led to the reduction in the reformate gas-air mixture temperature during the compression stroke. In addition, the higher specific heat capacity of the reformate gas-air mixture also decreased the temperature increment of the cylinder charge and hence resulted in longer ignition delays. The slightly decreased cylinder peak pressure was mainly due to the presence of inert gases (i.e. carbon dioxide and steam) in the combustion chamber which inhibits the burning velocity of the reformate gas-air mixture. The overall longer ignition delay caused the pilot diesel to auto-ignite at a later stage, which then starts burning the gaseous fuel surrounding the ignition region of the pilot diesel, hence contributing to the slightly higher ROHR at the diffusion combustion phase. In general, the overall combustion stability was not affected in the engine – reactor system.

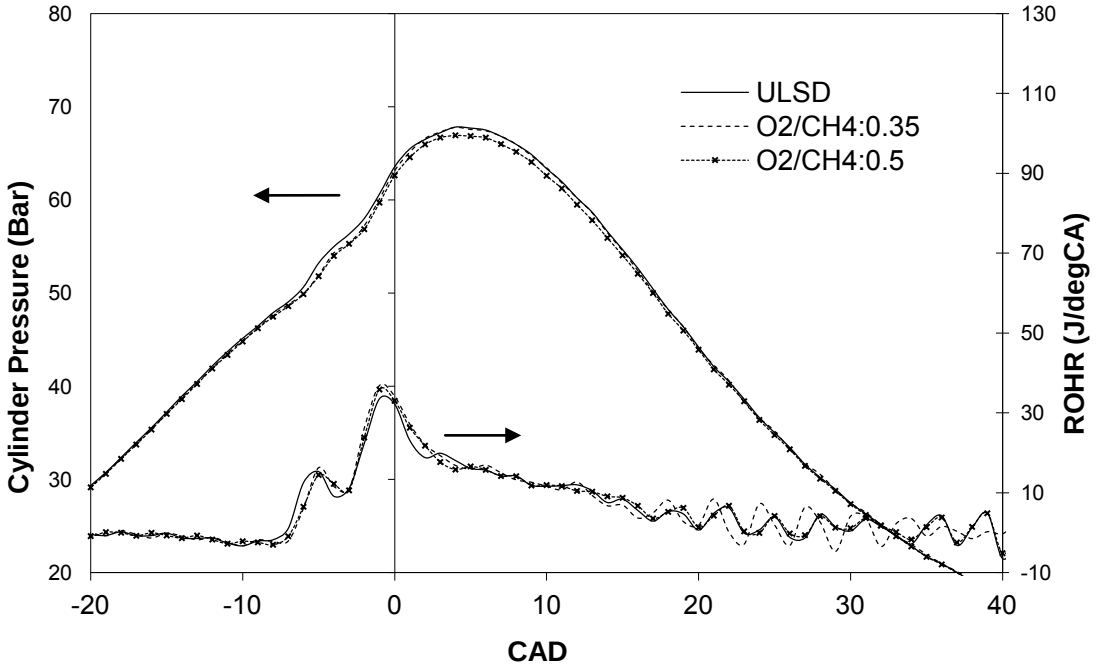


Figure 6.5: In-cylinder pressure and rate of heat release for pure diesel and reformate gas-diesel operations at 0% EGR engine condition.

### 6.3.3 Fossil Fuel Replacement

As stated in the Introduction section, the main goal of utilizing biogas for vehicular applications is that it is a renewable source of energy, hence potentially reducing dependence on the use of fossil fuels. Figure 6.6 shows the percentage replacement of fossil diesel fuel (i.e. ULSD) achieved for both biogas-diesel and reformate gas-diesel operations in energy basis. It can be seen that there was substantial amount of liquid diesel being replaced (maximum fossil fuel replacement of approximately 14%) even with small amount of gaseous fuel used (Table 6.1). In addition, the liquid diesel replacement was significantly higher in the engine – reactor system, mainly due to the higher energy content of reformate and less unburned methane being emitted into the atmosphere as wasted chemical energy through the engine exhaust.

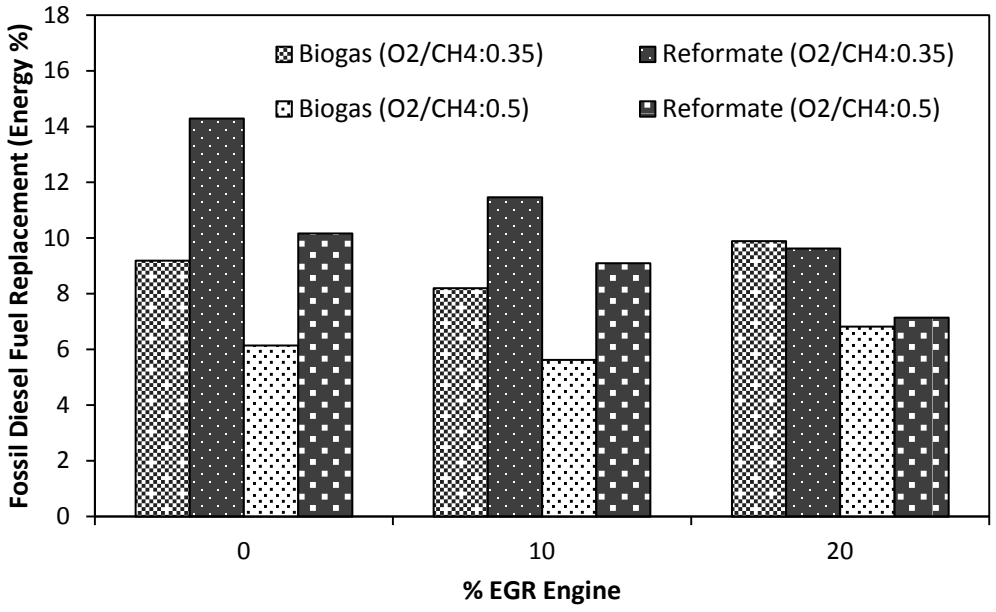


Figure 6.6: Percentage fossil fuel substitution for both dual fuel operations in energy basis.

### 6.3.4 UHC and CO Emissions

It was explained in the Literature Review section that one of the main disadvantage for using gaseous fuel is the high amount of unburned hydrocarbon (UHC) emissions present in the engine exhaust, especially at engine part load operating conditions. In this chapter, the main constituent of the UHC consists of unburned methane in the combustion chamber originating either from biogas or reformate gaseous fuel. Figure 6.7 shows the amount of unburned methane in the exhaust emissions for both the biogas-diesel and reformate gas-diesel operations. The pure diesel operation was represented at $O_2/CH_4$ molar ratio of 0. It can be seen that there is a significant reduction in unburned methane emission at all engine operating conditions when reformate is used compared to that of biogas-diesel operation. The main reason for this is the superior fuel properties of reformate over biogas which improves the combustion of the total gas-air mixture, hence reducing the amount of unburned methane in the combustion chamber. Another reason is due to the fact that part of the methane from biogas was being reformed into syngas, hence smaller amount of fresh methane was being inducted into the engine for the reformate gas-diesel operation. In addition, this reduction in unburned methane also contributed to the higher engine thermal efficiency as less gaseous fuel was being wasted in the engine exhaust.

Nonetheless, higher CO emission was found for the reformate gas-diesel operation (Figure 6.8). This is mainly due to the insufficient combustion of high amount of carbon monoxide present in reformate (Figure 6.1 and 6.2). For the biogas-diesel operation, the carbon monoxide was formed from the partial oxidation of the gaseous fuels in the vicinity of the pilot diesel combustion. It was also shown by Bari (1996) that the dissociation of carbon dioxide into carbon monoxide and oxygen is possible at high temperature conditions, leading to the high CO emissions during both dual fuel operations.

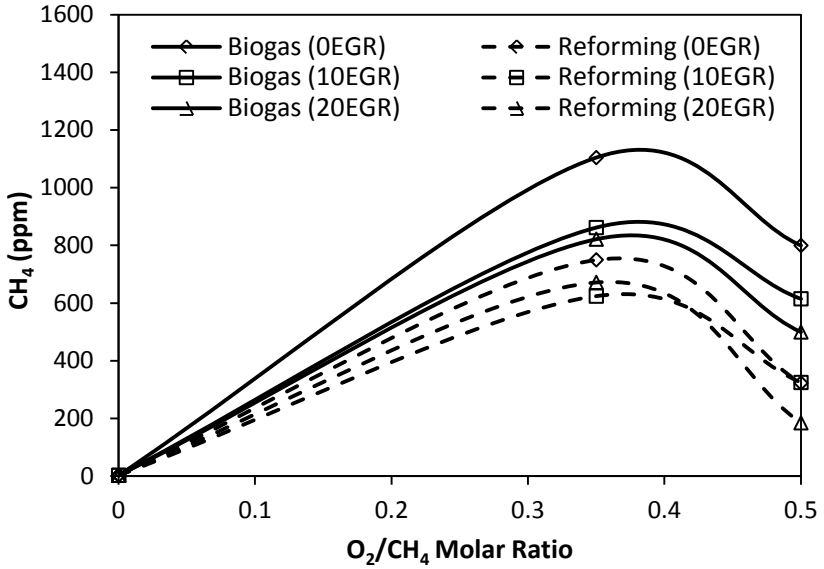


Figure 6.7: Unburned methane emission for the biogas-diesel and reformate gas-diesel operations at $O_2/CH_4$ molar ratio 0, 0.35, 0.50.

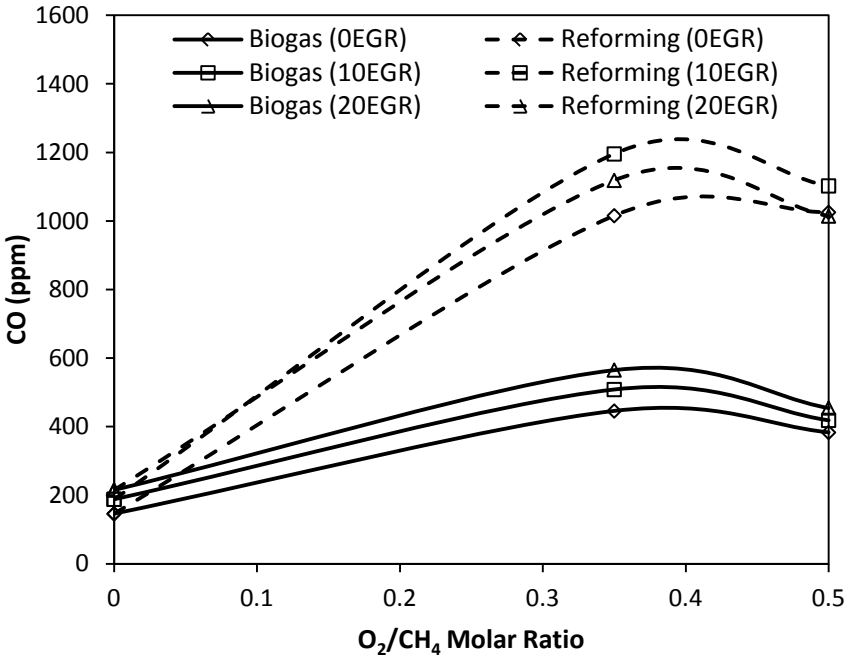


Figure 6.8: CO emission for the biogas-diesel and reformate gas-diesel operations at $O_2/CH_4$ molar ratio of 0, 0.35, 0.50.

### 6.3.5 NOx Emission

There was a significant drop in NOx emission level with the usage of both gaseous fuels (i.e. biogas and reformate) at all engine operating conditions compared to that of pure diesel operation (Figure 6.12). This reduction in NOx emission for dual fuel operations was mainly due to the lower cylinder charge temperature and it was explained in detailed in the Literature Review section. Moreover, from Figure 6.12, the use of reformate in the engine decreases the NOx emission level even further compared to when biogas is being used. It was shown by Shrestha et al. (2000) that small quantity of hydrogen (i.e. from reformate) present in the combustion chamber reduces the NOx formation due to its combustion characteristics. In general, hydrogen burns more rapidly and cleanly compared to both liquid diesel fuel and biogas as the smaller size molecules of hydrogen enters the combustion reaction at a higher velocity (hence the high flame propagation speed of hydrogen). In addition, the lower activation energy of hydrogen incurs more molecular collisions than other heavier molecules. These superior characteristics of hydrogen are believed to improve the combustion process of the gaseous fuel-air mixture and reduce hot spots within the combustion chamber which acts as the main contributor for the formation of NOx (Gomes Antunes et al., 2009). Additionally, Masood et al. (2007) also shows that adding hydrogen increases the mole fraction of steam present in the combustion chamber (from hydrogen combustion) which subsequently brought down the cylinder peak temperature and hence further decreasing the NOx emission level.

Figure 6.9 and 6.10 shows both NO and $NO_2$ distributions in the engine exhaust emissions. In overall, the use of gaseous fuels (i.e. either biogas or reformate) in the engine significantly reduces the NO level while increasing the $NO_2$ level in the engine emissions compared to that of pure diesel operation. The end result is a drop in the overall NOx emission due to the fact that NO is the main constituent of NOx emission and the reduction in

NO level is greater than the increment in the $NO_2$ level. In addition, the usage of reformate in the engine – reactor system was seen to further decrease the NO while increasing the $NO_2$ emissions at all engine operating conditions. The major path in the formation of $NO_2$ was via the oxidation of NO with $HO_2$ as shown in Eq. 6.3 (Kuo, 2005). The presence of hydrogen in reformate effectively increases the $HO_2$ level in the combustion chamber, as shown experimentally by Bika et al. (2008) and numerically by Lilik et al. (2010) which then subsequently resulted in the increase in $NO_2$ emission level.

$$NO + HO_2 \leftrightarrow NO_2 + OH \tag{6.3}$$

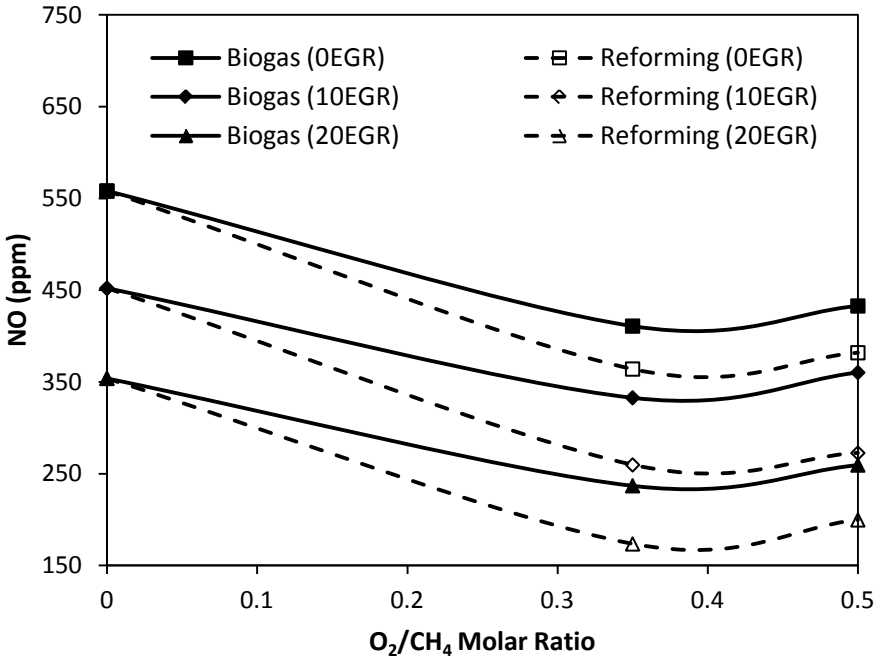


Figure 6.9: NO emission for biogas-diesel and reformate gas-diesel operations at $O_2/CH_4$ molar ratios of 0, 0.35, 0.50.

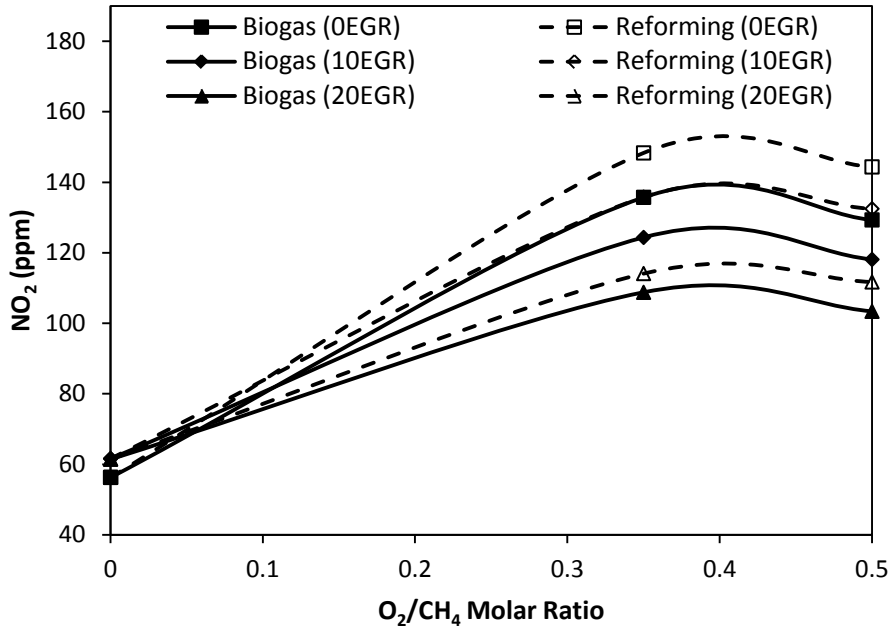


Figure 6.10: $NO_2$ emission for biogas-diesel and reformate gas-diesel operations at $O_2/CH_4$ molar ratios of 0, 0.35, 0.50.

### 6.3.6 Soot Emission

Figure 6.11 – 6.14 show the soot concentration and particle size distribution for both pure diesel and reformate gas-diesel operations. The total particle mass (Figure 6.13) were calculated using the particle number concentration distribution obtained from SMPS (Figure 6.11) and the density of the particles, by implementing the particle density calculation equation developed by Lapuerta et al. (2003). Based on Figure 6.11 – 6.14, it can be seen that increasing the EGR ratio increases the amount of particles in the engine exhaust for all test conditions, mainly due to the associated lower combustion temperature. In addition, the trend for the total particle mass (Figure 6.13) is consistent with the distribution of soot concentration (Figure 6.14).

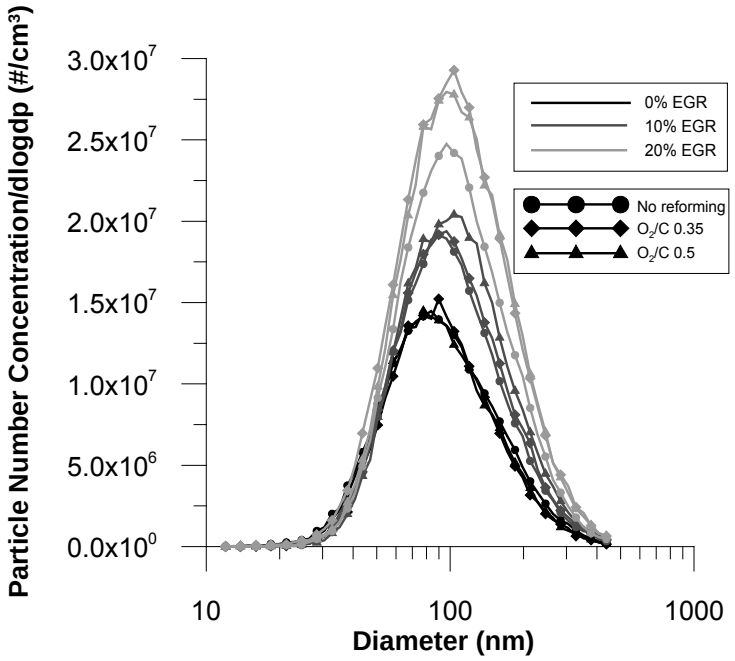


Figure 6.11: Particle number distribution for pure diesel operation (no reforming) and reformate gas-diesel dual fuel operation.

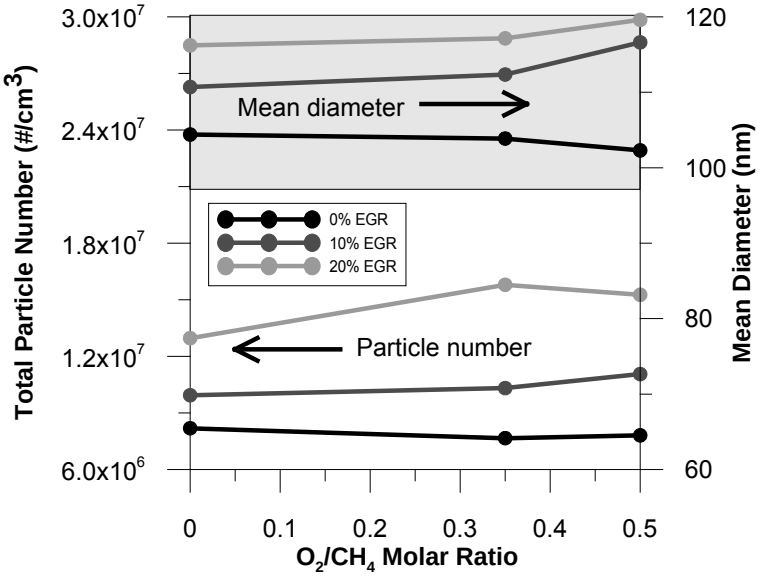


Figure 6.12: Total particle number and mean diameter for pure diesel operation and reformate gas-diesel dual fuel operation.

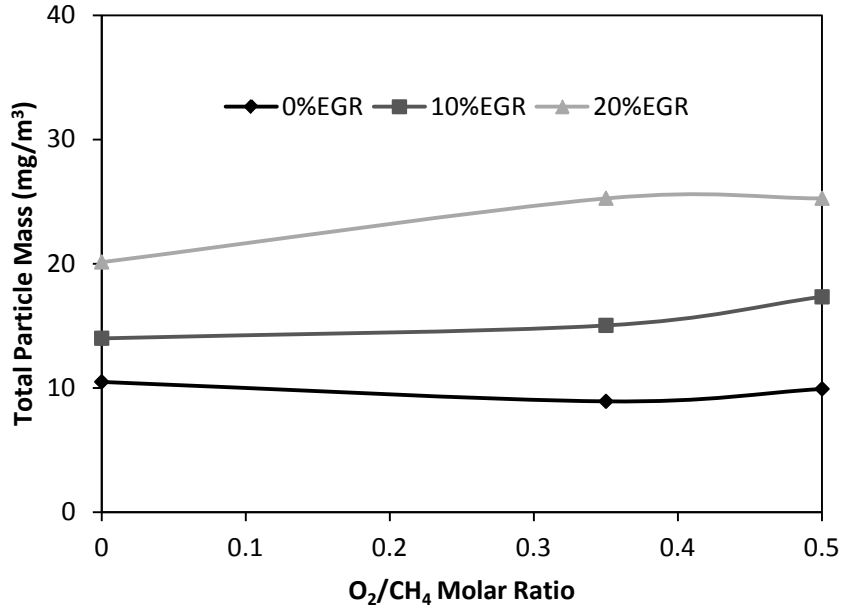


Figure 6.13: Total particle mass distribution for the pure diesel operation and reformate gas-diesel dual fuel operation.

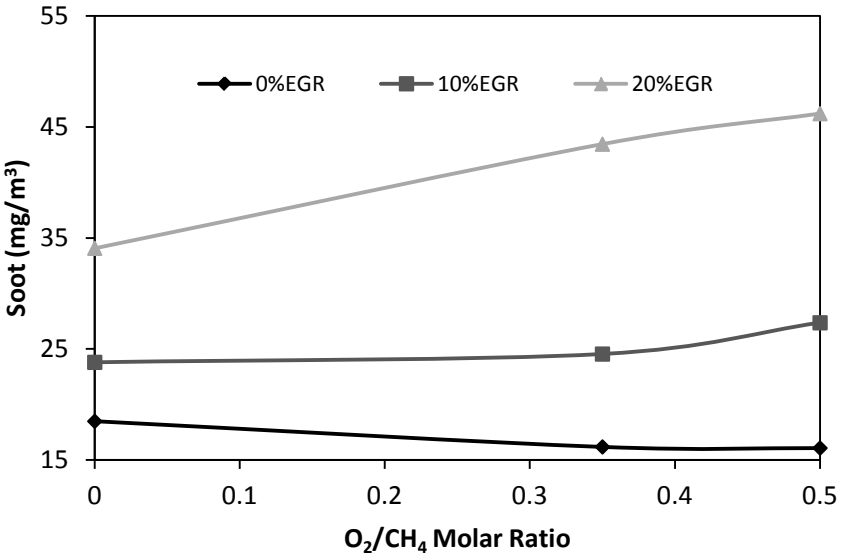


Figure 6.14: Soot concentration for pure diesel operation and reformate gas-diesel dual fuel operation.

At 0% EGR engine operating condition, the reduction in soot emission is mainly due to the reduction in pilot diesel fuel intake (i.e. main compound for soot formation) due to the gaseous fuel substitution. When comparing the use of both gaseous fuels (Figure 6.15), the higher energy content and the presence of less methane in the reformate compared to biogas resulted in the larger decrease in liquid fuel injected into the combustion chamber at constant engine power output, hence further decreasing the soot emission in the engine – reactor system at 0% EGR engine condition. Nonetheless, the simultaneous introduction of both EGR and reformate gaseous fuel (3% REGR) decreases the total volume of air intake into the engine and hence resulting in a drop in the λ value. The effect of adding gaseous fuel was only beneficial up to a certain level of engine intake air substitution level. Beyond that, the lack of oxygen in the combustion chamber (i.e. to reduce soot formation and promote soot oxidation) resulted in increasing soot emission (Mustafi and Raine, 2008). This resulted in the high soot emission level when reformate was being inducted into the engine at 20% EGR condition as the λ value decreases significantly from 2.93 (pure diesel operation) to 2.75 (reformate gas-diesel operation). This large drop in the λ value is mainly due to the fact that no oxygen is present in the REGR composition (i.e. reformate) for the combustion process. In addition, the lower cylinder charge temperature observed during the premixed combustion phase at low λ conditions demotes the soot oxidation process and hence further increases the soot emission level (Papagiannakis et al., 2010).

There is also the possibility of soot formation in the reforming reactor at 20% EGR engine condition which was then being fed directly into the engine. As shown by Pedersen-Mjaanes et al. (2005), the rich combustion of methane (i.e. POX reforming process) during the exhaust gas fuel reforming process promotes the formation of soot. Hence, it was speculated that at high EGR ratio, the high quantity of pre-existing soot present in the engine

exhaust which was then being fed into the reforming reactor could promote the formation of soot through both surface growth and coalescence process. This is shown in Figure 6.12 and 6.14 whereby at 20% EGR, the decrease in total particle number when $O_2/CH_4$ molar ratio was increased from 0.35 to 0.50 (increased exhaust gas feed rate into the reactor) was associated with the increase in both the particle mean diameter (coalescence) and soot mass concentration (surface growth).

### 6.3.7 Soot – NOx Emissions

Figure 6.15 summarizes the overall NOx and soot emissions for the different EGR ratios implemented in the engine system. It can be seen that the trade-off between soot and NOx is clear whereby as % EGR increases, there was a reduction in NOx emission together with an increase in soot emission. At low EGR ratio conditions the use of reformate is capable of reducing both NOx and soot simultaneously, breaking the trade-off. At 0% EGR, introducing reformate (at $O_2/CH_4$ molar ratio of 0.35) resulted in a reduction in NOx emission of up to 17% together with a 13% decrease in soot emission. Even though the addition of reformate at high EGR ratios further decreases the NOx emission, the overall soot emission was increased as explained earlier.

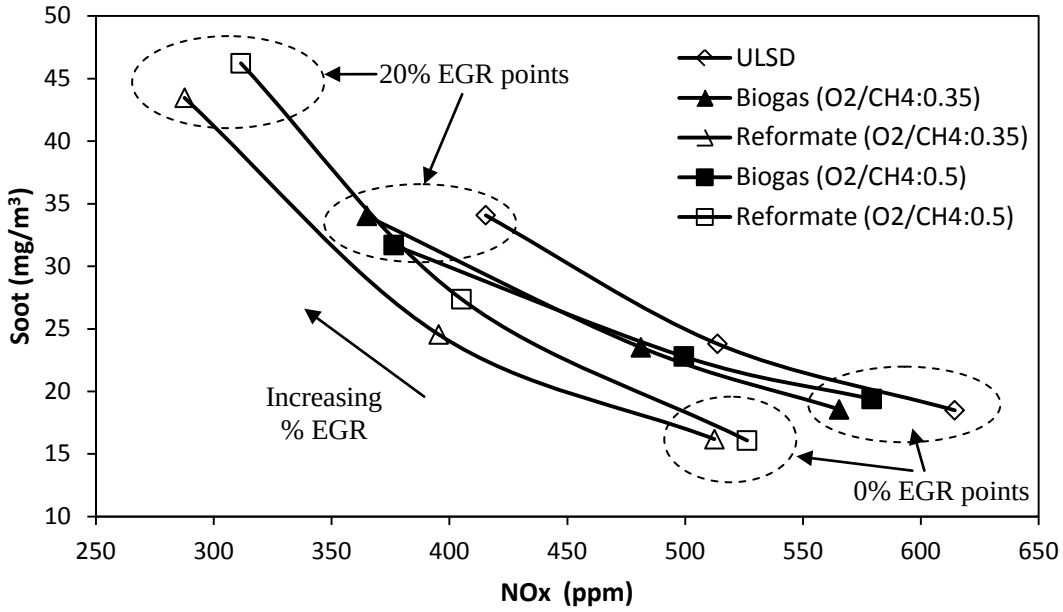


Figure 6.15: Soot – NOx emissions for pure diesel, biogas-diesel and reformate gas-diesel operations at all test conditions.

## 6.4 Summary

The investigation of the effects of implementing REGR in the engine – reactor system on both the biogas exhaust fuel reforming process and the engine performance for the gas-diesel operation was performed. The main findings were summarized as follow:

- Higher hydrogen production and an increase in the overall reforming process efficiency were observed in the engine – reactor system. This was mainly due to the increased endothermic SRR process of biogas resulted from the higher steam content (from hydrogen combustion) present in the engine exhaust gas.
- In terms of engine performance, it was shown that the engine indicated thermal efficiency for the reformate gas-diesel operation was significantly improved compared to that of biogas-diesel operation due to the superior properties of reformate gaseous fuel and the overall reduction in carbon dioxide content which improves the combustion process.

- Nonetheless, prolonged ignition delay and lower cylinder peak pressure was observed when both gaseous fuels (i.e. reformate and biogas) were inducted into the engine due to the reduced air intake and high specific heat capacity of the cylinder charge.
- The introduction of both biogas and reformate gaseous fuel into the engine have resulted in increased unburned methane and carbon monoxide emission levels compared to pure diesel operation due to insufficient combustion of both emission gases.
- During the dual fuel operations, NO emission was reduced while the $NO_2$ formation was somewhat enhanced and this trend was more prominent with the use of reformate. The overall NOx emission was significantly reduced with the induction of both gaseous fuels into the engine system due to the lower cylinder charge temperature.
- At low %EGR engine conditions, soot emission was decreased when REGR was implemented in the engine – reactor system as less liquid diesel fuel was injected due to substitution of liquid fuel by reformate. Nevertheless, a slight increase in soot emission was observed with increasing EGR ratio as high amount of inert gas and soot was being recirculated back into the engine system.
- In general, the engine – reactor system was deemed beneficial for dual fuel operations with higher engine thermal efficiency and greater fossil diesel fuel replacement. Moreover, both NOx and soot emission levels were reduced at low EGR ratios, hence breaking the PM-NOx trade off with the implementation of REGR in the engine – reactor system.

# CHAPTER 7

# CONCLUSIONS AND FUTURE WORK

## 7.1 Concluding Remarks

Preliminary equilibrium calculations and detailed experimental studies were done to investigate the potential of upgrading biogas into higher quality syngas. The upgrade of biogas through catalytic reforming reactions using a monolith reforming catalyst coated with 2%Pt and 1%Rh was first studied to understand the catalyst performance at various temperatures, gas hourly space velocities and feed rates test conditions. Subsequently, biogas upgrading at low exhaust temperature through catalytic exhaust gas fuel reforming process was investigated and reformate gaseous fuel (i.e. upgraded biogas) produced was fed directly into the engine air intake to study the system with REGR. The resulting effects of REGR on the biogas exhaust fuel reforming process were investigated. Finally, a comparison study was done to distinguish the key differences in the engine performance and emissions characteristics at part load condition when reformate and pure biogas were individually used as a fuel source for dual fuel operations. Equally important is the amount of fossil diesel fuel that was being successfully replaced in the dual fuel operations. The main findings of this research are further summarized as follow.

### 7.1.1 Biogas Upgrade to Syngas via Dry and Oxidative Reforming

Both equilibrium calculations and experimental work were done to investigate the reaction profile and process efficiency of biogas dry reforming and the effect of adding oxygen into the reactor at various $O_2/CH_4$ molar ratios on the overall reforming process. It

was concluded that syngas could be produced from biogas at high temperatures but the highly endothermic DRR process of biogas deteriorated at conditions of low temperature range and high GHSV, with low hydrogen yield generated. Nonetheless, the addition of oxygen into the reforming reactor significantly increased the hydrogen production at low temperatures due to the promotion of the exothermic oxidative reforming processes of methane present in biogas. In addition, the increase in temperature along the catalyst bed resulting from the exothermic processes also promoted the DRR process of biogas downstream the catalyst. As opposed to the slow reacting DRR process, the increase in GHSV promoted the POX reforming activity in the reactor. Nonetheless, at high temperatures the introduction of oxygen had little effect on the overall hydrogen yield as the DRR process of biogas remains the dominant reforming reaction.

### 7.1.2 Biogas Upgrade through Exhaust Gas Fuel Reforming Process with Engine Exhaust Waste Heat Recovery

Real exhaust gas from engine fuelled with ULSD at part load condition was fed directly into the reforming reactor together with biogas. Detailed studies were done on: (i) the reforming reaction temperature profiles and (ii) reformer product gas compositions for the catalytic exhaust gas fuel reforming process. It was shown that reformer product gas containing up to 20% hydrogen and having approximately similar energy content as the feed biogas can be produced at low exhaust temperature conditions. The maximum overall reforming process efficiency of approximately 95% was obtained. In addition, the reduction in carbon dioxide content in biogas resulting from converting it into high energy content reformate rendered it more suitable as a fuel source for use in IC engines.

Generally, increasing the $O_2/CH_4$ molar ratios of the feed gas into the reforming reactor increases the hydrogen production throughout all test conditions. When the engine is operated without EGR, the high oxygen and low steam content in the exhaust promoted the POX process of biogas and this reaction was further enhanced at high GHSVs. However, with the introduction of 20% EGR into the engine, the increased steam content in the engine exhaust caused the high hydrogen yielding SRR process and the WGSR side reaction to dominate in the reactor, hence significantly increased hydrogen production was obtained at low GHSVs. In addition, the increase in endothermic reactivity further promotes the recovery of waste heat and improves the overall reforming process efficiency. Therefore, with the optimization of the process, on-demand supply of high quality syngas produced from biogas could be achieved with minimal energy loss for dual fuel engine operations.

### 7.1.3 Performance of the Biogas Exhaust Gas Fuel Reforming Process and the Gas – Diesel Dual Fuel Operation with REGR

The engine – reactor system was implemented by feeding the reformer product gas (i.e. reformate gaseous fuel) from the reactor placed in the REGR loop into the air intake of the engine fuelled with ULSD. The effect of REGR on the overall reformer product composition and on reforming process efficiency was investigated and compared with that of biogas exhaust fuel reforming in previous chapter. Comparison studies on the engine performance and exhaust gas emissions for (i) pure diesel operation, (ii) biogas-diesel dual fuel operation and (iii) reformate gas-diesel dual fuel operation were also conducted.

The reforming activity for the biogas exhaust fuel reforming in the engine – reactor system was mainly influenced by the higher amount of steam present in the engine exhaust gas as a result of combusting hydrogen-enriched reformate gaseous fuel obtained through the

implementation of REGR. The increased steam content into the reforming reactor which further promotes the endothermic SRR process proved to be beneficial, with up to 24% hydrogen in the product. The resulting overall process efficiency was higher than 100% at optimum operating condition; hence exhaust waste heat recovery was achieved.

The beneficial effects of introducing reformate into the dual fuel system at engine part load operation was evident compared to that of using pure biogas. It is believed that the superior properties of hydrogen and carbon monoxide present in reformate and the substantial reduction in carbon dioxide content improved the turbulent flame propagation through the gaseous fuel-air mixture. This belief is further supported by decreased unburned methane emissions and simultaneous increased engine indicated thermal efficiency. Moreover, the achieved liquid diesel fuel replacement was also significantly higher in dual fuel reformate gas-diesel operation than in biogas-diesel operation. At low EGR ratio, both NOx and soot emissions were substantially reduced with the introduction of reformate compared to both that of biogas-diesel and pure diesel operations. Alas, the use of reformate increased the soot emission at high EGR ratio even though the NOx emission level still remained the lowest with the use of reformate.

## 7.2 General Closing Remarks

The use of gaseous fuels for dual fuel operations can retain most of the positive traits of a diesel engine while providing better engine exhaust emissions. Nonetheless, the use of biogas especially during engine part load operation resulted in lower engine thermal efficiency and high UHC emission. The engine - reactor system has shown great potential in improving the engine performance and emissions of dual fuel operation by upgrading biogas into hydrogen-enriched syngas through the exhaust gas fuel reforming process. As a result of

this work, it was observed that the exhaust gas fuel reforming process using biogas was influenced by both the reactor operating conditions and the compositions of engine exhaust being fed into the reforming reactor. Process optimisation is thus essential in order to achieve high hydrogen content in the reactor gas product with minimal energy loss in the reforming process. With the implementation of REGR in the engine – reactor system, the high steam content in the engine exhaust gas proved to be beneficial by increasing hydrogen yield in the reactor gas product and improving the overall reforming process efficiency. At low EGR ratio engine operating conditions, simultaneous reduction in NOx, soot and UHC emissions were observed in the reformate gas-diesel operation compared to that of biogas-diesel operation. Moreover, at all engine operating conditions, higher engine thermal efficiency and greater fossil diesel fuel replacement were achieved in the engine – reactor system.

## 7.3 Future Work

It can be seen that the equilibrium calculation method is a convenient tool to predict the results of the reactor reforming products for preliminary studies. Nonetheless, the STANJAN equilibrium model used in this thesis is only capable of performing steady state calculations (i.e. constant temperature and pressure conditions). Based on the experimental studies for the exhaust gas fuel reforming process presented in this thesis, it was clear that the reactor temperature changes along the monolith catalyst bed and hence resulting in a non-uniform reactor temperature profile. It was proposed that an in-house model built from software such as ANSYS FLUENT or MATLAB that could predict the chemical kinetics of the various reforming processes at a non-uniform temperature profile would be useful for the preliminary studies of the exhaust gas fuel reforming process. This would also enable the

study for the optimization of the exhaust gas fuel reforming process in various engine exhaust compositions and reactor conditions without incurring the cost of laboratory work.

In terms of engine performance and emission characteristics, it was shown in this thesis that the use of reformate gaseous fuel in the engine – reactor system proves to be superior compared to that of biogas-diesel dual fuel operation even at low REGR condition of only 3%. A full scale engine - reactor configuration capable of providing reformate gas at a higher flow rate should be set up to study the effect of adding reformate into the diesel engine at higher % REGR conditions. This study would enable further investigations of the exhaust gas fuel reforming process at various GHSV conditions and subsequently different engine intake air substitution levels for the engine – reactor system. In addition, part of the hydrogen-enriched reformate gaseous fuel produced from the full scale reformer reactor could be utilized in the diesel after-treatment systems, further reducing engine exhaust emissions.

Lastly, research into the formation of soot in the reforming reactor would be necessary as the next step in studying the engine – reactor system. The high amount of soot present in the engine exhaust, especially at high % EGR engine conditions could potentially promote the undesirable soot formation during the exhaust gas fuel reforming process. Detailed study on the amount of soot formed in the reforming reactor would give an insight into the cause for the high soot emission at high % EGR conditions as shown in Chapter 6. In addition, by thoroughly understanding the soot formation in the reforming rector, the possible deactivation of reforming catalyst due to coking (i.e. carbon deposition on catalyst surface) especially with the introduction of long-chain hydrocarbon fuels in the exhaust gas fuel reforming process could be avoided in the future.

# APPENDIX

# A. Technical Data for Measuring Equipment

Table A.1: Technical data for the MKS Type MultiGas Analyzer Model 2030.

| Measurement Specifications | |
|---|---|
| Measuring Technique | FT-IR spectroscopy |
| Gases and Vapor Measurable | Most molecules with dipole moments except for $N_2$, $H_2$, and $O_2$ |
| Ranges | Concentration between low ppb and 100 ppm scale |
| FT-IR | 2102 Process FT-IR |
| Spectral Resolution | 0.5-128 $cm^{-1}$ |
| Scan Speed | 1 scans / sec @ 0.5 $cm^{-1}$ |
| Scan Time | 1-300 sec |
| Infrared Source | Silicon Carbibe at 1100°C |
| Reference Laser | Helium – Neon (15798.2 $cm^{-1}$) – dependent upon detector |
| Detector | $LN_2$-cooled MCT; TE-cooled MCT |
| Pressure Transducer | MKS Baratron (0-1000 torr 0-3000 torr standard; consult model code) |

Table A.2: Technical data for the AVL Digas 440 analyzer.

| Gas | Measuring range | Resolution | Accuracy |
|---|---|---|---|
| CO | 0-10% vol. | 0.01% vol. | <0.6% vol.: ±0.03% vol.<br>≥0.6% vol.: ±5% of ind. val. |
| $CO_2$ | 0-20% vol. | 0.1% vol. | <10% vol.: ±0.5% vol.<br>≥10% vol.: ±5% of ind. val. |
| HC | 0-20000ppm vol. | ≤2000 ppm: 1ppm vol.<br>>2000 ppm: 10 ppm vol. | <200 ppm vol.: ±10ppm vol.<br>≥200 ppm vol.: ±5% of ind. val. |
| $O_2$ | 0-22% vol. | 0.01% vol. | <2% vol.: ±0.1% vol.<br>≥2% vol.: ±5% of ind. val. |
| NO | 0-5000ppm vol. | 1 ppm vol. | <500 ppm vol.: ± 50ppm vol.<br>≥500 ppm vol.: ±10% of ind. val. |

# B. Test Spread Sheet

Table B.1: Engine emissions recording spreadsheet.

| No | Engine Condition | EGR (%) | GHSV (k/h) | Reformate (l/min) | CO2 | CO(l) | O2 | Nox | THC | THC | NO(H) | λ |
|---|---|---|---|---|---|---|---|---|---|---|---|---|
| 1 | 1500rpm/ 4bar | 0 | 25.5 | 15 | | | | | | | | |
| 2 | | | | | | | | | | | | |
| 3 | | 20 | | | | | | | | | | |
| 4 | | | | | | | | | | | | |
| 5 | | 0 | 16.5 | 10 | | | | | | | | |
| 6 | | | | | | | | | | | | |
| 7 | | 20 | | | | | | | | | | |
| 8 | | | | | | | | | | | | |

Table B.2: Reformer reactor product gas recording spreadsheet.

| No | Engine Condition | EGR (%) | GHSV (k/h) | Reformate (l/min) | Product Gas (%) | | | | |
|---|---|---|---|---|---|---|---|---|---|
| | | | | | H2 | CO | CH4 | CO2 | O2 |
| 1 | 1500rpm/ 4bar | 0 | 25.5 | 15 | | | | | |
| 2 | | | | | | | | | |
| 3 | | 20 | | | | | | | |
| 4 | | | | | | | | | |
| 5 | | 0 | 16.5 | 10 | | | | | |
| 6 | | | | | | | | | |
| 7 | | 20 | | | | | | | |
| 8 | | | | | | | | | |

Table B.3: Reactor temperature profile recording spreadsheet.

| No | Engine Condition | EGR (%) | GHSV (k/h) | Reformate (l/min) | Temperature Profile Along Monolith (C) | | | | | | | | | | |
|---|---|---|---|---|---|---|---|---|---|---|---|---|---|---|---|
| | | | | | 1 | 2 | 3 | 4 | 5 | 6 | 7 | 8 | 9 | 10 | 11 |
| 1 | 1500rpm/ 4bar | 0 | 25.5 | 15 | | | | | | | | | | | |
| 2 | | | | | | | | | | | | | | | |
| 3 | | 20 | | | | | | | | | | | | | |
| 4 | | | | | | | | | | | | | | | |
| 5 | | 0 | 16.5 | 10 | | | | | | | | | | | |
| 6 | | | | | | | | | | | | | | | |
| 7 | | 20 | | | | | | | | | | | | | |
| 8 | | | | | | | | | | | | | | | |

# C. Author's Publications and Award

## C1 Author Publications

- **Lau, C. S.,** Tsolakis, A., Wyszynski, M. L. 2011. Biogas Upgrade to Syngas ($H_2$-CO) via Dry and Oxidative Reforming. **International Journal of Hydrogen Energy**, 36(1), 397-404.
- **Lau, C. S.,** Allen, D., Tsolakis, A., Golunski, S. E., Wyszynski, M. L. 2012. Biogas Upgrade to Syngas Through Thermochemical Recovery using Exhaust Gas Reforming. **Biomass and Bioenergy**, 40(0), 86-95.
- **Lau, C. S.,** Herreros, J. M., Tsolakis, A. 2012. Engine – Reactor Closed Loop Exhaust Reforming of Biogas for Improved Dual Fuel Performance and Emissions. Submitted to **Renewable Energy**.
- Leung, C. P., **Lau, C. S.,** Tsolakis, A., Wyszynski, M. L. 2010. Fuel Reforming for Gasoline and Alternative Fuels. *Presented by the Author at the **UnICEG** Meeting at University of Nottingham 2010.*

## C2 Author Award

- **Guest Keen and Nettlefolds Scholarship** for outstanding academic achievements.

# List of References

Abd-Alla, G. H. 2002. Using Exhaust Gas Recirculation in Internal Combustion Engines: A Review. **Energy Conversion and Management**, 43, 1027-1042.

Abd-Alla, G. H., Badr, O. A., Soliman, H. A., Rabbo, A. M. F. 2000. Exhaust Emissions from an Indirect Injection Dual-Fuel Engine. **Proceedings of the Institute of Mechanical Engineer**, 214 (D), 333-340.

Abd-Alla, G. H., Soliman, H. A., Badr, O. A., Abd Rabbo, M. F. 2000. Effect of Pilot Fuel Quantity on the Performance of a Dual Fuel Engine. **Energy Conversion and Management**, 41, 559-572.

Abu-Jrai, A., Tsolakis, A. 2007. The Effect of $H_2$ and CO on the Selective Catalytic Reduction of NOx Under Real Diesel Engine Exhaust Conditions over Pt/Al2O3. **International Journal of Hydrogen Energy**, 32, 2073-2080.

AEBIOM, **European Biomass Association**. 2009. A Biogas Road Map for Europe.

Ahluwalia, R. K., Hua, T. Q., Peng, J. K. 2011. On-board and Off-board Performance of Hydrogen Storage Options for Light-duty Vehicles. **International Journal of Hydrogen Energy**, In Press.

Ahmed, S., Krumpelt, M. 2001. Hydrogen from Hydrocarbon Fuels for Fuel Cells. **International Journal of Hydrogen Energy**, 26, 291-301.

Andujar, J. M., Segura, F. 2009. Fuel Cells: History and Updating. A Walk along Two Centuries. **Renewable and Sustainable Energy Reviews**, 13, 2309-2322.

Badr, O., Karim, G. A., Liu, B. 1999. An Examination of the Flame Spread Limits in a Dual Fuel Engine. **Applied Thermal Engineerin**g, 19, 1071-1080.

Bari, S. 1996. Effect of Carbon Dioxide on the Performance of Biogas/Diesel Dual-Fuel Engine. **Renewable Energy**, 9, 1007-1010.

Bedoya, I. D., Arrieta, A. A., Cadavid, F. J. 2009. Effects of Mixing System and Pilot Fuel Quality on Diesel-Biogas Dual Fuel Engine Performance. **Bioresource Technology**, 100, 6624-6629.

Bika, A., Franklin, L., Kittleson, D. 2008. Emissions Effects of Hydrogen as a Supplemental Fuel with Diesel and Biodiesel. **SAE Paper**, 2008-01-0648.

Bittner, R. W., Aboujaoude, F. W. 1992. Catalytic Control of NOx, CO, and NMHC Emissions From Stationary Diesel and Dual-Fuel Engines. **Journal of Engineering for Gas Turbines and Power**, 114, 597-601.

Bradford, M. C. J., Vannice, M. A. 1996. Catalytic Reforming of Methane with Carbon Dioxide over Nickel Catalysts II. Reaction kinetics. **Applied Catalysis A: General**, 142, 97-122.

Chigier, N. 1981. **Energy, Combustion, and Environment**, USA, McGraw Hill Company.

Deublein, D., Steinhauser, A. 2008. **Biogas from Waste and Renewable Resources: An Introduction**, Wiley-VCH.

Ding, O. L., Chan, S. H. 2008. Autothermal Reforming of Methane Gas-Modelling and Experimental Validation. **International Journal of Hydrogen Energy**, 33, 633-643.

DOE., U.S. Department of Energy. 2008. Metal hydrides [Online]. Available: http://www1.eere.energy.gov/hydrogenandfuelcells/storage/metal_hydrides.html [Accessed 14 October 2011].

DOE., U.S. Department of Energy. 2009. Targets for onboard hydrogen storage systems for light-duty vehicles [Online]. Available: http://www1.eere.energy.gov/hydrogenandfuelcells/storage/index.html [Accessed 14 October 2011].

Duc, P. M., Wattanavichien, K. 2007. Study on Biogas Premixed Charge Diesel Dual Fuelled Engine. **Energy Conversion and Management**, 48, 2286-2308.

EEA, European Environmental Agency. 2011. Transport Introduction [Online]. Available: http://www.eea.europa.eu/themes/transport [Accessed 17 August 2011].

El-Shinnawi, M. M., El-Shimi, S. A., Badawi, M. A. 1988. Enzyme Activities in Manured Soils. **Biological Wastes**, 24, 283-295.

Enerdata. 2011. **World Energy Use in 2010: over 5% growth**.

Frusteri, F., Freni, S., Chiodo, V., Spadaro, L., Di Blasi, O., Bonura, G., Cavallaro, S. 2004. Steam Reforming of Bio-Ethanol on Alkali-Doped Ni/MgO Catalysts: Hydrogen Production for MC Fuel Cell. **Applied Catalysis A: General**, 270, 1-7.

Gomes Antunes, J. M., Mikalsen, R., Roskilly, A. P. 2009. An Experimental Study of a Direct Injection Compression Ignition Hydrogen Engine. **International Journal of Hydrogen Energy**, 34, 6516-6522.

Graf, P. O., Mojet, B. L., Van Ommen, J. G., Lefferts, L. 2007. Comparative Study of Steam Reforming of Methane, Ethane and Ethylene on Pt, Rh and Pd Supported on Ytrium-Stabilized Zirconia. **Applied Catalysis A: General**, 332, 310-317.

Henham, A., Makkar, M. K. 1998. Combustion of Simulated Biogas in a Dual-Fuel Diesel Engine. **Energy Conversion and Management**, 39, 2001-2009.

Heywood, J. B. 1988. **Internal Combustion Engine Fundamentals**, New York ; London : McGraw-Hill, c1988.

Horn, R., Williams, K. A., Degenstein, N. J., Bitsch-Larsen, A., Dalle Nogare, D., Tupy, S. A., Schmidt, L. D. 2007. Methane Catalytic Partial Oxidation on Autothermal Rh and Pt Foam Catalysts: Oxidation and Reforming Zones, Transport Effects, and Approach to Thermodynamic Equilibrium. **Journal of Catalysis**, 249, 380-393.

IEA, International Energy Agency. 2009. **Key World Energy Statistics 2009**. Paris.

Jing, Q. S., Zheng, X. M. 2006. Combined Catalytic Partial Oxidation and CO2 Reforming of Methane over ZrO2-modified Ni/SiO2 Catalysts Using Fluidized-bed Reactor. **Energy**, 31, 2184-2192.

Jonsson, O. 2004. Biogas upgrading and use as transport fuel.

Jonsson, O., Persson, M., Seifert, M. 2007. European Experience of Upgrading Biogas to Vehicle Fuel and for Gas Grid Injection. In: **Proceedings of 15th European Biomass Conference & Exhibition**, 2007 Berlin, Germany.

Karim, G. A. 2003. Combustion in Gas Fueled Compression: Ignition Engines of the Dual Fuel Type. **Journal of Engineering for Gas Turbines and Power**, 125, 827-836.

Karim, G. A., Wierzba, I. 1992. Methane-Carbon Dioxide Mixtures as a Fuel. **SAE Paper**, 921557.

Kibert, C. J. 2008. **Sustainable Construction: Green Building Design and Delivery**, John Wiley & Sons.

Kobayashi, H., Hagiwara, H., Kaneko, H., Ogami, Y. 2007. Effects of CO2 Dilution on Turbulent Premixed Flames at High Pressure and High Temperature. **Proceedings of the Combustion Institute**, 31, 1451-1458.

Korakianitis, T., Namasivayam, A. M., Crookes, R. J. 2011. Diesel and Rapeseed Methyl ester (RME) Pilot Fuels for Hydrogen and Natural Gas Dual-Fuel Combustion in Compression-Ignition Engines. **Fuel**, 90, 2384-2395.

Kratzeisen, M., Starcevic, N., Martinov, M., Maurer, C. & Muller, J. 2010. Applicability of Biogas Digestate as Solid Fuel. **Fuel**, 89, 2544-2548.

Kuo, K. K.Y. 2005. **Principles of Combustion. 2nd Ed**, WILEY-Interscience.

Lapuerta, M., Armas, O., Gomez, A. A. 2003. Diesel Particle Size Distribution Estimation from Digital Image Analysis. **Aerosol Science and Technology**, 37, 369-381.

Lee, F. B. 2001. A Comparative Study of Fuels for On-Board Hydrogen Production for Fuel-Cell-Powered Automobiles. **International Journal of Hydrogen Energy**, 26, 381-397.

Lee, J., Ohn, H., Choi, J.Y., Kim, S. J., Min, B. 2011. Development of Effective Exhaust Gas Heat Recovery System for a Hybrid Electric Vehicle. **SAE Paper**, 2011-01-1171.

Li, B., Kado, S., Mukainakano, Y., Nurunnabi, M., Miyao, T., Naito, S., Kunimori, K., Tomishige, K. 2006. Temperature Profile of Catalyst Bed during Oxidative Steam Reforming of Methane over Pt-Ni Bimetallic Catalysts. **Applied Catalysis A: General**, 304, 62-71.

Lilik, G. K., Zhang, H., Herreros, J. M., Haworth, D. C., Boehman, A. L. 2010. Hydrogen Assisted Diesel Combustion. **International Journal of Hydrogen Energy**, 35, 4382-4398.

Liu, Z., Karim, G. A. 1997. Simulation of Combustion Processes in Gas-Fuelled Diesel Engines. **Proceedings of the Institution of Mechanical Engineers, Part A: Journal of Power and Energy**, 211, 159-169.

Liu, Z., Karim, G. A. 1998. An Examination of the Ignition Delay Period in Gas-Fueled Diesel Engines. **Journal of Engineering for Gas Turbines and Power**, 120, 225-231.

Masood, M., Ishrat, M. M., Reddy, A. S. 2007. Computational Combustion and Emission Analysis of Hydrogen-Diesel Blends with Experimental Verification. **International Journal of Hydrogen Energy**, 32, 2539-2547.

Mezzulo, W. G. 2010. **An Interdisciplinary Assessment of Biogas Production and The Bioenergy Potential Within the South West of England**. Philisophy of Doctor, University of Bath.

Mukainakano, Y., Li, B., Kado, S., Miyazawa, T., Okumura, K., Miyao, T., Naito, S., Kunimori, K., Tomishige, K. 2007. Surface Modification of Ni Catalysts with Trace Pd and Rh for Oxidative Steam Reforming of Methane. **Applied Catalysis A:General**, 318, 252-264.

Mustafi, N. N., Raine, R. R. 2008. A Study of the Emissions of a Dual Fuel Engine Operating with Alternative Gaseous Fuels. **SAE Paper**, 2008-01-1394.

Nagai, M., Nakahira, K., Ozawa, Y., Namiki, Y., Suzuki, Y. 2007. $CO_2$ Reforming of Methane on Rh/Al2O3 Catalyst. **Chemical Engineering Science**, 62, 4998-5000.

Nielsen, O. B., Qvale, B., Sorenson, S. 1987. Ignition Delay in the Dual Fuel Engine. **SAE Paper**, 870589.

NRC. 2010. **Advancing the Science of Climate Change**, Washington, DC. The National Academic Press.

Ono, R., Nifuku, M., Fujiwara, S., Horiguchi, S., Oda, T. 2007. Minimum Ignition Energy of Hydrogen–Air Mixture: Effects of Humidity and Spark Duration. **Journal of Electrostatics**, 65, 87-93.

Owen, K., Coley, T. 1995. **Automotive fuels reference book**, Warrendale, PA. USA, Society of Automotive Engineers, Inc.

Papagiannakis, R. G., Hountalas, D. T. 2004. Combustion and Exhaust Emission Characteristics of a Dual Fuel Compression Ignition Engine Operated with Pilot Diesel Fuel and Natural Gas. **Energy Conversion and Management**, 45, 2971-2987.

Papagiannakis, R. G., Hountalas, D. T., Rakopoulos, C. D. 2007. Theoretical Study of the Effects of Pilot Fuel Quantity and its Injection Timing on the Performance and Emissions of a Dual Fuel Diesel Engine. **Energy Conversion and Management**, 48, 2951-2961.

Papagiannakis, R. G., Hountalas, D. T., Rakopoulos, C. D., Rakopoulos, D. C. 2008. Combustion and Performance Characteristics of a DI Diesel Engine Operating from Low to High Natural Gas Supplement Ratios at Various Operating Conditions. **SAE Paper**, 2008-01-1392.

Papagiannakis, R. G., Rakopoulos, C. D., Hountalas, D. T., Rakopoulus, D. C. 2010. Emission Characteristics of High Speed, Dual Fuel, Compression Ignition Engine Operating in a Wide Range of Natural Gas/Diesel Fuel Proportions. **Fuel**, 89, 1397-1406.

Patterson, T., Esteves, S., Dinsdale, R., Guwy, A. 2011. An Evaluation of the Policy and Techno-Economic Factors Affecting the Potential for Biogas Upgrading for Transport Fuel Use in the UK. **Energy Policy**, 39, 1806-1816.

Pedersen-Mjaanes, H., Chan, L., Mastorakos, E. 2005. Hydrogen Production from Rich Combustion in Porous Media. **International Journal of Hydrogen Energy**, 30, 579-592.

Peucheret, S., Feaviour, M., Golunski, S.E. 2006. Exhaust-gas Reforming using Precious Metal Catalysts. **Applied Catalysis B: Environment**, 65, 201-206.

Poschl, M., Ward, S., Owende, P. 2010. Evaluation of Energy Efficiency of Various Biogas Production and Utilization Pathways. **Applied Energy**, 87, 3305-3321.

Prakash, G., Ramesh, A., Shaik, A. B. 1999. An Approach for Estimation of Ignition Delay in a Dual Fuel Engine. **SAE Paper**, 1999-01-0232

Rasi, S., Veijanen, A., Rintala, J. 2007. Trace Compounds of Biogas from Different Biogas Production Plants. **Energy**, 32, 1375-1380.

REN21, **Renewable Energy Policy Network for the 21st Century**. 2009. Renewables 2011 Global Status Report.

Reynolds, W. C. 1986. **The Element Potential Method for Chemical Equilibrium Analysis: Implementation in the Interactive Program STANJAN**. Department of Mechanical Engineering, Stanford University.

Richardson, J. T., Garrait, M., Hung, J. K. 2003. Carbon Dioxide Reforming with Rh and Pt–Re Catalysts Dispersed on Ceramic Foam Supports. **Applied Catalysis A: General**, 255, 69-82.

Richardson, J. T., Paripatyadar, S. A. 1990. Carbon Dioxide Reforming of Methane with Supported Rhodium. **Applied Catalysis**, 61, 293-309.

Rose, J. W., Cooper, J. R. 1977. **Technical Data on Fuel**, British National Committee, World Energy Conference Edinburgh : distributed by Scottish Academic Press.

Roy, M. M., Tomita, E., Kawahara, N., Harada, Y., Sakane, A. 2011. Comparison of Performance and Emissions of a Supercharged Dual-Fuel Engine Fueled by Hydrogen and Hydrogen-Containing Gaseous Fuels. **International Journal of Hydrogen Energy**, 36, 7339-7352.

Ryi, S.K., Park, J.S., Kim, D.K., Kim, T.H., Kim, S.H. 2009. Methane Steam Reforming with a Novel Catalytic Nickel Membrane for Effective Hydrogen Production. **Journal of Membrane Science**, 339, 189-194.

Shrestha, S. O. B., Leblanc, G., Balan, G., Souza, M. D. 2000. A Before Treatment Method for Reduction of Emissions in Diesel Engines. **SAE Paper**, 2000-01-2791.

Simeone, M., Salemme, L., Allouis, C. 2008. Reactor Temperature Profile during Autothermal Methane Reforming on Rh/Al2O3 Catalyst by IR Imaging. **International Journal of Hydrogen Energy**, 33, 4798-4808.

Stone, R. 1992. **Introduction to Internal Combustion Engines**, The Macmillan Press Ltd.

Themelis, N. J., Ulloa, P. A. 2007. Methane Generation in Landfills. **Renewable Energy**, 32, 1243-1257.

Tinaut, F. V., Melgar, A., Giménez, B., Reyes, M. 2011. Prediction of performance and emissions of an engine fuelled with natural gas/hydrogen blends. **International Journal of Hydrogen Energy**, 36, 947-956.

Tomishige, K., Matsuo, Y., Sekine, Y., Fujimoto, K. 2001. Effective Methane Reforming with CO2 and O2 Under Pressurized Condition using NiO-MgO and Fluidized Bed Reactor. **Catalysis Communications**, 2, 11-15.

Tree, D. R., Svensson, K. I. 2007. Soot Processes in Compression Ignition Engines. **Progress in Energy and Combustion Science**, 33, 272-309.

Tsolakis, A. 2004. **Exhaust Gas Fuel Reforming for Compression Ignition Engines Fuelled by Diesel and Biodiesel**. Philosophy of Doctor, University of Birmingham.

Tsolakis, A., Golunski, S. E. 2006. Sensitivity of Process Efficiency to Reaction Routes in Exhaust-Gas Reforming of Diesel Fuel. **Chemical Engineering Journal**, 117, 131-136.

Tsolakis, A., Megaritis, A. 2004. Catalytic Exhaust Gas Fuel Reforming for Diesel Engines-Effects of Water Addition on Hydrogen Production and Fuel Conversion Efficiency. **International Journal of Hydrogen Energy**, 29, 1409-1419.

Tsolakis, A., Megaritis, A., Wyszynski, M. L. 2004. Low Temperature Exhaust Gas Fuel Reforming of Diesel Fuel. **Fuel**, 83, 1837-1845.

UNEP, United Nations Environment Programme. 2009. **Towards Sustainable Production and Use of Resources: Assessing Biofuels**.

UN, United Nations. 2008. **Kyoto Protocol Reference Manual on Accounting of Emissions and Assigned Amount**. Bonn, Germany: United Nations Climate Change Secretariat.

Weaver, C. S., Turner, S. H. 1994. Dual Fuel Natural Gas/Diesel Engines: Technology, Performance, and Emissions. **SAE Paper**, 911766.

Wierzba, P., Karim, G. A., Wierzba, I. 1995. An Analytical Examination of the Combustion of a Turbulent Jet in an Environment of Air Containing a Premixed Fuel or a Diluent. **Journal of Energy Resources Technology**, 117, 234-238.

Yoon, S. H., Lee, C. S. 2011. Experimental Investigation on the Combustion and Exhaust Emission Characteristics of Biogas-Biodiesel Dual-Fuel Combustion in a CI engine. **Fuel Processing Technology**, 92, 992-1000.